4-28-2017

Alginate Hydrogels for Bone Tissue Regeneration

Stephanie T. Bendtsen
University of Connecticut, stephanie.bendtsen@uconn.edu

Alginate Hydrogels for Bone Tissue Regeneration

Stephanie Teresa Bendtsen, Ph.D.

University of Connecticut, 2017

Bone tissue engineering is employed to help enhance regeneration of bone tissue that may have difficulty of achieving sufficient healing on its own. As bones tend to break in irregular manners, methods to produce engineered scaffolds more closely fitting the geometry of the defective tissue are desirable. Current techniques to produce engineered bone tissue constructs result in stiff, rigid scaffolds with limited plasticity and ability to form irregular architectures. Additionally, processing methods limit the feasibility to uniformly incorporate live cells into the scaffolds for enhanced uniform healing. The use of hydrogel materials for bone tissue engineering has gained interest due to their high water content and interwoven structure mimicking that of the natural extracellular matrix, rendering them favorable for live cell incorporation. Alginate is a hydrogel with materials properties allowing manipulation in a variety of ways for numerous applications, including injectable fillers, 3D printing, drug and growth factor delivery, cell encapsulation and many more.

In this work, the gelation properties of a series of alginate hydrogel formulations were thoroughly studied and control of the gelation rate was established by varying component concentrations. An optimal hydrogel system was developed with a gelation time appropriate in a surgical setting and composition capable of aiding in new bone formation, confirmed through various characterization techniques. A systematic investigation was then conducted using the knowledge gained to determine the feasibility of their use in 3D printing. As a result, an alginate-

polyvinyl alcohol-hydroxyapatite formulation was developed with optimal rheological properties allowing encapsulation of MC3T3 cells and 3D bioprinting of scaffolds with high shape fidelity and cell viability. Degradation studies showed the scaffolds maintained sufficient mechanical stability to support cell life in culture. *In vitro* evaluations were then conducted to determine the capacity of the formulations to support cell viability and promote cell proliferation. A synergistic effect was discovered, highlighting the need for both sufficient cell adhesion modalities in the matrix and appropriate scaffold mechanical rigidity.

Thus, the development of these alginate hydrogel systems can provide more personalized treatment options for bone repair with potential to enhance bone tissue regeneration.

Alginate Hydrogels for Bone Tissue Regeneration

Stephanie Teresa Bendtsen

B.S., University of Connecticut, 2012

A Dissertation

Submitted in Partial Fulfillment of the

Requirements for the Degree of

Doctor of Philosophy

at the

University of Connecticut

2017

APPROVAL PAGE

Doctor of Philosophy Dissertation

Alginate Hydrogels for Bone Tissue Regeneration

Presented by

Stephanie Teresa Bendtsen, B.S.

Major Advisor _____
Mei Wei

Associate Advisor _____
Anson Ma

Associate Advisor _____
Kelly Burke

University of Connecticut

2017

Acknowledgements

I would like to first thank my advisor, Dr. Mei Wei, for her support and guidance throughout the duration of my doctoral studies here at the University of Connecticut. I am grateful for the opportunity to further my education and gain invaluable research experience and skills that will greatly benefit me in my future endeavors. Also, I would like to thank my associate advisors, Dr. Anson Ma and Dr. Kelly Burke, as well as committee members Dr. Wendy Vanden Berg-Foels and Dr. Harold Brody for their support and input along the way.

I would also like to extend my gratitude to Aida Ghiaei for providing me with the opportunity to be a part of the GK-12 program here at UConn as a fellow, traveling to H.H. Ellis Technical High School once a week to share my knowledge with the students and promote involvement in STEM by engaging them in fun, hands-on activities. It was such a rewarding experience to be involved in such a great outreach program and I am grateful for the professional development and travel experience I gained through the program as well. I would also like to acknowledge my GK-12 members for their teamwork and support.

Additionally, I'd like to thank all the members of the Wei lab, past and present, for their input including Dr. Erica Kramer, Dr. Zengmin Xia, Dr. Max Villa, Dr. Michael Zilm, Jonathan Russo, Drew Clearfield, Changmin Hu, Bryant Heimbach, Seamus Thomson, and Le Yu. I would also like to thank my undergraduate student, Sean Quinnell, who provided substantial contributions to our 3D printing efforts. I'd also like to thank Dr. Pinatti and Dr. Shaw for providing me with their technical expertise. I'd like to thank Dr. Alpay for giving me the opportunity to be his teaching assistant, as well as Lorri LaFontaine and all of the Institute of Materials Science staff for all of their assistance.

Most importantly, I would like to express my deepest gratitude towards my family and friends for all of their unconditional love and constant support throughout this challenging journey. I'd like to thank Dr. Lydie Louis, for being a great mentor and friend; providing me with advice, support, and encouragement throughout my studies. I'd like to dedicate this work to the most supportive people I know: my parents, Todd and Teresa, my brothers, Christopher and Nicholas, and my boyfriend Ryan. Words cannot describe how much it means to me that I could count on you all to encourage me through tough times and celebrate my accomplishments with me. I could not have done this without you.

Table of contents

Copyright……..... ii

Approval page…… iii

Acknowledgements…… iv

Table of contents…… vi

List of tables……... xi

List of figures……..... xii

Chapter 1: Introduction……..... 1

1.1 Personalized medicine and tissue engineering……..... 1

1.2 Bone tissue engineering…… 1

1.3 Hydrogel biomaterials……... 2

1.4 Alginate hydrogels…… 4

1.4.1 Composition…… 4

1.4.2 Gelation and mechanical properties…… 5

1.4.3 Degradation mechanism…….. 7

1.4.4 Applications…… 8

1.4.4.1 Delivery vehicles……..... 8

1.4.4.2 Cell encapsulation……. 10

1.4.4.3 Injectable purposes…… 11

1.5 Three-dimensional printing……. 12

1.6 Current shortcomings…….. 15

1.7 Research objectives……. 16

Chapter 2: Synthesis and characterization of a novel injectable alginate–collagen–hydroxyapatite hydrogel for bone tissue regeneration

2.1 Introduction……. 19

2.2 Materials and methods…… 22

2.2.1 Preparation of alginate hydrogels…… 22

2.2.2 Preparation of alginate-collagen (A-C) hydrogels……... 23

2.2.3 Preparation of alginate-mineralized collagen (A-MC) hydrogels……... 24

2.2.4 Characterization……... 26

2.2.5 Statistical analysis…… 28

2.3 Results…….... 28

2.3.1 Gelation time……..... 28

2.3.2 Dynamic mechanical analysis…….. 32

2.3.3 Thermogravimetric analysis……. 34

2.3.4 X-Ray diffraction……. 35

2.3.5 Fourier transform infrared spectroscopy…….. 36

2.4 Discussion……... 38

2.4.1 Gelation time and mechanical properties……. 38

2.4.2 Characterization of hydrogel inorganic composition……... 44

2.5 Conclusions……. 46

Chapter 3: Development of a novel alginate-polyvinyl alcohol-hydroxyapatite hydrogel for 3D bioprinting bone tissue engineered scaffolds

3.1 Introduction……. 47

3.2 Materials and methods…… 50

3.2.1 Preparation of hydrogel formulations…….. 50

3.2.2 3D printing and hydrogel printability…….. 51

3.2.3 Rheology…….. 52

3.2.4 Optimal formulation characterization……..... 52

3.2.5 Degradation studies in α-MEM…… 53

3.2.5.1 Diameter change……..... 53

3.2.5.2 Dynamic mechanical analysis……... 53

3.2.6 3D bioprinting…….. 54

3.2.6.1 Cell encapsulation and bioprinting……... 54

3.2.6.2 Assessment of cell viability…….. 55

3.2.7 Statistical analysis…… 56

3.3 Results……. 56

3.3.1 Hydrogel printability…… 56

3.3.2 Rheology…….. 58

3.3.3 Optimal formulation characterization…….. 60

3.3.4 Degradation studies α-MEM…… 62

3.3.4.1 Diameter change……... 62

3.3.4.2 Dynamic mechanical analysis……..... 64

3.3.5 Bioprinting and viability of encapsulated MC3T3 cells…….. 65

3.4 Discussion……... 66

3.4.1 Hydrogel printability…… 66

3.4.2 Rheology……..... 69

3.4.3 Optimal formulation characterization…….. 70

3.4.4 Degradation studies α-MEM……..…….. 71

3.4.4.1 Diameter change……... 71

3.4.4.2 Dynamic mechanical analysis……... 73

3.4.5 Bioprinting and viability of encapsulated MC3T3 cells…….. 74

3.5.5 Conclusions…….. 76

Chapter 4: *In vitro* evaluation of 3D bioprinted tri-polymer network scaffolds for bone tissue regeneration

4.1 Introduction……. 77

4.2 Materials and methods…… 79

4.2.1 Preparation of hydrogel-cell suspension…….. 79

4.2.2 3D bioprinting…….. 80

4.2.3 *In vitro* proliferation……. 81

4.2.4 Effects of calcium bath…… 82

4.2.4.1 Diffusion properties of 3D printed scaffolds…… 82

4.2.4.2 Calcium cytotoxicity analysis……... 83

4.2.5 Addition of collagen gel…...…… 83

4.2.6 Mechanical properties…….. 84

4.2.7 Statistical analysis…… 85

4.3 Results……. 85

4.3.1 3D printing of scaffolds with different infill geometries……. 85

4.3.2 Evaluation of proliferation……... 86

4.3.2.1 Infill geometry…….. 86

4.3.2.2 Effects of calcium bath……. 87

4.3.2.2.2 Calcium cytotoxicity analysis…… 88

4.3.2.2.3 Scaffold diffusion properties…….. 88

4.3.2.3 Effect of collagen content……..... 92

4.3.3 Mechanical properties…….. 94

4.4 Discussion……... 95

4.4.1 Proliferation……. 95

4.4.1.1 Effects of infill geometry…….. 96

4.4.1.2 Effects of calcium bath……. 98

4.4.1.2.1 Calcium cytotoxicity analysis…… 98

4.4.1.2.2 Scaffold diffusion properties…….. 99

4.4.1.3 Effect of collagen content……... 101

4.4.2 Mechanical properties…… 103

4.4.3 Conclusions…… 105

Chapter 5: Conclusions and Future work…… 106

5.1 Conclusions……... 106

5.2 Future work……..... 108

5.2.1 Drug delivery……. 108

5.2.2 3D printing scaffolds of irregular architecture……... 108

5.2.2 Further *in vitro* evaluation……. 110

5.2.3 *In vivo* evaluation……... 111

References……... 112

List of Tables

Chapter 2

Table 2.1: Compositions of A-Ca and A-P hydrogels……. 23

Table 2.2: Composition of A-C and A-MC hydrogels……. 24

Table 2.3: Compositions of selected hydrogels for characterization of inorganic content…….. 27

Chapter 3

Table 3.1: Final compositions of various hydrogels for 3D printing……... 51

Table 3.2: Summary of formulation printability…….. 57

Table 3.3: Summary of rheological values after 20 minute gelation period…… 59

Chapter 4

Table 4.1: Diffusion coefficients of FITC-dextran for 3D printed scaffolds……... 92

List of Figures

Chapter 1

Figure 1.1: Sol-gel transition of PECE-collagen-nHA hydrogel at 37 °C [34]……. 3

Figure 1.2: Polymeric structure of alginate [48]……..... 5

Figure 1.3: Ionic crosslinking mechanism of alginate G blocks with calcium ions[50]……... 6

Figure 1.4: Alginate microbeads for drug delivery [70] ……... 9

Figure 1.5: Schematic of 3D printing process [91]…….. 13

Figure 1.6: Figure 1.6 3D printed alginate scaffold [98] …… 15

Figure 1.7: Figure 1.7 3D printed scaffolds for bone tissue engineering [92] …… 16

Chapter 2

Figure 2.1: Alginate suspension (left) and gel (right) states…… 28

Figure 2.2: Average gelation times of alginate hydrogels with varying Na_2HPO_4 and $CaSO_4$ concentrations…….. 29

Figure 2.3: FESEM images of air dried a) pure collagen fibers and b) mineralized collagen fibers……. 30

Figure 2.4: Gelation times of alginate hydrogels with varying pure collagen (C) or mineralized collagen (MC) fiber content…….. 31

Figure 2.5: Compressive moduli of alginate hydrogels of varying Na_2HPO_4 and $CaSO_4$ content……... 32

Figure 2.6: Compressive moduli of various (a) A–C and (b) A–MC hydrogels……. 33

Figure 2.7: TGA curves of alginate hydrogels containing (a) A–MC-2, (b) A–P-9 (0.40% Ca–0.12% P) and (c) A–Ca-1 (0.20% Ca–0% P)…… 35

Figure 2.8: XRD patterns of (a) A–Ca-1, (b) A–P-9, (c) A–C-1, (d) A–MC-1a and (e) A–MC-2 hydrogels……... 36

Figure 2.9: FTIR spectra of (a) A–Ca-1, (b) A–P-9, (c) A–C-1, (d) A–MC-1a and (e) A–MC-2 hydrogels……... 37

Figure 2.10: Schematic of the hypothesized "pre-mature" alginate crosslinking mechanism…. 42

Chapter 3

Figure 3.1: Storage moduli profile of hydrogel formulations during 20 minute time sweep …. 58

Figure 3.2: Recovery profile of select formulations after applied pre-shear, time period defied by dotted lines…… 60

Figure 3.3: XRD patterns of a) formulation 5, b) formulation 6, c) hydroxyapatite and d) control (*) indicates major additional NaCl peak……. 61

Figure 3.4: TGA curves of a) control, b) formulation 5 and c) formulation 6…… 62

Figure 3.5: Diameter change of select scaffold formulations at various time points throughout degradation study……..... 63

Figure 3.6: Compressive moduli of select scaffold formulations throughout degradation Study……. 64

Figure 3.7: Images of 3D bioprinted a) control and b) optimal alginate-polyvinyl alcohol-hydroxyapatite hydrogel formulations embedded with MC3T3-E1 cells …… 65

Figure 3.8: Cell viability after 3D printing and incubation in the calcium bath…….. 66

Chapter 4

Figure 4.1: Schematic of 3D bioprinting process……..... 81

Figure 4.2: 3D printed a) original design b) alternating design and c) control scaffolds…… 85

Figure 4.3: Proliferation of 3D bioprinted scaffolds after 1 % (w/v) $CaCl_2$ bath……..... 86

Figure 4.4: Proliferation of 3D bioprinted scaffolds after 0.5 % (w/v) $CaCl_2$ bath……. 87

Figure 4.5: Cytotoxic study of MC3T3 cells incubated in calcium baths of various concentrations……... 88

Figure 4.6: a) Cumulative release profile of FITC-dextran from scaffolds with control (C), original (O) and alternating (A) infill designs incubated in 0.5 % or 1 % $CaCl_2$ b) Magnified release profile from 1.5-3 hours…….. 89-90

Figure 4.7: Permeability coefficients of FITC-dextran released from 3D printed scaffolds…... 91

Figure 4.8: AlamarBlue reduction by cells 3D printed into scaffolds with a) 5 % (w/v) and b) 6.5 % (w/v) collagen incubated in 0.5 % (w/v) and 1 % (w/v) $CaCl_2$ baths……. 93-94

Figure 4.9: Compressive moduli of increased collagen scaffolds throughout degradation study……. 95

Chapter 5

Figure 5.1: Example of a) CAD model and b) sliced .stl file of proposed irregular scaffold design…….. 109

Chapter 1

Introduction

1.1 Personalized medicine and tissue engineering

The recent advancement of personalized medicine involves individualized treatment to meet the specific needs of patients on a case to case basis as opposed to employing a "one size fits all" mentality. When considering defective tissue, one method of treatment may not be suitable for all patients. Depending on the severity of the injury or damage, some patients may need complete tissue replacement or transplantation whereas some may benefit from tissue repair.[1] Tissue engineering, the use of biomaterials alone or in combination with cells and/or growth factors, has been extensively practiced in hope to enhance healing of all tissue types.[2,3] When suitable, this method provides an alternative to tissue and organ transplantation. This alleviates reliance on the limited availability and negative side effects associated with the use of donor tissue, such as tissue rejection and encapsulation.[4-6] The practice of tissue engineering involves the production of biomaterial scaffolds used as tissue substitutes and reinforcements that promote faster healing of the natural tissue while the defected area undergoes regeneration.[7,8] It is of the most importance that the material of choice be biocompatible, not eliciting an adverse immune response from the host, and biodegradable, degrading within the body at the same rate it promotes new tissue ingrowth for optimized healing.[9,10]

1.2 Bone tissue engineering

Natural bone is composed of inorganic hydroxyapatite (HA) minerals and organic collagen fibrils.[11] Thus, tissue engineering applied to enhance bone regeneration employs biomaterials most often incorporating a combination of HA, collagen, and/or additional materials

with composition and innate material properties closely resembling those of natural bone.[12-14] It is also of interest that these materials be osteoconductive, promoting bone growth on the surface of the material, and osteoinductive, inducing the native *in vivo* environment to produce new bone.[15,16] Originally, the most common materials used were ceramics composed of calcium phosphates.[17] Conventional methods to construct such scaffolds include porogen leaching, solvent casting and lyophilization, creating stiff structures with controlled porosity.[18,19] Porosity is necessary for nutrient transport and cellular migration throughout the scaffold, which are both essential for new bone formation.[20] However, these materials can often form brittle structures lacking the elasticity of natural bone.[21] Thus, additional polymeric materials, such as polycaprolactone (PCL), polylactic acid (PLA), and polyglycolic acid (PLGA), have been implemented in combination with osteoconductive materials such as HA, to increase the elasticity of the scaffolds while maintaining sufficient mechanical strength, biocompatibility and biodegradability.[22,23] However, these scaffolds still suffer from limited ability to easily fit irregular shaped defects, often created by bone fractures.[24] Thus, recent research in bone tissue engineering has focused on hydrogel materials which although are significantly weaker, are able to form scaffolds of irregular dimensions, making them ideal for the practice of personalized medicine and treatment of individualized defective tissues.

1.3 Hydrogel biomaterials

Hydrogels are composed of long chains of polymeric networks and are able to retain a large quantity of water due to hydrophilic functional groups on the polymer backbone.[25] Hydrogel biomaterial applications range from the formation of physical products such as contact lenses and wound dressings, to their application in tissue engineering, drug delivery, cell

encapsulation and 3D printing.[26-30] They are often highly biocompatible and flexible due to their high water content (over 90%) and interwoven structure resembling that of the natural extracellular matrix (ECM), making them a favorable environment for cellular activities such as migration and proliferation.[31,32]

Hydrogels are most often formed via sol-gel polymerization in which they transition from a fluid, flowing state (sol) to a solid, non-flowing state (gel).[33] Thermogelation is a sol-gel mechanism in which the transition is induced at a particular temperature, most often body temperature (37 °C) for biomedical applications.[34] Figure 1.1 depicts the thermogelation of a polyethylene glycol (PEG)-PCL-PEG-collagen-nanohydroxyapatite (PECE-collagen-nHA) hydrogel occurring at 37 °C.[34]

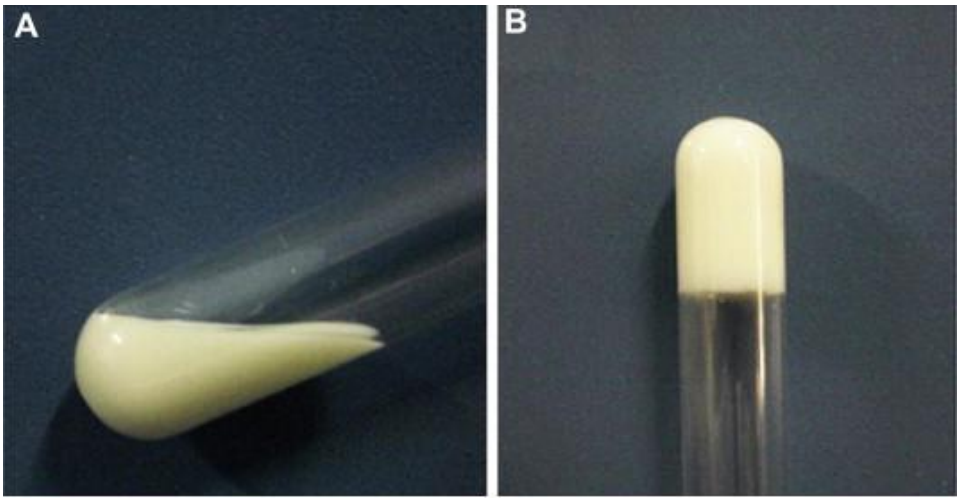

Figure 1.1: Sol-gel transition of PECE-collagen-nHA hydrogel at 37 °C [34]

An alternative method is photopolymerization, which occurs as a result of polymerization of an acrylic or methacrylic side group on the polymer backbone in the presence of a photoinitiator and UV light.[35,36] Additional sol-gel polymerization methods include those that are ionic and result from chemical reactions, only occurring under a specific set of conditions.[37,38] These transitions are often easier to control and vary the materials properties of the resulting hydrogel, including mechanical strength and degradation rate. They are also more biocompatible due to the absence of cytotoxic side groups and non-biodegradable byproducts, commonly associated with photopolymerization and thermogelation, respectively.[39,40]

Hydrogels can be either of synthetic or natural origin, both extensively researched for use as biomaterials. Popular synthetic hydrogels, commonly formed through thermogelation and photopolymerization, include PEG, polyhydroxyethyl methacrylate (PHEMA), and polyvinyl alcohol (PVA).[41,42] Natural hydrogels include chitosan, gelatin, and alginate, all derived from natural sources.[43,44] Although hydrogels are often implemented for soft tissue regeneration such as skin and muscle, recent research has expanded into bone tissue engineering, though less commonly explored.[45,46]

1.4 Alginate hydrogels

1.4.1 Composition

Alginate is a naturally occurring polysaccharide derived from brown algae.[47] The linear co-polymer backbone is composed of consecutive blocks of (1–4) linked α-L-guluronate (G-blocks) and β-D-mannuronate (M-blocks) followed by segments of alternating MG blocks.[48] Figure 1.2 shows the composition of the G and M blocks.

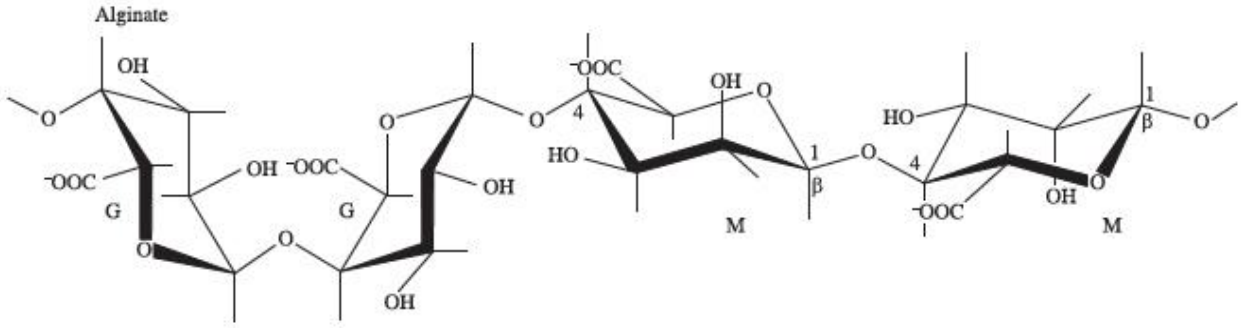

Figure 1.2: Polymeric structure of alginate [48]

Alginate hydrogels will have specific materials properties according to the source, or type of algae, it is derived from. This can be attributed to the ratio of G to M blocks present in the polymer backbone, which varies from source to source.[49] For example, sources with a high ratio, or high G block content, such as *Laminaria hyperborea*, are known as high viscosity sources, and form strong hydrogels. Medium viscosity sources, such as *Macrocystis pyrifera*, form medium strength hydrogels due to the medium ratio of G:M blocks, while low viscosity sources such as *Ascophyllum rodosum*, form the weakest hydrogels due to the high content of M blocks within the polymer structure.[49] The composition of the alginate polymer chains is responsible for gelation and mechanical properties, which will be further explained in the next section.

1.4.2 Gelation and mechanical properties

The mechanism in which alginate experiences a sol-gel transition is ionic in nature. The G blocks of the alginate polymer chain undergo formation of what is described as an "egg box" structure in the presence of divalent cations.[50] The divalent cations form intermolecular bonds

with two deprotonated carboxylate groups and two hydroxyl groups of the alginate G blocks, shown in Figure 1.3. Lateral crosslinking of these egg boxes results in hydrogel formation.

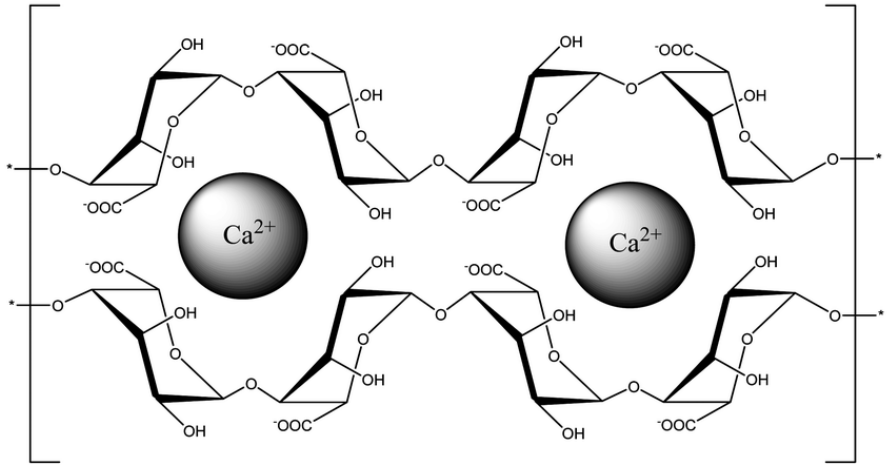

Figure 1.3: Ionic crosslinking mechanism of alginate G blocks with calcium ions[51]

As previously mentioned, the ratio of G to M blocks in the alginate structure plays a crucial role in the materials properties of the resulting hydrogel, as the G blocks have a great affinity for divalent cations whereas the M blocks form weak interactions with divalent cations and don't partake in crosslinking.[52] Thus, the greater amount of G blocks present in the structure, the greater number of crosslinks formed, and the stronger the resulting hydrogel will be. Calcium is the most commonly used divalent cation to induce alginate gelation as the G blocks have a high affinity for forming strong bonds with it and it is the most biocompatible.[53] Additional divalent cations used include magnesium, barium and strontium, forming bonds weakest to strongest, respectively.[54]

The rate in which this gelation occurs can be tailored via varying the concentrations of the constituents and/or the addition of retardation agents.[52] It has been shown that an increase in calcium concentration results in an increase in gelation rate, as the increase in available calcium ions allows crosslinks with alginate G blocks to form quickly. The addition of a retardation such as Na_2HPO_4 can interrupt the gelation process thereby slowing the rate in which it occurs.[55] The calcium source also plays a role in the gelation rate, with highly soluble sources such as $CaCl_2$ releasing ions rapidly into the media supplying ions for immediate gelation. Intermediate sources such as $CaSO_4$, supply ions over time for gradual gelation, and sources with low solubility such as $CaCO_3$, supply ions over an extended period of time resulting in slow gelation.[55] Thus, the gelation rate can be tailored ranging from immediate, in which alginate microbeads are formed instantly, to over a desired amount of time to achieve gradual gelation for injectable and filling purposes.

1.4.3 Degradation mechanism

The mechanism by which alginate hydrogels degrade is through a natural ion exchange with sodium ions or other monovalent ions in the surrounding environment.[56,57] As the alginate G blocks only form strong bonds with divalent cations, as monovalent ions replace them in the egg box structure, the crosslinks are destroyed. This results in media uptake and swelling of the hydrogel structure. Over time, as more crosslinks are broken, the gel will lose its mechanical stability and break down into small pieces. As this process is not enzymatic, alginate is a favorable option for use in the body as it won't be broken down immediately by enzymes or macrophages.[58] Thus, alginate hydrogels have the capability of remaining within the body for time periods necessary to support tissue regeneration. As previously discussed, as the extent of

crosslinking directly affects the mechanical properties and stability of alginate hydrogels, their degradation can be tailored to match the required time necessary for the application. Highly crosslinked, stronger gels will maintain their integrity longer than weaker gels with fewer crosslinks.

1.4.4 Applications

Alginate hydrogels have been extensively researched and used in a wide variety of applications ranging from thickening agents in foods to immobilization agents and scaffold systems in tissue engineering.[52,54] As previously discussed, alginate's innate biocompatibility renders it favorable for use in many biomedical applications. It's gelation properties allow encapsulation of cells, drugs, growth factors for treatment of a variety of aliments including infections, ulcers and wound healing.[59,60] Alginate has been extensively studied for implementation in wound healing in the form of wound dressings as thin films are easily achievable through control of its gelation properties.[61] As an alternative to gauze, alginate provides exudate absorbance properties, water retention for a moist environment, and the ability to incorporate antibiotics and other healing agents within the gel while enhancing skin regeneration.[62] The ability for alginate to serve as delivery vehicles, cell encapsulation and an injectable systems will be further discussed in the following sections.

1.4.4.1 Delivery vehicles

The formation of alginate microspheres, most often as a result of immediate crosslinking in $CaCl_2$, is favorable for many applications. In pharmacology, drugs can be homogeneously mixed throughout an alginate suspension and effectively trapped within the alginate matrix once

the calcium crosslinks are formed. [63,64] Alginate microspheres can used for oral intake or be injected and transported to the site of interest to deliver the drug of choice, such as antibiotics or anti-inflammatory drugs, thus increasing the bioavailability and avoiding rapid drug clearance.[65-67] As alginate is not degraded enzymatically, the drugs are released via diffusion out of the matrix or erosion of the microbeads.[68] Additionally, burst release of the drug can be suppressed and controlled release can be achieved by coating the microspheres or adding additional biomaterials to form composite drug carrier systems. [69,70] Alginate-HA composite beads for oral drug delivery can be seen in Figure 1.4.[70] This method also allows for the incorporation of multi-drug systems which may be difficult to obtain through conventional methods.[52]

Proteins and growth factors such as VEGF can also be encapsulated in microbeads or bulk hydrogels and released in a controlled manner over an extended period of time to enhance tissue regeneration in a defected area.[71-73]

Figure 1.4: Alginate-HA microbeads for drug delivery[70]

1.4.4.2 Cell encapsulation

Similar to drug and growth factor encapsulation, live cells can also be mixed homogeneously throughout an alginate suspension and immobilized via crosslinking with calcium or other divalent cations.[74-76] As the gelation rate can be easily tailored as previously described, mild conditions not harmful to the cells can be achieved, such as gradual gelation at room or body temperature, attributing to high cell viability.[77] Thus, these "donor" cells can be encapsulated and delivered to an area of defective tissue to help enhance regeneration. For example, fibroblasts can be delivered to a wound site to secrete biological agents promoting deposition of ECM components, leading to new epithelial tissue formation.[78] Donor cells can also release chemical signals to recruit host cells to invade the defected area and begin to form new tissue as well.

Although cells can be easily encapsulated in alginate at high viability rates, the matrix must resemble that of the native extracellular matrix in order for cells to proliferate, differentiate, and begin new tissue deposition.[79] Cells need to attach and migrate throughout their extracellular matrix in order to form a network and carry out appropriate physiological behaviors such as proliferation. In the native ECM, elements such as ligands, cell adhesion molecules (CAMs) and additional proteins exist that promote binding to integrins, or transmembrane receptors, on the cytoskeleton.[80] Alginate alone has been reported to induced limited interactions with cells due to its polymer structure, providing minimal cell adhesion sites.[81,82] As alginate does not promote formation of these adhesive contacts, elements that possess ligands, such as collagen and fibronectin, are often added to enhance cellular interactions within the hydrogel matrix.[83,84] Alternatively, the alginate polymer backbone can be chemically modified and coupled with RGD

peptides to mimic the presence of adhesion proteins in the matrix and promote integrin binding.[85,86]

Furthermore, the alginate hydrogel matrix is often combined with additional elements to promote cellular differentiation and progression of mature cells capable of depositing new tissue of choice. For example, tissue engineered constructs aimed to promote new bone formation often include collagen and hydroxyapatite, the main components of natural bone.[87] Thus, pre-osteoblastic cells will sense an environment simulating natural bone and will be more inclined to differentiate into osteoblasts.

1.4.4.3 Injectable purposes

Control of the gelation kinetics of alginate also renders it an optimal base system for injectable applications such as dermal fillers and wound dressings. Injectable hydrogels can also be used to treat additional tissue defects including cartilage and bone, which has been less extensively investigated.[37] In general, treatment via injectable means are favored because they are less invasive and don't require open surgery, which is associated with more pain and longer healing times for patients. Thus, injectable options are most often preferred as they improve the quality of patients' lives during healing, which is a vulnerable time period. Alginate hydrogel injectable systems are advantageous as the gelation rate can be controlled to completely fill a tissue defect and set as a mechanically stable gel within minutes.[38] Thus, irregularity in defect geometry is not an issue, which can be the case when using other static materials or scaffolds constructed under conventional methods.[24] As previously discussed, applying injectable hydrogels for treatment of defected bone tissue is especially favorable as bone most often breaks in irregular manners.

Additionally, as discussed in the previous section, drugs, growth factors, cells, and additional biological components can be encapsulated within the alginate hydrogel and injected into a defected tissue area to aid in enhanced regeneration, thus combining many treatment elements and methods into one superior alternative.

1.4 Three-Dimensional Printing

Three-dimensional (3D) printing is an additive manufacturing technique that implements the production of structures layer by layer.[88] First, a 3D CAD model is created of the desired structure, saved as a .stl file and sliced into G-code, or the computer language that 3D printing software reads. The G-code file dictates the path in which the extruder should follow in order to deposit the material in a way that results in the desired structure.[89] Then, the user chooses various printing conditions, such as printer speed and flow rate, to instruct the printer on how the material should be deposited. 3D printed structures can then be printed ranging from minutes to hours, depending on the size and complexity of the CAD design.[90]

Many types of 3D printing methods exist each with specific requirements for the materials used. 3D printing of metals involves direct metal laser sintering (DMLS), a process in which a laser is directed at a bed of metal powder and melts the metal selectively, fusing the particles into the desired structure.[91] Similarly, inkjet printing, also known as binder jetting, requires deposition of a powder resin followed by printing a layer of a liquid binder material to selectively bind particles together.[92] Stereolithography, often denoted as the first rapid prototyping technique, utilizes a laser to spatially control the photopolymerization of a liquid resin.[93] When the current layer is cured, more resin is added to pattern and cure the succeeding layer. A popular polymer 3D printing method includes fused deposition modeling (FDM), in

which a filamentous thermoplastic is required to melt upon heating and re-solidify once deposited, thereby fusing with the previous layer. Materials employed often include synthetic polymers such as PCL and PLGA.[94] Although all of the previously discussed methods are capable of producing 3D structures of high shape fidelity and mechanical strength, limitations exist when employing these methods for 3D printing for tissue engineering. Reconstruction of damaged or defective tissue can be achieved via 3D printing of repaired CAD files obtained from a patient's MRI or CT scan, thus producing individualized structures with precise geometry and porosity necessary for enhanced tissue healing.[95] A schematic of the 3D printing process is shown in Figure 1.5.

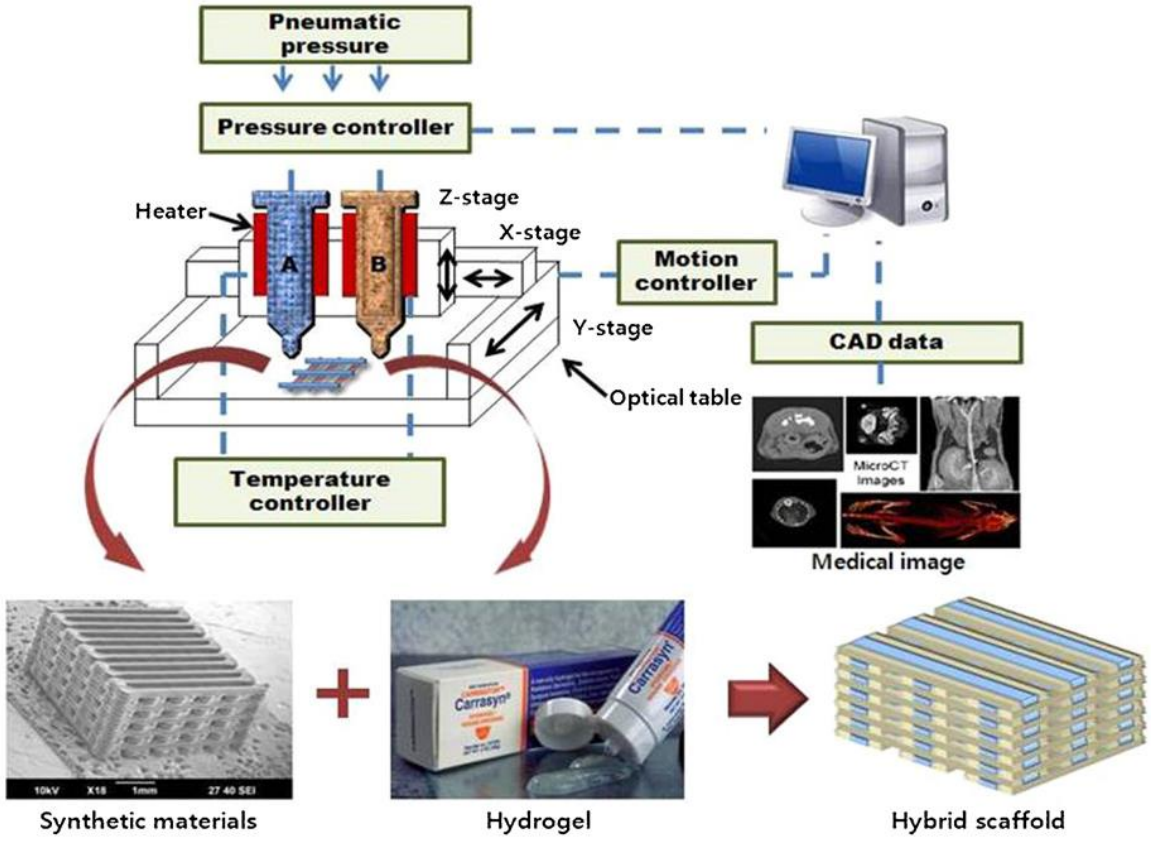

Figure 1.5: Schematic of 3D printing process [96]

As previously mentioned, tissue regeneration can be enhanced even further via inclusion of a patient's own cells distributed homogeneously throughout the engineered tissue substitute. Thus, 3D "bioprinting" or printing of live cells within a biomaterial into scaffolds has emerged and progressed rapidly in hope to achieve such advanced healing.[97-99] Conventional 3D printing processing techniques include chemical components or high temperatures making them unsuitable for incorporation of live cells. Thus, as hydrogels are extensively used for cell encapsulation, 3D printing of hydrogels with more gentle techniques such as piston-driven extrusion have recently been implemented.[100]

Alginate is an ideal candidate for 3D bioprinting due to its innate material properties. An example of a 3D bioprinted alginate scaffold for encapsulating endothelial cells is shown in Figure 1.6. [98] Alginate's rheological properties allow shear-thinning, or a reduction in viscosity under increased shear.[101] This attribute is favorable for 3D printing as a less viscous material requires less stress and pressure to be extruded through a nozzle. Thus, cells encapsulated within alginate are subjected to less stress. Additionally, the formation of crosslinks between alginate G blocks and divalent cations can form a protective barrier for the cells, sheltering them from applied pressure.

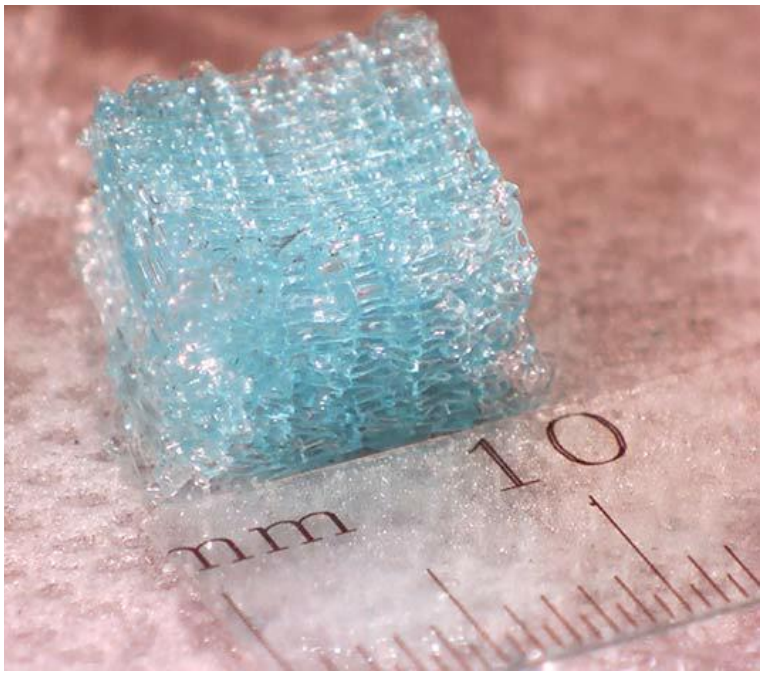

Figure 1.6 3D printed alginate scaffold [98]

1.5 Current shortcomings

Although there are emerging biomaterials and technology capable of treating patients on an individual basis for tissue regeneration, there remains a few limitations present in the field. For example, personalized treatment is less popularly applied to bone tissue regeneration due to the relatively weak structures formed with hydrogel materials. However, injectable hydrogels have the capability of completely filling irregular shapes not achievable by conventional scaffold processing techniques, which result in rigid scaffolds of limited plasticity. Additionally, these rigid scaffolds pose difficulties for uniform cell infiltration via traditional seeding techniques. Similarly, 3D printing methods used to produce scaffolds for bone tissue regeneration have largely focused on producing structures composed of calcium phosphates of high mechanical strength, shown in Figure 1.7.[92] As a result, the feasibility of incorporating of live cells within the biomaterial and printing structures with high cell viability is limited.[102,103] Thus, there is a

need to progress the practice of bone tissue engineering towards a more individualized healing practice, which can be achievable through the use of hydrogels such as alginate.

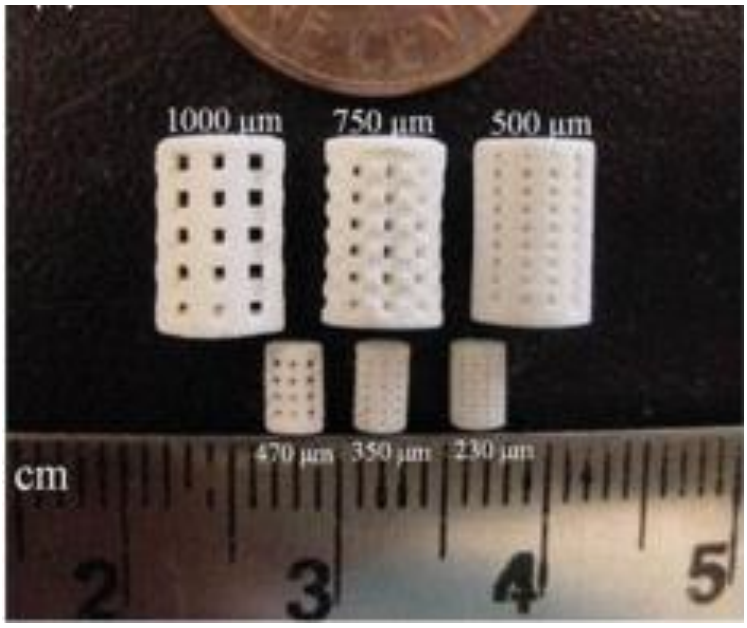

Figure 1.7 3D printed scaffolds for bone tissue engineering [92]

1.6 Research objectives

As previously discussed, hydrogel systems for individualized treatment for enhanced bone tissue regeneration is less commonly explored. However, they have the potential to provide patients with scaffolds of perfectly fitting geometry to heal their specific defects as well as incorporate the patients' own cells within the matrix for the possibility of enhanced, homogeneous regeneration and healing.

Thus, the objective of this research is to develop a novel hydrogel system capable of multiple applications for enhanced, individualized treatment and regeneration of defective bone

tissue. Alginate was chosen as the hydrogel base element due to its biocompatibility, biodegradability, and ability to readily mix with additional components while maintaining its innate gelation properties. An alginate-collagen-hydroxyapatite hydrogel system was developed and the gelation properties were thoroughly investigated. Establishment of control of the gelation kinetics to result in a system suitable for injectable applications was of interest, as it is crucial the hydrogel formulation completely fills a defect and sets in an appropriate amount of time. Collagen was incorporated and hydroxyapatite was formed *in situ*, confirmed through various characterization techniques, resulting in an environment more closely mimicking natural bone and providing elements capable of contributing to enhanced bone regeneration. We next aimed to develop a hydrogel system for 3D bioprinting for scaffolds capable of supporting cell life and enhanced, individualized bone defect regeneration. A systematic investigation based on the previously well-established knowledge of the properties of alginate gelation led to the development of a novel alginate-polyvinyl alcohol-hydroxyapatite system suitable for 3D printing. The printability of various concentrations and combinations of components were studied via 3D printing and rheology to understand rheological properties necessary to allow the hydrogel to be easily extruded and recover upon deposition to create 3D scaffolds of high shape fidelity. As the main goal was to bioprint live cells into the scaffolds with high viability, scaffold degradation properties were investigated to determine if they maintained mechanical stability and had the capacity to support cell life *in vitro*. MC3T3 cells were then incorporated into the alginate system and 3D bioprinted at high viability. *In vitro* evaluations of 3D bioprinted alginate-polyvinyl alcohol-hydroxyapatite scaffolds were then conducted to assess the scaffolds' ability to support cell life and proliferation. A systematic study to increase cell proliferation was conducted, including investigations of the effects of the calcium bath and addition of collagen

gel on proliferation. This shed light on the components necessary to support cell proliferation and led to the development of a novel tri-polymer hydrogel network capable of 3D bioprinting and supporting cell proliferation and potential to support differentiation *in vitro*.

Chapter 2

Synthesis and characterization of a novel injectable alginate–collagen–hydroxyapatite hydrogel for bone tissue regeneration

2.1 Introduction

Bone tissue engineering scaffolds have been researched extensively in hope to find an ideal construct that is biocompatible, biodegradable, promotes bone regeneration and mimics the distinctive properties of natural bone. It is especially important that the composition closely resembles that of bone and the native extracellular matrix in order to promote favorable cell attachment and proliferation. The main components of natural bone found in the human body include inorganic hydroxyapatite nanocrystals and organic collagen fibrils.[11] The first bone tissue engineered scaffolds aimed to mimic the composition of natural bone and possess regeneration capabilities were developed in the form of calcium phosphate ceramic implants.[103,104] Since then, calcium phosphate cements and scaffolds have been constructed in combination with various biopolymers such as polycaprolactone, chitosan and collagen to produce biocompatible composites capable of promoting bone regeneration.[12,13,17,105–107] Specifically, a well known co-precipitation method first developed by Kikuchi *et al.* has been followed to fabricate scaffolds in which hydroxyapatite nanocrystals are nucleated onto collagen fibers that precipitate out of solution.[108] Many variations of this self-assembling method have since been established.[19,109] Recently, our group has developed a novel co-precipitation method involving the nucleation of apatite onto collagen fibers in a modified simulated body fluid (m-SBF).[110,111] These lyophilized scaffolds have been proven to be biocompatible and promote new bone growth.[112]

Despite the early success in the preparation of lyophilized bone tissue engineering scaffolds, they must be surgically implanted into the bone defect of the patient. Thus, researchers have been gravitating towards the development of novel, noninvasive, injectable hydrogel scaffolds for bone tissue engineering. The current most widely used technique is the use of sol–gel polymerization. Sol -gel mechanisms include photopolymerization, thermogelation, concentration dependent chemical reactions and various additional mechanisms.[34,113,114] Photopolymerization techniques involve the radical chain polymerization of a polymer in which an acrylic or methacrylic side group is initiated and polymerized by a photoinitiator (I2959) under UV light.[113] Similarly, many thermogelation techniques involve the monomeric polymerization of polymers with non-degradable backbones, for example pNiPAAm based polymers, which introduces side groups that are potential cytotoxic agents.[115,116] This possibility of cytotoxicity and additional adverse immune responses render these polymer modification processes less biocompatible for injectable hydrogel purposes. Thus, injectable systems without polymeric modification such as ionically crosslinked systems are more suitable.

An extensively researched ionically crosslinked injectable hydrogel system includes the use of the naturally occurring polysaccharide alginate, produced by brown algae such as Macrocystis pyrifera (kelp).[117] Applications in which alginate is used range from food stabilizers in ice cream to biomedical applications such as dental molds, wound dressings, cell immobilization, drug delivery and bone tissue engineered scaffolds.[54,77,118,119] Alginate is a linear co-polymer composed of consecutive blocks of (1–4) linked a-L-guluronate (G-blocks) and b-D-mannuronate (M-blocks) followed by segments of alternating MG blocks.[58] Grant *et al*. first described the formation of an ‘‘egg box structure’’ as a result of the G blocks in the presence of divalent cations such as calcium, barium and strontium. [50] The divalent cations form

intermolecular bonds with two deprotonated carboxylate groups of one G block and with two hydroxyl groups of another.[120] The β- glycolic linkage of the M blocks has a low affinity for divalent cations, resulting in weak interactions. The G blocks are therefore most significant in the crosslinking process.[121] As a result of this crosslinking of lateral egg box multimers, the alginate undergoes a sol–gel transition.[114]

Martinsen *et al*. found that the sol–gel transition occurs instantaneously to form alginate gel microspheres when alginate is added dropwise to a calcium chloride solution.[118] Although this property may be favorable for some applications such as cell immobilization, the fast gelation rate may not be ideal for others, such as injectable purposes.[77] Cho *et al.* proposed the use of $CaSO_4$ as a gelling agent and Na_2HPO_4 as a retardation agent to control the gelation rate of an alginate gel.[55] Controlling the gelation rate allows for homogeneous gel formation and uniform material properties.[38]

Unfortunately, alginate on its own has shown to induce reduced cell attachment in vitro due to its hydrophilic and negatively charged properties as well as poor osteoconductivity.[58] Therefore researchers have expanded to using combinations of alginate with more biocompatible components such as PVA, hydroxyapatite, collagen and chitosan.[55,122–125] Particularly, the combination of alginate, collagen and hydroxyapatite has been extensively researched.[119,87,125,126] Commonly, pre-fabricated, lyophilized collagen-apatite powder is added to an alginate suspension which is then gelled and lyophilized for further characterization. *In vitro* studies have shown that the addition of collagen and hydroxyapatite to the alginate hydrogel provided a favorable environment for osteoblast attachment and proliferation.[87] Thus, the focus of our work in this chapter was to develop a novel combination of an injectable alginate–collagen hydrogel with in situ hydroxyapatite nucleation onto collagen fibers. This combination provides

appropriate mechanical strength as a bone tissue substitute and the components necessary to promote bone regeneration without lyophilization, proving its potential as an injectable regenerative material.

2.2 Materials and methods

2.2.1 Preparation of alginate hydrogels

Alginic acid sodium salt (medium viscosity; MP Biomedicals LLC, USA) was added to 6 mL of deionized water in polystyrene vials (25.9 mL; ID x H: 26 x 51 mm) and mixed with 2 mL of sodium phosphate dibasic anhydrous (Na_2HPO_4, ≥ 99%, Fisher Scientific, USA) solutions at varying concentrations according to Table 2.1. The suspensions then sat for 1 hour at room temperature before 8 mL of calcium sulfate anhydrous ($CaSO_4$, 99%, Alfa Aesar, USA) solutions of varying concentrations were added and mixed for 30 seconds. The gelation time was observed and recorded as defined by the test tube tilting method.[31] Briefly, the vial was tilted 90° every minute after initial mixing and the time at which the meniscus of the suspension no longer moved was designated as the gelation point. As shown in Table 1, the final weight percent of alginate was 1.5% (w/v) while the final weight percentages of Na_2HPO_4 and $CaSO_4$ ranged from 0–0.12% (w/v) and 0.20–0.40% (w/v), respectively. Alginate hydrogels with 0.12% (w/v) P (Na_2HPO_4) and 0.40% (w/v) Ca ($CaSO_4$) were chosen for the addition of pure collagen fibers and mineralized collagen fibers.

After the gelation test, A–P-4, A–P-5 and A–P-9 hydrogels were chosen to proceed with mechanical testing as their gelation times fell in the range of 5–30 minutes, defined as ideal in a surgical setting.[126] The A–Ca-1 hydrogel was selected to act as the control.

Table 2.1: Compositions of A-Ca and A-P hydrogels

Hydrogel	Alginate Final % (w/v)	$CaSO_4$ Final % (w/v)	Na_2HPO_4 Final % (w/v)
A-Ca-1	1.5	0.20	0
A-Ca-2	1.5	0.30	0
A-Ca-3	1.5	0.40	0
A-P-1	1.5	0.20	0.04
A-P-2	1.5	0.30	0.04
A-P-3	1.5	0.40	0.04
A-P-4	1.5	0.20	0.08
A-P-5	1.5	0.30	0.08
A-P-6	1.5	0.40	0.08
A-P-7	1.5	0.20	0.12
A-P-8	1.5	0.30	0.12
A-P-9	1.5	0.40	0.12

2.2.2 Preparation of alginate–collagen (A–C) hydrogels

Type I collagen was extracted from rat tails following a protocol by Rajan *et al.*[127] Briefly, the collagen was extracted and dissolved in 0.02 M acetic acid at 4°C. The pH of the collagen solution was raised to 7 using sodium hydroxide. 30 mL of the collagen solution with a concentration of 4.5 mg/mL was then covered placed in a waterbath at 37 °C for 24 hours at constant stirring using a magnetic stir bar and stir plate. The precipitates were then collected via filtration and rinsed with deionized water. The fibers were then allowed to air dry for 1 hour. A small amount of fibers was air dried overnight and imaged using FESEM to observe the morphology.

Final compositions of the A–C hydrogels can be seen in Table 2.2. Collagen fibers were added at 2.5, 5.0, 10.0 and 20.0% (w/v) to alginate suspensions and mixed until homogeneously distributed throughout the alginate suspensions. Na_2HPO_4 solution was added to the mixture after 20 minutes at 0.12% (w/v) of the final hydrogel. After 1 hour, $CaSO_4$ solution of 0.40%

(w/v) of the final hydrogel volume was added and the gelation time was recorded as previously described.

Table 2.2: Composition of A-C and A-MC hydrogels

Hydrogel	Alginate Final % (w/v)	$CaSO_4$ Final % (w/v)	Na_2HPO_4 Final % (w/v)	Pure Collagen Fiber Final % (w/v)	Mineralized Collagen Fiber Final % (w/v)
A-C-1	1.5	0.40	0.12	2.5	0
A-C-2	1.5	0.40	0.12	5.0	0
A-C-3	1.5	0.40	0.12	10.0	0
A-C-4	1.5	0.40	0.12	20.0	0
A-MC-1a	1.5	0.40	0.12	0	2.5
A-MC-1b	1.5	0.40	0.12	0	5.0
A-MC-2*	1.5	0.40	0.12	0	2.5

*Phosphate solution was added to mineralized collagen suspension before the addition of alginate powder

2.2.3 Preparation of alginate–mineralized collagen (A–MC) hydrogels

Alginate–mineralized collagen (A–MC) hydrogels were composed of alginate, mineralized collagen fibers, Na_2HPO_4 and $CaSO_4$. A–MC hydrogels differed in the order in which the remaining components were added to the mineralized collagen fiber suspension. A–MC-1 hydrogels were prepared by adding alginate powder prior to the phosphate solution addition whereas for A–MC-2 hydrogels, the phosphate solution was added prior to the alginate powder. To prepare mineralized collagen fibers, a solution of modified simulated body fluid (m-SBF) was used as the source to provide calcium and phosphate ions.[13,15] Briefly, SBF is composed of inorganic ions similar to the natural composition of human blood plasma. The modified SBF contains ion concentrations 3 times that of normal SBF to ensure mineralization of

collagen fibers. The first two salts in the m-SBF recipe were dissolved in 20 mL of deionized water. A collagen solution of concentration 4.5 mg/mL was then added to the solution and mixed on ice for 10 minutes. The next 3 salts were added to 10 mL of deionized in order after the complete dissolution of the previous ion. This solution was then added to the collagen solution containing the first two ions, which remained on ice, and mixed for an additional 10 minutes. The sodium bicarbonate was added to the collagen–SBF solution and mixed until completely dissolved. The pH of the solution was raised to 7 using sodium hydroxide. The collagen–SBF solution was then removed from ice and added to a waterbath at 37 °C under moderate stirring for 1.5 hours. The stir bar was then removed and the suspension was aged at 37 °C overnight. After 24 hours, the mineralized collagen fiber precipitates were collected via filtration, rinsed twice with deionized water and allowed to air dry. The fibers were weighed at 2.5 and 5.0% (w/v) of the final hydrogel. The fibers were re-suspended in 6 mL of deionized water under moderate stirring to re-disperse them in the suspension. For A–MC-1 hydrogels, 0.24 g alginate powder was then added to the collagen suspension and mixed to form a homogeneous suspension. 0.12% (w/v) P and 0.40% (w/v) Ca solutions were then added as previously described. The final A–MC-1 hydrogel compositions can be seen in Table 2.2. The gelation time was recorded according to the test tube tilting method as previously described.

To further investigate gelation properties, A–MC-2 hydrogels (2.5% w/v) were prepared. Mineralized collagen fibers, prepared as previously described, were added to deionized water followed by an addition of the phosphate solution at 0.12% (w/v) of the final hydrogel. Alginate powder was then added to the solution at a final concentration of 1.5% (w/v). $CaSO_4$ at 0.40% (w/v) final concentration was added and gelation proceeded as previously described.

2.2.4 Characterization

The morphology of pure collagen fibers and mineralized collagen fibers were observed using field emission scanning electron microscopy (FESEM, JEOL JSM-6335F, Japan) at an accelerating voltage of 5 kV.

Dynamic mechanical analysis (DMA) was completed using a DMA 2980 Dynamic Mechanical Analyzer (TA instrument Inc., New Castle, DE) in compression mode using 40 mm sandwich fixtures. Pre-determined A–Ca (n = 8) and A–P (n = 8) hydrogel samples were sliced to an average thickness of 4.5 mm. The hydrogels were loaded into the DMA, ramped to 37 °C and held isothermally for 5 minutes. A preload force of 0.01 N was applied, followed by a force ramped up to 18 N at a uniform stress rate of 0.5 N per minute. The compressive modulus was determined from the slope of the initial 20% linear elastic region of the obtained stress–strain curve. The same procedure was implemented for A–C (n = 5), A–MC-1 (n = 5) and A–MC-2 (n = 5) hydrogels.

After DMA testing, remaining hydrogel slices were frozen at -25 °C and lyophilized using a freeze-dryer (Free Zones, Labconco, USA). The freeze-dried hydrogels of selected compositions, as listed in Table 2.3, were subjected to a series of evaluations, including thermogravimetric analysis (TGA), X-ray diffraction (XRD), and Fourier transform infrared spectroscopy (FTIR).

Table 2.3: Compositions of selected hydrogels for characterization of inorganic content

Hydrogel	Alginate % (w/v)	$CaSO_4$ % (w/v)	Na_2HPO_4 % (w/v)	Collagen Fibers % (w/v)	Mineralized Collagen Fibers % (w/v)
A-Ca-1: Alginate-CaSO4	1.5	0.20	0	0	0
A-P-9: Alginate-Phosphate	1.5	0.40	0.12	0	0
A-C: Alginate-Collagen	1.5	0.40	0.12	2.5	0
A-MC-1: Alginate-Mineralized Collagen	1.5	0.40	0.12	0	2.5
A-MC-2: Alginate-Mineralized Collagen	1.5	0.40	0.12	0	2.5

TGA was conducted using a TG analyzer (TGA-1000, Rheometric Scientific, UK) to determine the weight percentage of the inorganic components present in the hydrogels. The freeze-dried hydrogels were loaded into the TG analyzer at an average weight of 20 mg. The weight loss profile was recorded from 25 °C to 900 °C in air at a rate of 10 °C per minute and the weight percent residue was determined. X-ray diffraction (XRD, Bruker AXS D5005) was performed on the freeze-dried hydrogels to determine the composition of the inorganic components present in the hydrogels. Scans were collected over a 2θ range of 10-50° at a step size of 0.02° and a scan rate of 0.2° per minute with Cu Kα radiation (k = 1.54056 nm). FTIR was used to determine the functional groups present in the alginate hydrogels. FTIR spectra were obtained with a Nicolet Magna-IR 560 Spectrometer and a Specac-Onest Single Bounce Diamond ATR Accessory. A small slice of the freeze-dried hydrogel was placed over the diamond and compressed until sufficient contact was made. The spectra were recorded using 32 scans over the range of 400 to 4000 cm^{-1} using OMNIAC software.

2.2.5 Statistical analysis

Results were statistically analyzed using one or two-way analysis of variance (ANOVA) and expressed as mean ± standard deviation. Statistical significance was defined as $p < 0.05$.

2.3 Results

2.3.1 Gelation time

The solution and gel states of alginate are shown in Fig. 2.1.

Figure 2.1: Alginate suspension (left) and gel (right) states

Average gelation times of alginate hydrogels with varying $CaSO_4$ and Na_2HPO_4 concentrations are shown in Fig. 2.2. Within groups A–P-1-3 (0.04% (w/v) Na_2HPO_4) and A–P-7–9 (0.12% (w/v) Na_2HPO_4), an increase in calcium concentrations resulted in a decrease in gelation time. The slight increase in gelation times seen in groups A–Ca-1–3 (0% (w/v) Na_2HPO_4) and A–P-4–6 (0.08% (w/v) Na_2HPO_4) was not statistically significant. Comparing gelation times of alginates

composed of the same calcium concentrations displayed an increase in gelation time with increasing Na_2HPO_4 concentration. Variations from this increase in gelation time were not statistically significant. The control group exhibited variation from the expected increase in gelation time due to the instantaneous, inhomogeneous gelation of the alginate chains and hindered diffusion of calcium ions throughout the suspension. The differences in average gelation times of the selected, starred hydrogels were not statistically significant from the control.

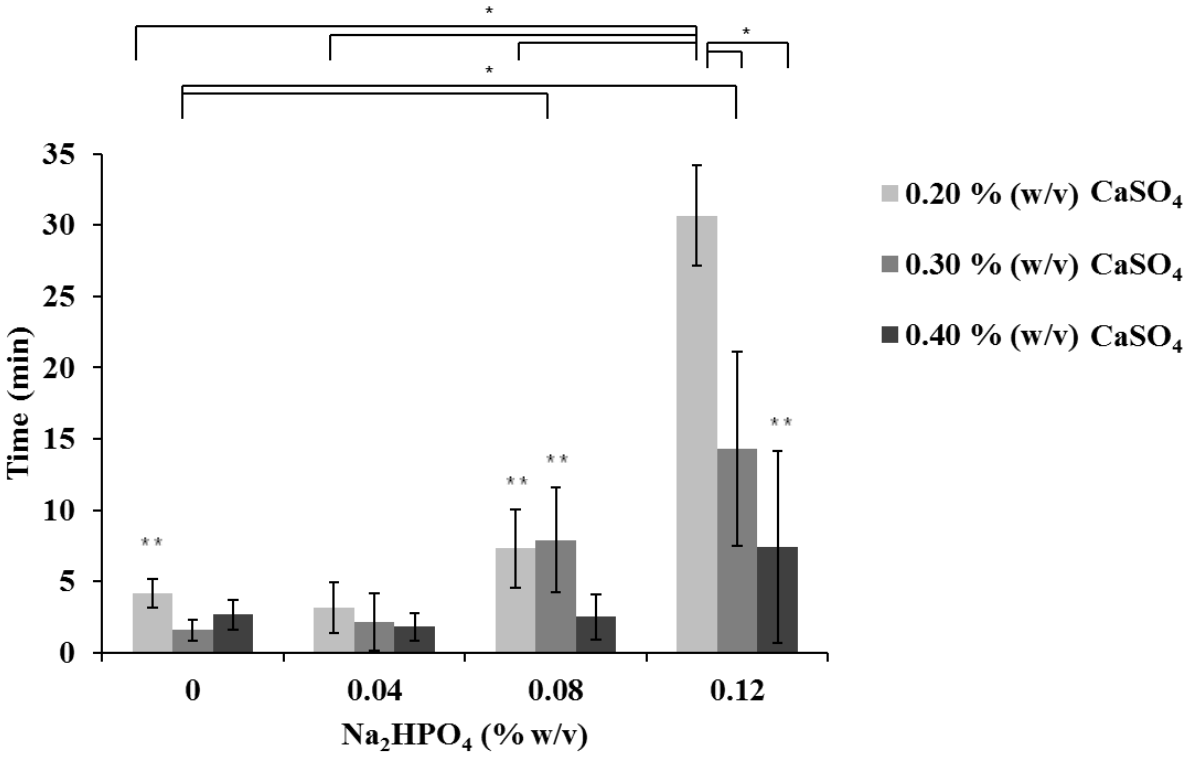

Figure 2.2: Average gelation times of alginate hydrogels with varying Na_2HPO_4 and $CaSO_4$ concentrations. *Statistically significant from each other ($p < 0.05$, ANOVA), ** selected compositions for mechanical testing

Fig. 2.3a displays a FESEM image of pure collagen fibers added to the alginate hydrogels. The collagen fibers are about 200 nm in width and on the order of micrometers in length. Debanding patterns characteristic of collagen fibers are observed. Fig. 2.3b shows a FESEM image of mineralized collagen fibers in which apatite particles are deposited along the collagen fibers.

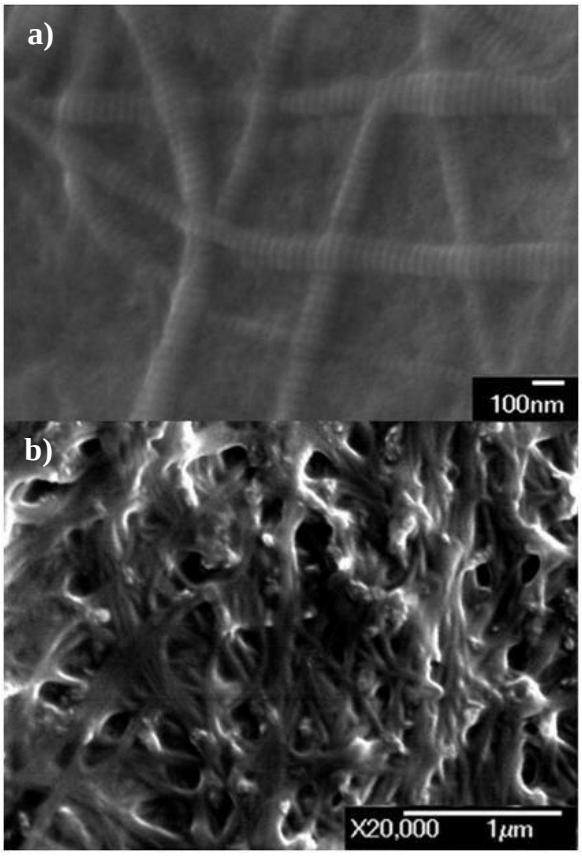

Figure 2.3: FESEM images of air dried a) pure collagen fibers and b) mineralized collagen fibers

The average gelation times of alginate hydrogels with varying weight percentages of pure collagen fibers and mineralized fibers are shown in Fig. 2.4. The addition of pure collagen fibers at all percentages did not significantly impact the gelation times of the hydrogels when compared to the control. The addition of alginate directly following the mineralized fibers (A–MC-1 hydrogels) resulted in a decrease in average gelation times yet differences are not statistically significant from the control. However, the average gelation times of A–MC-1 hydrogels (2.5% w/v and 5% w/v) did display a statistically significant decrease compared to A–C-1 hydrogels (2.5% (w/v) pure collagen fibers). When the order of the phosphate addition was modified to be before the alginate (A–MC-2), the gelation time was not significantly different from the control and was slower than those of A–MC-1 hydrogels. A statistically significant difference in gelation time was observed between 5% (w/v) A–MC-1b and 2.5% (w/v) A–MC-2 hydrogels.

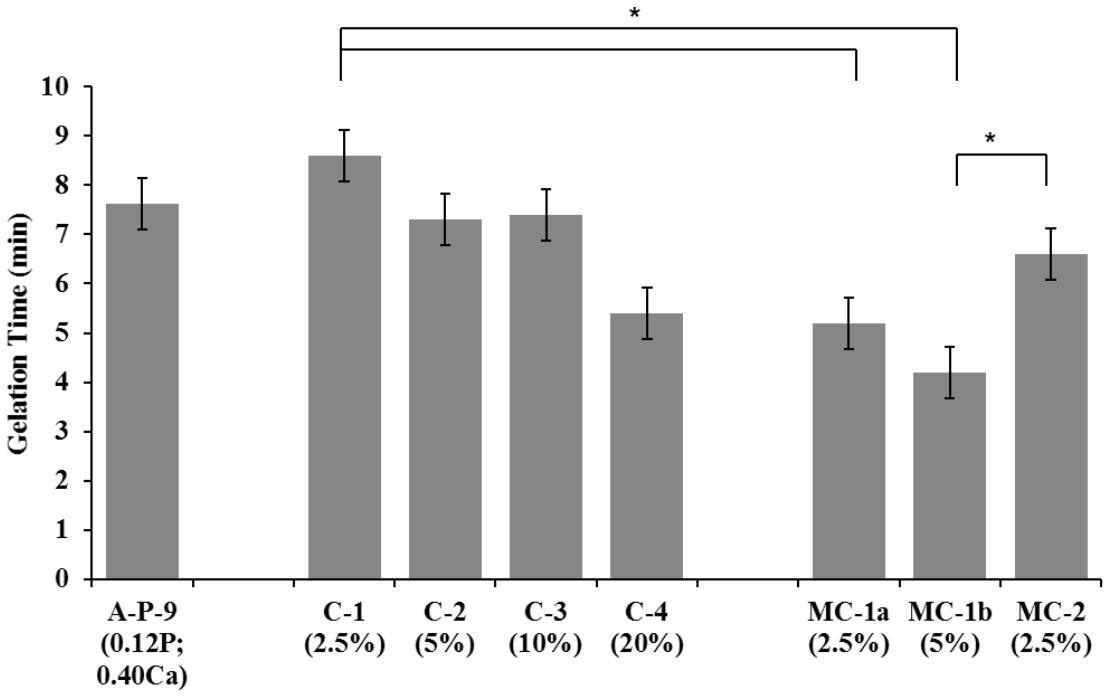

Figure 2.4: Gelation times of alginate hydrogels with varying pure collagen (C) or mineralized collagen (MC) fiber content. *Statistically significant from each other ($p < 0.05$, ANOVA)

2.3.2 Dynamic mechanical analysis

The average compressive moduli of alginate hydrogels of varying phosphate and calcium concentrations are shown in Fig. 2.5. A–Ca-1 hydrogels (0 % (w/v) Na_2HPO_4; 0.20% (w/v) $CaSO_4$) displayed an average compressive modulus of 1.6 kPa. An increase to 0.08% (w/v) P and 0.20% (w/v) Ca increased the average modulus to 2.3 kPa. The addition of 0.08% (w/v) P and 0.30% (w/v) Ca increased the average modulus to 3.2 kPa. The average compressive modulus peaked at a value of 5.1 kPa for alginate hydrogels of 0.12% Na_2HPO_4 and 0.40% $CaSO_4$, which was significantly higher than the other hydrogels.

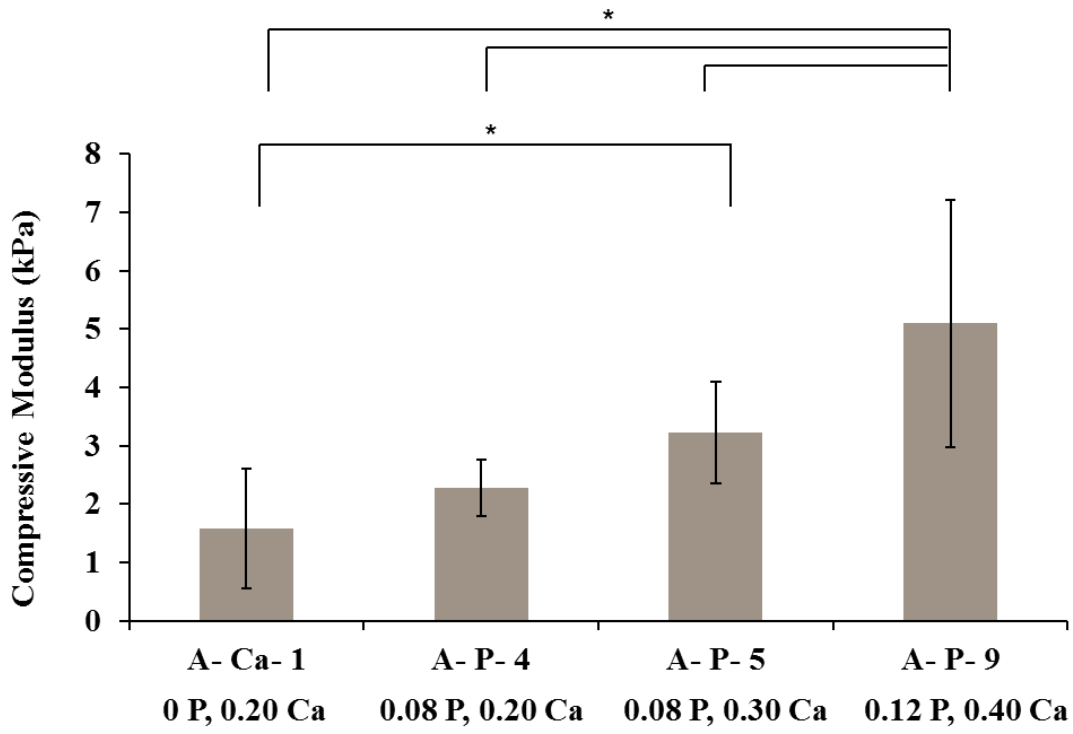

Figure 2.5: Compressive moduli of alginate hydrogels of varying Na_2HPO_4 and $CaSO_4$ content. *Statistically significant from each other ($p < 0.05$, ANOVA)

The average compression moduli of A–C and A–MC hydrogels are shown in Fig. 2.6. As a result of the addition of pure collagen fibers at 2.5, 5 and 10% (w/v) to alginate hydrogels composed of 0.12% P and 0.40% Ca, the compressive moduli of these hydrogels increased significantly. The average compressive modulus peaked at a value of 7.5 kPa for A–C-1 (2.5% (w/v)) hydrogels. The addition of alginate immediately after the mineralized collagen fibers (A–MC-1) did not result in statistically significant differences in compressive moduli compared to the control. The modulus of the A–MC-1a (2.5% (w/v)) hydrogels (6.6 kPa) was significantly lower than that of A–C-2 (5% (w/v)) hydrogels. The modulus of the A–MC-1b hydrogels (5.9 kPa) was significantly lower than that of both the A–C-1 and A–C-2 hydrogels. When the phosphate solution was added before the alginate (A–MC-2), the modulus reached the maximum of 8.0 kPa. This increased value was statistically significantly different from the original A–MC hydrogels (A–MC-1a and A–MC-1b) and the control.

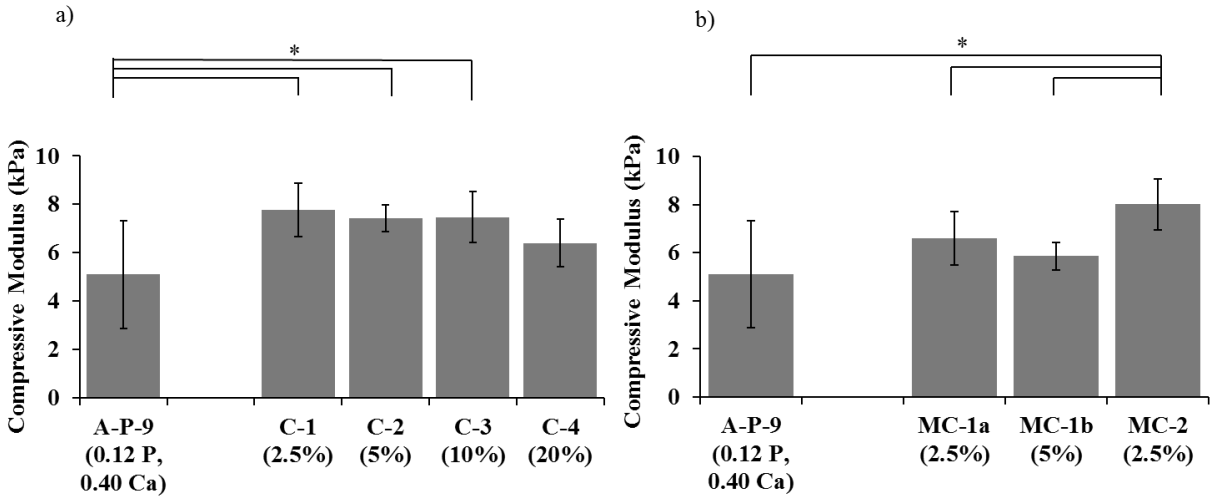

Figure 2.6: Compressive moduli of various (a) A–C and (b) A–MC hydrogels. *Statistically significant from each other ($p < 0.05$, ANOVA)

2.3.3 Thermogravimetric analysis

The TGA profiles for alginate hydrogels of various compositions can be seen in Fig. 2.7. Decomposition of the alginate hydrogels begins around 26 °C with the loss of water, followed by the rupture of the alginate chains and monomers around 190 °C and 620 °C. The residue includes elements that decompose above 900 °C. The average percent residue for A–Ca-1, A–P 9, A–C-1, A–MC-1a (2.5% w/v) and A–MC-2 (2.5% w/v) hydrogels was determined to be 26.8%, 33.0%, 32.8%, 31.4% and 35.0%, respectively. The increase in percent residue with the addition of phosphate, collagen fibers or mineralized collagen fibers to the control (A–Ca hydrogel) was statistically significant for all samples. The addition of pure collagen fibers (A–C) or mineralized collagen fibers (A–MC-1) did not result in a statistically significant increase in the percent residue compared to the alginate phosphate hydrogel (A–P-9), nor were they statistically significant from each other. The altered order of the addition of the phosphate solution (A–MC-2) resulted in an increase in residue that was statistically significant from the A–Ca-1, A–C-1 and A–MC-1a hydrogels.

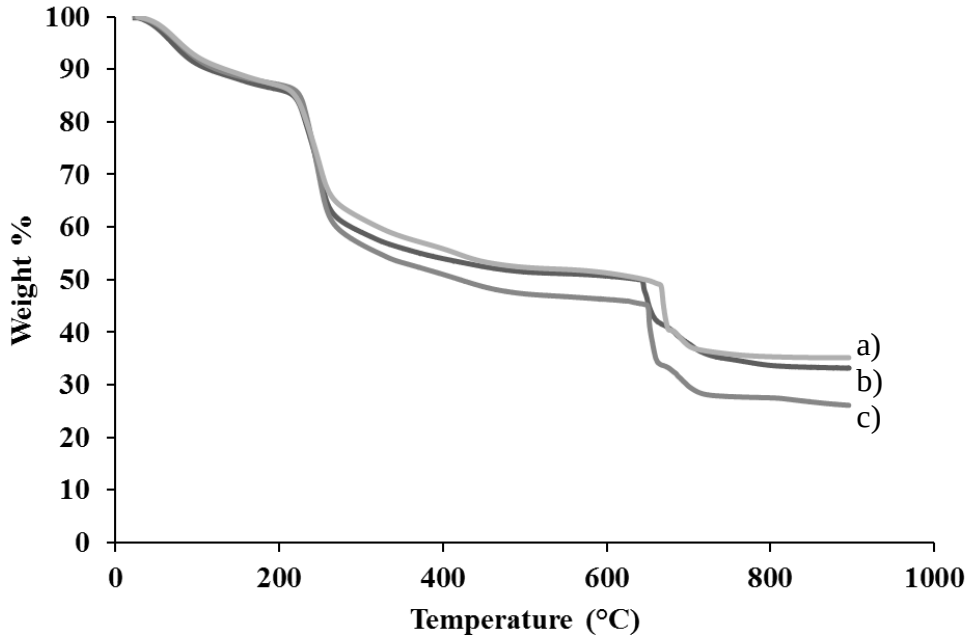

Figure 2.7: TGA curves of alginate hydrogels containing (a) A–MC-2, (b) A–P-9 (0.40% Ca–0.12% P) and (c) A–Ca-1 (0.20% Ca–0% P)

2.3.4 X-ray diffraction

Fig. 2.8 shows X-ray diffraction patterns of A–Ca-1, A–P-9, A–C-1, A–MC-1a and A–MC-2 hydrogels. The A–Ca spectrum depicts characteristic peaks of sodium calcium sulfate hydrate, sodium sulfate and calcium sulfate. The addition of phosphate to the A–Ca hydrogel results in additional peaks of sodium hydrogen phosphate and calcium phosphate carbonate. The addition of pure collagen fibers to the A–P hydrogels (A–C hydrogels) exhibits peaks characteristic of carbonate apatite around 29° and 32°. The A–MC-1a hydrogel with mineralized collagen fibers spectrum displays a greater amount of peaks characteristic of carbonate-hydroxyapatite around 25° and 29° and calcium phosphate carbonate around 19°, 23°, 34° and 38°. The A–MC-2 spectrum displays peaks at the same positions as the A–MC-1a spectrum but

with increased broadening. Peak broadening and shifting amongst spectra may be attributed to the overlapping of peaks of the various components of the hydrogels.

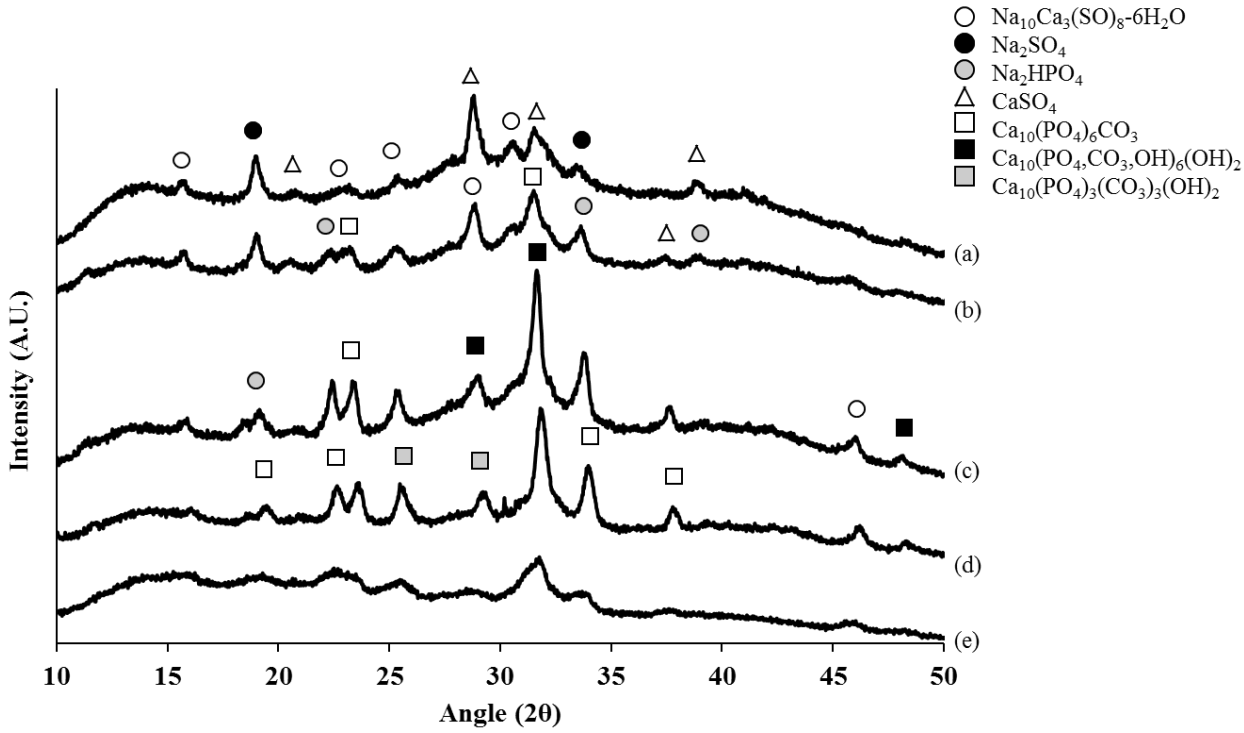

Figure 2.8: XRD patterns of (a) A–Ca-1, (b) A–P-9, (c) A–C-1, (d) A–MC-1a and (e) A–MC-2 hydrogels

2.3.5 Fourier transform infrared spectroscopy

The FTIR spectra of A–Ca-1 (0.20% Ca), A–P-9 (0.40% Ca–0.12% P), A–C-1 (2.5% pure collagen fibers), A–MC-1a (2.5% mineralized collagen fibers) and A–MC-2 (2.5% mineralized collagen fibers) hydrogels are shown in Fig. 2.9. The alginate alone spectrum displays characteristic alginate bands denoting asymmetric and symmetric stretching of $–COO^{-1}$ modes, found at 1595 cm^{-1} and 1410 cm^{-1}, respectively. C–O stretching vibration modes occur at

1080 cm^{-1}; and hydroxyl stretching bands at 3294 cm^{-1}. Bending of the OH group of the carboxyl is depicted at 889 cm^{-1}. With the addition of phosphate, a shift of the $–COO^-$ bands to higher wavelengths is observed. Bending and stretching of the phosphate modes are observed at 611 cm^{-1} and 997 cm^{-1}, respectively. The addition of pure collagen fibers and mineralized collagen fibers also results in a shift of the carboxyl absorption bands to higher wavelengths. Amide absorption bands of the collagen fibers characteristic of C=O and O–H stretching, N–H stretching and C–N stretching can be found at 1670 cm^{-1} and 1630 cm^{-1}, 1550 cm^{-1}, and 1200 cm^{-1}, respectively. Stretching of the PO_4^{3-} groups of the in situ formed apatite is located at 1200–965 cm^{-1} and 600–500 cm^{-1}. All of these signature peaks of collagen overlap with characteristic peaks of the A–Ca and A–P hydrogel systems.

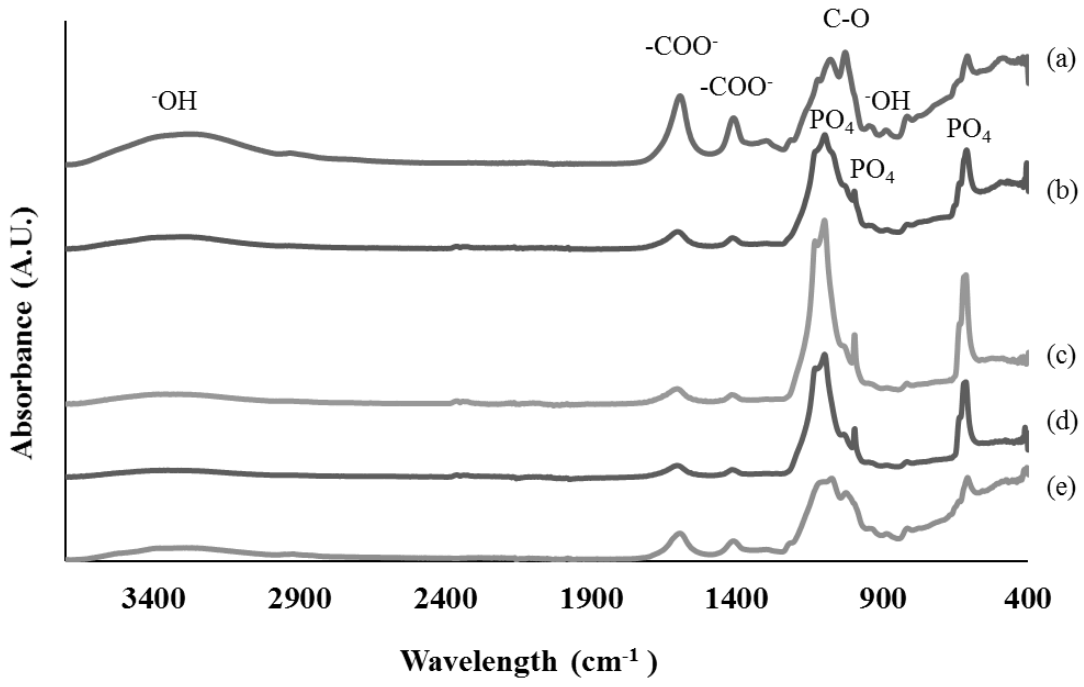

Figure 2.9: FTIR spectra of (a) A–Ca-1, (b) A–P-9, (c) A–C-1, (d) A–MC-1a and (e) A–MC-2 hydrogels

2.4. Discussion

2.4.1 Gelation time and mechanical properties

The ability to tailor the gelation time and strength of alginate hydrogels as desired is one of the greatest incentives for using alginate in a variety of applications. For injectable hydrogels used in bone tissue engineering, it is ideal that the composition can be adjusted so that the gelation rate is slow enough to allow surgical handling yet fast enough for the hydrogel to achieve *in vivo* stability and functionality soon after injection. The optimal gelation time range has been defined as 5–30 minutes.[126]

The variation in gelation time among the alginate hydrogels with different concentrations of sodium phosphate and calcium sulfate exhibits a strong trend as the time increases with an increase in phosphate concentration and decreases with an increase in calcium concentration, as seen in Fig. 2.2. The control hydrogels gelled immediately in various regions as the calcium sulfate solution was added without the presence of sodium phosphate. This resulted in inhomogeneous hydrogels. It was difficult for the remaining calcium to diffuse through the immediately gelled sections to reach the unreacted alginate, increasing the time for complete gelation of the whole suspension.[38] Kuo *et al*. suggested that the use of a calcium source with lower solubility in water allows for a more gradual gelation rate and thereby results in a more homogeneous gel. This is because that as the calcium particles are less readily released into the solution, they disperse more evenly throughout the medium over time before massive gelation occurs.

Thus, Cho *et al.* proposed the use of a gelling agent with intermediate solubility, $CaSO_4$, and a retardation agent, Na_2HPO_4, to control the gelation rate of an alginate hydrogel.[55] The mechanism by which Na_2HPO_4 slows down the gelation of alginate is through a chemical

reaction with $CaSO_4$, resulting in the formation of calcium phosphate. Due to the sparing solubility of $CaSO_4$, calcium ions are made available in solution over time. As the calcium is released through the suspension as ions, a high concentration of phosphate ions will quickly react with them to form calcium phosphate precipitates. This precipitation leaves less calcium available in solution for the immediate gelation of alginate. During this period, the rest of the $CaSO_4$ has more time to disperse throughout the alginate suspension. Thus, once all of the phosphate ions have precipitated with calcium ions, the calcium is then made available to crosslink the alginate G blocks via formation of the egg box structure uniformly throughout the suspension. Therefore, the order of stability of calcium in the composite and thus order of formation can be inferred to be calcium phosphate as the most stable, followed by calcium alginate and finally calcium sulfate.[126] The precipitation mechanism is an advantageous addition to the system to help control the gelation rate but the solubility of the calcium source plays a more dominate role. If a retardation agent is used with a highly soluble source, inhomogeneous gelation would still occur because the calcium ions would not be evenly distributed throughout the suspension. Only a combination of the two approaches can result in the greatest control of the gelation rate of the alginate as well as the homogeneity of the resulting hydrogel.

Our data shows that the rate of gelation does in fact decrease with increasing phosphate and decreasing calcium concentrations (and vice versa) for an unchanged concentration of alginate, corroborating previous studies.[55,126] An increase in calcium concentration at a constant concentration of phosphate decreases the gelation time as more calcium ions are made available to participate in the crosslinking with the G blocks of the alginate. This also results in an increase in the ultimate hydrogel strength.[118] A lower phosphate concentration will allow the sol–gel transition to occur more rapidly as the calcium phosphate precipitation will be completed more

quickly. The result is a decrease in the homogeneity of the hydrogel and thus its mechanical properties.[126] This was also confirmed by our data as the inhomogeneous controls (without phosphate) exhibited the lowest compressive moduli.

Although the reported compressive moduli of the alginate hydrogels are relatively weak, the results are within the same order of magnitude (kPa) as those of alginate hydrogels reported previously.[38,57,126,128] A–P-9 hydrogels (0.40 (w/v%) Ca–0.12 (w/v%) P) exhibited the greatest compressive modulus among tested hydrogels of various calcium and phosphate compositions. This can be attributed to a greater number of alginate–calcium bonds formed at a higher calcium concentration. As previously mentioned, the highest phosphate concentration postponed the gelation process via precipitation with calcium ions. This allowed for controlled diffusion of the remaining calcium throughout the alginate before the ions contributed to gelation, which resulted in uniform hydrogels.

The addition of various weight percentages of pure collagen fibers did not significantly affect the gelation time of the alginate hydrogels. Also, the differences in time were not statistically significant from that of the control. However, the compressive moduli of the hydrogels with 2.5, 5 and 10 weight percent pure collagen fibers did significantly increase compared to the control (A–P-9). This can be attributed to the composite rule of mixtures which explains that the mechanical strength of a composite is in between those of the continuous, matrix phase and reinforcement phase.[129] As the compressive modulus of collagen fibers is greater than that of alginate, it is reasonable that the average compressive modulus of A–C hydrogels is greater than that of A–P hydrogels.

Fig. 2.4 shows that the average gelation times of A–MC-1a and A–MC-1b hydrogels with 2.5% (w/v) and 5% (w/v) mineralized collagen fibers, respectively, were shorter than that of the

control and the differences in times were statistically significant. The average gelation times were also significantly shorter than that of hydrogels with 2.5% (w/v) pure collagen fibers. This eludes to the fact that the mineralized fibers have an impact on the gelation rate of the alginate hydrogels.

Kikuchi *et al*. explain that the in situ formation of hydroxyapatite onto collagen fibers is initiated by the nucleation of calcium ions onto the carboxyl groups of the collagen fibers.[108,109] The calcium ions then bind to the phosphate ions added to the collagen solution, forming hydroxyapatite. This in situ nucleation process has been adapted in our m-SBF method to form apatite onto our collagen fibers (mineralized collagen fibers) before alginate addition. The particles deposited onto the collagen fibers are apparent in Fig. 2.3. This apatite precipitation technique has been extensively researched in our lab and hydroxyapatite formation onto collagen hydrogel fibers has been confirmed using various characterization analyses in previous studies.[111,112] Tampieri *et al.* have indicated that apatite particles could provide calcium ions capable of crosslinking alginate chains.[125] Lu *et al.* also suggested that in situ, calcium ions are released from apatite particles to aid in alginate gelation.[128] Thus, it is hypothesized that the apatite nucleated onto our collagen fibers can also release calcium ions into solution. The released calcium is then available to bind to the deprotonated carboxyl groups of the alginate chains, resulting in premature partial crosslinking. In other words, the crosslinking of alginate G blocks occurred before the addition of $CaSO_4$. The proposed process is depicted in Fig. 2.10.

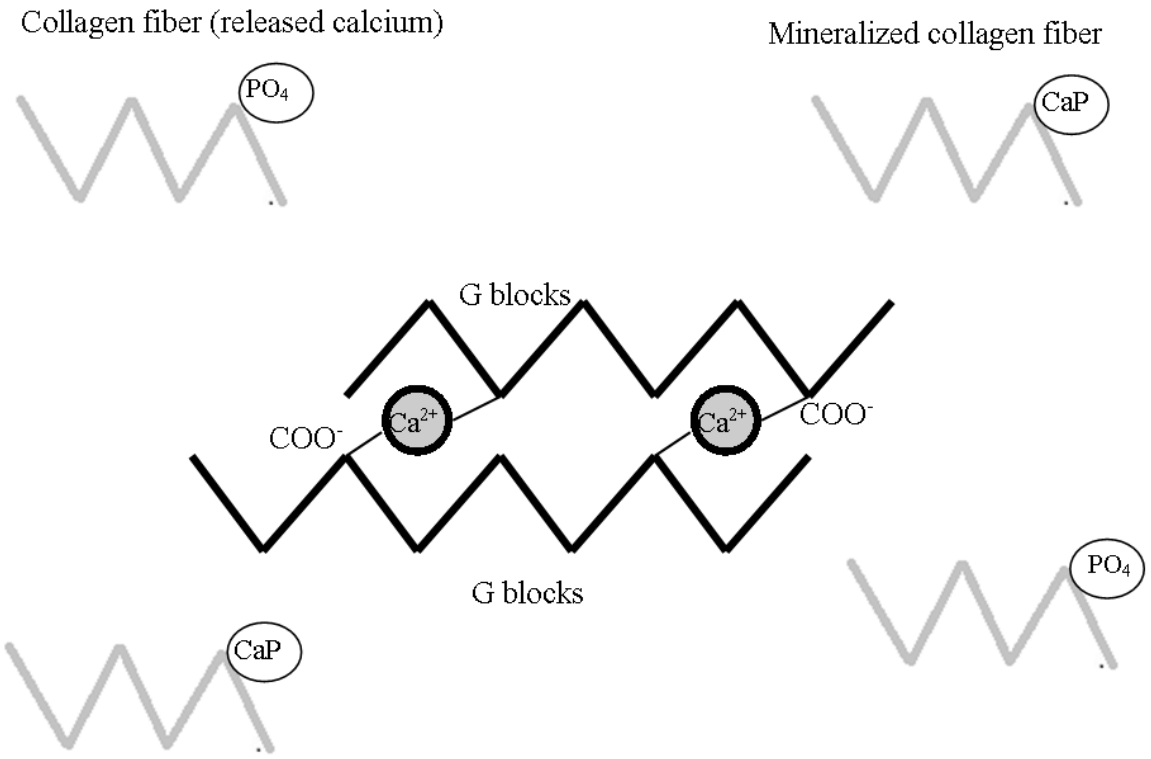

Figure 2.10: Schematic of the hypothesized "pre-mature" alginate crosslinking mechanism

The proposed partial crosslinking of alginate chains before the addition of $CaSO_4$ is supported by the observed increase in viscosity and gelation rate of the alginate suspension with mineralized collagen fibers (A–MC-1) when compared to the pure alginate suspension. This also provides an explanation as to why the addition of pure collagen fibers to the alginate suspension resulted in a significant increase in compressive modulus while the addition of mineralized collagen fibers in A–MC-1 hydrogels did not. Because the pure collagen fibers are not hindering the binding of the G blocks to the calcium, they are able to serve as reinforcements.

To further investigate the hypothesis that premature alginate crosslinking occurred, the order in which the constituents were added to form the hydrogel was modified so that the phosphate solution was added before the alginate powder (A–MC-2). Thus, any calcium released from the mineralized collagen fibers would precipitate with the phosphate ions to form calcium

phosphate, which would prevent premature partial gelation of the alginate. This is supported by our experimental data as an increase in gelation time of the A–MC-2 hydrogels compared to that of A–MC-1 hydrogels was observed. Therefore, the calcium ions had more time to disperse throughout the suspension before gelation occurred, resulting in a more controlled, uniform gelation process. As previously explained, hydrogels with more homogeneous material properties demonstrate higher mechanical properties than inhomogeneous hydrogels. This was exhibited by the A–MC-2 hydrogels which had the strongest compressive modulus out of all of the hydrogel samples studied. It is proposed that this is because the G block-calcium crosslinks were no longer disrupted by the mineralized collagen fibers and the fibers were able to serve as reinforcements in the alginate matrix.

The order in which the phosphate is added to the system plays a crucial role in the resulting material properties. By modifying the order of phosphate addition, the 2.5 % (w/v) A–MC-2 demonstrates the highest compressive modulus and appropriate gelation time. As such, it was identified as the most promising candidate as an injectable hydrogel for bone tissue engineering. The A–MC-2 gelation time is within the time defined as an ‘‘ideal surgical time’’ of 5–30 minutes and its compressive modulus is deemed sufficient for the proposed non-load bearing applications. These may include maxillofacial reconstruction or reinforcement purposes such as filling bone micro-fractures or osteoporotic bone to simply increase the rate of healing.[106,113,130,131] Injection of the hydrogel into areas of weakened bone may help restore bone density by promoting bone growth. New bone formation induced by the hydrogel will enhance the mechanical strength of the area and hopefully prevent further bone breakage and weakening. Additionally, the compressive modulus of the hydrogel has the potential to be increased even further with an increase in calcium concentration, resulting in an increase in alginate-calcium

crosslinks. The compressive modulus would increase as long as the calcium is released slowly and a homogeneous hydrogel is produced. Furthermore, because the biocompatibility of the alginate hydrogel should increase substantially with the presence of mineralized collagen fibers, it is a worthwhile addition to the system.

2.4.2 Characterization of hydrogel inorganic composition

Thermogravimetric analysis (TGA) of the hydrogel samples after heating to 900 °C removed all of the organic components from the sample, leaving behind the inorganic residue. In this case, the inorganic components are calcium phosphate phases and sulfate salts, proven by XRD and FTIR analyses. The addition of phosphate to A–Ca hydrogels resulted in a statistically significant increase in weight percent residue. The addition of pure collagen to the A–P hydrogels did not significantly affect the weight percent residue after 900 °C as the same amount of salts are present in the composition of both A–P and A–C hydrogels. The percent residue also does not significantly change with the addition of mineralized collagen fibers (A–MC-1) to the A–P hydrogels. However, when phosphate was added before alginate to prevent premature gelation (A–MC-2), a significant increase in percent residue was observed. This could be attributed to the fact that an increase in calcium ions took part in the formation of calcium phosphates in A–MC-2 compared to that of the A–MC-1 hydrogels. In the A–MC-1 hydrogels, a high concentration of calcium released from mineralized collagen fibers may have accumulated in local areas, contributing to early gelation and formation of less homogeneous hydrogels. In contrast, the calcium ions released from mineralized collagen fibers in A–MC-2 reacted with phosphate pre-added to the solution, which effectively prevented pre-mature gelation. As a result, an increase in inorganic residue was observed. Thus, only remaining calcium ions from

$CaSO_4$ contributed to organic crosslinks with the alginate chains, forming a homogeneous hydrogel.

XRD spectra show the change in composition of the alginate hydrogels as the result of the addition of phosphate, pure collagen and mineralized collagen fibers. The peaks of each hydrogel are relatively broad, indicating poorly crystalline samples. A slight shift in peaks may be present in the A–C and A–MC spectra due to the addition of calcium phosphate phases. In the A–C hydrogels, phosphate has the capability of nucleating onto the collagen fibers and precipitating with calcium ions to form calcium phosphate. A–MC hydrogels have apatite present on the collagen fibers to begin with. The interaction between alginate and calcium phosphate may result in compression of the polymer matrix, leading to peak to shifts.[132] Pure hydroxyapatite exhibits characteristic peaks of the (211), (300) and (202) planes as three separate, sharp peaks.[133] These peaks are overlapped into a broad peak in the A–MC spectra. This broadness of the apatite peaks can be attributed to the in situ formation of apatite, suggesting that hydroxyapatite is nano-sized and of low crystallinity.[132,134] An increase in peak broadening is observed in the A–MC-2 spectrum due to the increase in the nano-sized inorganic components in the hydrogel. However, these characteristics closely resemble that of natural bone, making this composition suitable as a bone substitute.[105]

FTIR spectra of the various alginate hydrogels show that the main alginate carboxyl absorption bands are present in each sample yet are not in the same exact location for each type of hydrogel. The addition of phosphate to A–Ca hydrogels results in the shifting of these bands at 1595 cm^{-1} and 1410 cm^{-1} to higher wavelengths, also known as a blue shift. This suggests an interaction between the alginate and the calcium phosphate formed. The shifts in the PO_4^{3-} group bending and O–H stretching bands also confirm the interaction.[122] A shift to higher wave

numbers is also seen after the addition of pure collagen fibers. When comparing A–C and A–MC hydrogels, a shift to a slightly lower wave number, or red shift, is seen in most absorbance bands. As Teng *et al.* explained, this is indicative of an interaction between organic and inorganic phases in the sample, supporting the idea that the in situ formed apatite crystals are in fact bonding with the collagen and alginate components.[132]

2.5 Conclusions

In the work in this chapter, a novel, biocompatible injectable hydrogel for bone tissue regeneration has been developed. The gelation time has been optimized so that the injectability of the system is appropriate in a surgical setting, rendering a less invasive method for bone repair compared to implantation of bone tissue engineered scaffolds. Utilizing our in situ collagen fiber mineralization method, we were able to produce an alginate hydrogel comprised of collagen and apatite, the two main components of natural bone, which was proven via numerous material characterization techniques. Thus, this injectable hydrogel system contains the components necessary to promote new bone growth and can be a promising biomaterial for bone repair and regeneration.

Chapter 3

Development of a novel alginate-polyvinyl alcohol-hydroxyapatite hydrogel for 3D bioprinting bone tissue engineered scaffolds

3.1. Introduction

The practice of personalized medicine has recently shaped the progression of leading research and innovative technology in all areas of tissue engineering. Specifically, the technique of additive manufacturing and three-dimensional (3D) printing technology originally used in metal processing has been applied to meet the needs of patient-specific treatment in biomedical engineering and tissue regeneration.[92,135,136] In a clinical setting, a patient's CT scan or MRI can be used to re-construct a repaired CAD model of a damaged tissue or organ, which can then be 3D printed within 24 hours.[95] Thus, a patient can receive an individualized, biocompatible tissue with precise size and geometry in a timely fashion, alleviating reliance on organs for transplantation which are sparsely available.[137] Using this method, tissue substitutes can be printed layer by layer to create constructs capable of promoting new tissue growth once placed *in vivo*. 3D printing of various tissues and organs for regeneration, including osteochondral, bone, skin, liver and heart valves have all been achieved in the laboratory.[100,138-140] Additionally, live cells have been successfully incorporated into hydrogel materials prior to printing and supported by the 3D printed scaffold, in hope to enhance tissue regeneration.[99,141-143]

As bone is a hard tissue commonly fractured in various manners resulting in irregularly shaped defects, the implementation of 3D printing to precisely fill these defects is of popular interest. Common 3D printing approaches for bone tissue regeneration include powder bed fusion and binder jetting of a ceramic particles, such as calcium phosphate phases, in hope to

achieve scaffolds with composition and mechanical properties similar to those of natural bone.[102,144] These processes require the use of lasers or sintering, respectively, to selectively bind particles. Although these scaffolds are often biocompatible and may promote cell proliferation *in vitro*, these common processing techniques are not suitable for bioprinting, or incorporation of cells throughout the material and subsequent printing of scaffolds with uniform cell distribution.[103] Thus, bone tissue regeneration of the defect site treated with such scaffolds most often relies on uniform cell seeding and subsequent migration throughout the scaffold. These processes may be difficult if the 3D printed scaffold design is intricate; posing barriers for cells to pass by during seeding or migrate through to form a network. If cells are unable to distribute uniformly throughout the scaffold, the defect may suffer from incomplete healing.[102] Similarly, 3D printing synthetic polymers, such as PCL and PLA, have been frequently investigated for bone tissue engineering purposes due to their exceptional printability but the high processing temperature necessary for extrusion results in limited capability for cell encapsulation.[145,146] Thus, natural biopolymer hydrogels, such as alginate and chitosan, have been recently implemented for 3D bioprinting due to their inherent biocompatibility, high water content, and molecular structure similar to that of the natural extracellular matrix.[126,147] This renders them easily biodegradable and favorable for cell incorporation and migration.[148] Additionally, under the right processing conditions, these biopolymers have the capacity to possess optimal printability, or rheological properties that allow it to be extruded through a thin nozzle and maintain a stable printed 3D structure once deposited. The selection of a hydrogel material with both printability and biocompatibility is crucial to the success of the 3D printed scaffold applied both *in vitro* and *in vivo*.[97,149]

A widely investigated hydrogel is alginate, a natural polysaccharide derived from algae. Its co-polymer structure is composed of consecutive units of α-L-guluronate (G-blocks) and, β-D-mannuronate (M-blocks) followed by alternating MG segments.[58] Alginate is unique in that it undergoes a sol-gel transition in the presence of divalent cations such as calcium, forming an "egg box" structure.[50] Precise control over the gelation process presents alginate with ideal properties as an optimal candidate for a biomaterial used in 3D printing.[150] Moreover, alginate possesses optimal cell encapsulation properties as the slow gelation process at room temperature is gentle and not harmful to the cells.[151] 3D printed cells encapsulated in alginate have shown to be protected from stress and pressure involved in extrusion, resulting in high viability rates.[98,152,153] Bioprinting of alginate isn't commonly implemented for bone regeneration due to the low mechanical properties of the hydrogel compared to those of natural bone, however, it is hypothesized that the ability to encapsulate cells throughout the scaffold may result in enhanced regeneration.

Thus, in this chapter, 3D printing of alginate hydrogels has been thoroughly investigated to produce biocompatible, osteoconductive scaffolds suitable for bone defect repair. Our focus on the material rheological properties responsible for printability allowed us to develop a novel printable material, of optimal gelation time and viscosity, capable of providing a suitable environment for cell encapsulation. Hydroxyapatite, the main inorganic component of natural bone, was incorporated in a polyvinyl alcohol suspension to increase the viscosity of the hydrogel formulation, while simultaneously increasing the biocompatibility and osteoconductivity of the printed scaffold. Additionally, mouse calvaria 3T3-E1 cells have been incorporated in the alginate hydrogel and 3D printed to produce scaffolds of high shape fidelity and cell viability.

3.2. Materials and methods

3.2.1 Preparation of hydrogel formulations

Seven hydrogel formulations of varying composition were developed and are listed in Table 3.1. Each component was added to the same volume of deionized water across all formulations. For formulations 1-7, alginic acid sodium salt (medium viscosity; MP Biomedicals LLS, USA) was added to 3 mL of deionized water to form a suspension and mixed with 1 mL of a sodium phosphate dibasic anhydrous (Na_2HPO_4, ≥ 99%, Fisher Scientific, USA) solution. For formulation 6, sodium chloride (NaCl, Fisher Scientific, USA) was also added to the sodium phosphate solution at 0.72% (w/v) of the final suspension. A suspension of hydroxyapatite (HA) was added to formulations 3-6. Briefly, HA was prepared via a metathesis reaction.[133,154] HA powder was then added to 5 mL of a 1% (w/v) PVA (Fisher Scientific, USA) solution and mixed on a stirring plate for 15 minutes. The HA-PVA suspension was then added to the alginate-phosphate suspension and mixed until homogeneous. For all formulations, 4 mL of a calcium sulfate anhydrous ($CaSO_4$, 99%, Alfa Aesar, USA) solution of a final concentration defined in Table 3.1 was then added to the suspension and mixed for 40 seconds. The suspensions were then loaded into the HyRel extruder for 3D printing. Formulation 6 contained the total amount of sodium ions present when formulation 5 is made with α-MEM for investigation of degradation properties of hydrogels made for cell encapsulation studies. The control is of the same composition as formulation 5 with the absence of the PVA-hydroxyapatite suspension so as to investigate the role that the suspension plays on printability, cell viability and future proliferation studies.

Table 3.1: Final compositions of various hydrogels for 3D printing

Formulations
1) 1.5% alginate, 0.12% Na_2HPO_4, 0.40% $CaSO_4$
2) **2% alginate,** 0.12% Na_2HPO_4, 0.40% $CaSO_4$
3) 2% alginate, 0.12% Na_2HPO_4, 0.40% $CaSO_4$, **2.5% HA**
4) 2% alginate, 0.12% Na_2HPO_4, **0.20% $CaSO_4$,** 2.5% HA
5) **2.5% alginate, 0.15% Na_2HPO_4**, 0.20% $CaSO_4$, 2.5% HA
6) 2.5% alginate, 0.15% Na_2HPO_4, 0.20% $CaSO_4$, 2.5% HA, **0.72% NaCl**
7) **Control:** 2.5% alginate, 0.15% Na_2HPO_4, 0.20% $CaSO_4$

(*Bold font indicates difference in composition compared to previous formulation)

3.2.2 3D Printing and hydrogel printability

The HyRel System 30 3D printer with a modified EMO-25 extruder was used to conduct 3D printing of various alginate hydrogel formulations, defined in Table 3.1. Formulations were prepared as previously described in section 3.2.1 and allowed to gelate in the extruder for 20 minutes. They were then printed using a 23 gauge needle (430 μm inner diameter) to form 7-layer porous, cylindrical scaffolds with a diameter of 1.5 cm and a height of 0.2 cm. Formulations were assessed qualitatively on the continuity of the alginate strands as extruded through the needle in addition to the shape fidelity of the printed scaffold. Formulations that produced continuous prints with high shape fidelity were defined as optimal and chosen for further characterization.

3.2.3 Rheology

To characterize the physical properties of the ideal alginate hydrogel system for 3D printing, rheological analyses were conducted using an ARG2 rheometer (TA instruments). The 60 mm cone and plate fixture was used. To simulate the printing process, the hydrogels were mixed until homogeneous and added directly to the rheometer. A time sweep was conducted for 20 minutes at 25 °C, a low oscillatory stress value of 1.0 Pa, and frequency of 1 Hz to obtain a gelation profile. As formulations 5 and 6 exhibited printed scaffolds of high shape fidelity, the recovery profile of the hydrogel after simulated extrusion was obtained. A pre-shear conditioning step at 50.44/second was conducted for 30 seconds following the initial time sweep to simulate extrusion during 3D printing and to break up the hydrogel. The pre-shear value was calculated using the printing volumetric flow rate divided by the area of the needle. The recovery profile was then obtained via a time sweep at 25 °C, an oscillatory stress of 1.0 Pa, and frequency of 1 Hz for 20 minutes. Formulation 7 was included as a control.

3.2.4 Optimal formulation characterization

The inorganic compositions of hydrogel formulations 5, 6 and 7 were analyzed using thermogravimetric analysis (TGA) and X-ray diffraction (XRD). First, hydrogels were frozen at -25 °C and lyophilized using a freeze-dryer (Free Zone®, Labconco, USA). The inorganic weight percent present in the hydrogels was determined using a TG analyzer (TGA-1000, Rheometric Scientific, UK). 20 mg of the freeze-dried scaffolds were loaded into the TG analyzer and ramped from 25 °C to 800 °C in air at a rate of 10 °C per minute. The weight loss profile was recorded and the weight percent of the inorganic residue was calculated. X-ray diffraction (XRD, Bruker AXS D5005) was completed to determine the composition of the hydrogels' inorganic

components. Scans were collected over a 2-θ range of 10-50 ° at a step size of 0.02 ° and a scan rate of 0.2 ° per minute with Cu K α radiation (k= 1.54056 nm).

3.2.5 Degradation studies in α-MEM

3.2.5.1 Diameter change

Hydrogel formulations 5, 6, and 7 (control) were chosen for investigation of degradation properties for 14 days. For each formulation, scaffolds were printed as previously described (n=6) and the diameters were measured using a micrometer. Printed scaffolds were then transferred to a 100 mM $CaCl_2$ (Calcium chloride anhydrous, Fisher Scientific, USA) bath for 1 hour for further crosslinking of the alginate chains. The diameters were measured and the scaffolds were then added to a 24 well plate with 3 mL of alpha modified eagles medium (α-MEM, Fisher Scientific, USA). On days 1, 3, 5, 7 and 14 of incubation, the media was exchanged and a sample was chosen for diameter measurement and mechanical testing (n=3).

3.2.5.2 Dynamic mechanical analysis

Dynamic mechanical analysis (DMA) was completed using a DMA 2980 Dynamic Mechanical Analyzer (TA instrument Inc., New Castle, DE) in compression mode using 40 mm sandwich fixtures. At each previously mentioned designated time point, the diameter of the selected printed scaffold (n=3) was measured and the print was loaded into the DMA. A preload force of 0.01 N was applied, followed by a ramped force at a uniform stress rate of 0.5 N per minute up to 18 N. The stress-strain curve was obtained and the compressive modulus was calculated from the slope of the initial 20 % linear elastic region.

3.2.6 3D bioprinting

3.2.6.1 Cell encapsulation and bioprinting

Mouse calvaria 3T3-E1 (MC3T3) cells were incorporated into the alginate hydrogel for 3D-printing. Cells were cultured in α-MEM supplemented with 10% fetal bovine serum (FBS, Corning Cellgro, USA) and 1% penicillin-streptomycin (Fisher Scientific, USA) under an atmosphere of 5% CO_2 at 37°C. At 90% confluence, cells were harvested and re-concentrated in the supplemented α-MEM for encapsulation.

Formulation 5 was chosen for bioprinting of MC3T3 cells as it was identified as having optimal printability and rheological properties. The control was also chosen to investigate the effect of the addition of hydroxyapatite on hydrogel printability and resulting cell viability. 5 mL of the hydrogel formulations were prepared as previously described yet components were suspended in sterile α-MEM cell culture media with 10% FBS and 1% penicillin-streptomycin instead of deionized water, with the exception of the PVA solution. The volume of media to which the components were added played a significant role in the viscosity and thus printability of the hydrogel. Briefly, alginate powder was added to 1.5 mL of cell culture media to form a homogeneous suspension. Na_2HPO_4 was added to 0.5 mL of cell culture media, which was then mixed with the alginate suspension. HA powder was added to 1.5 mL of a sterile-filtered, 1% (w/v) PVA solution and stirred for 15 minutes. The HA suspension was then added to the alginate-phosphate suspension, mixed until homogeneous, and incubated in a waterbath at 37°C while the MC3T3 cells were prepared for encapsulation. For the control formulation, alginate was added to 2.5 mL cell culture media and Na_2HPO_4 was added to 1.0 mL media so that the cells were added to a hydrogel of equi-volume with the alginate-HA formulation. 100 µL of the MC3T3 cell suspension at a concentration of 2.5×10^5 cells/mL was added to the formulations

and mixed gently until homogeneously suspended. The $CaSO_4$ solution, prepared in 1.5 mL α-MEM cell culture media, was then added and mixed gently to form a homogeneous suspension. The hydrogel was transferred to the EMO-25 extruder and allowed to gelate for 20 minutes before printing. 3D printing was then executed as previously described. Printed scaffolds were transferred to a 2 mL of a $CaCl_2$ bath, which was prepared by adding 0.10 g $CaCl_2$ in 10 mL sterile α-MEM with 10% FBS and 1% penicillin-streptomycin. The printed scaffolds were then moved to the incubator at 37°C and 5% CO_2 for 1 hour.

3.2.6.2 Assessment of cell viability

Cell viability was assessed after 3D printing and incubation in the calcium bath to ensure the procedure was not harmful to the cells. To assess the viability of cells encapsulated in the optimal alginate-PVA-HA and the control formulations (n=10 each) directly after printing, 0.80 mL of a 0.10 M sodium citrate solution was added to the printed scaffold in a 1.5 mL centrifuge tube and incubated for 1 hour to dissociate the alginate-calcium bonds. Aliquots were then taken from the suspension, mixed 1:1 with Trypan Blue solution (0.4 %, Sigma Aldrich, USA), and cells were counted under the light microscope using a hemacytometer. The number of cells throughout the suspension was calculated and the viability was determined as a percent of the cells seeded. As prints were approximately 0.20 mL in volume, the dilution factor incorporated in the calculation was 10. To assess the viability after incubation in the calcium bath, optimal and control scaffolds (n=4 each) were incubated in sodium citrate as previously described but for 2.5 hours as the increased number of calcium-alginate crosslinks formed in the calcium bath required more time to dissociate the bonds. Cells were counted and the viability was calculated as previously described.

3.2.7 Statistical Analysis

Results were statistically analyzed using one-way analysis of variance (ANOVA) and expressed as mean ± standard deviation. Statistical significance was defined as $p < 0.05$.

3.3 Results

3.3.1 Hydrogel printability

Hydrogel formulations were assessed on the continuity of the gel strands as extruded through the needle as well as by the shape fidelity of the printed scaffold. Images of hydrogel formulations 3D printed into scaffolds 1.5 cm in diameter are seen in Table 3.2. All scaffold images are of the same magnification. Formulations 1, 2, 4 and the control were not viscous enough to maintain separate lines, causing the lines to spread and connect which resulted in limited porosity. These formulations also did not support consecutive, distinct layers, further contributing to gel spreading and filling in of pores. Formulation 3 was too viscous to be extruded continuously, which resulted in discontinuous prints with limited integration. Formulations 5 and 6 presented optimal printability, with distinct porosity and shape fidelity.

Table 3.2: Summary of formulation printability (Scale bar 3.75 mm)

Formulation	**Reasoning**	**Printability**	**Storage Modulus**	**Image**
1) 1.5% alginate, 0.12% Na_2HPO_4, 0.40% $CaSO_4$	Initial optimal injectable formulation developed in previous studies	Not viscous enough to maintain shape fidelity Lines spread	275 Pa	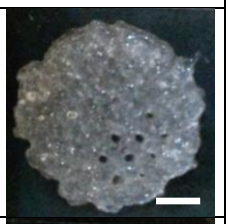
2) 2% alginate, 0.12% Na_2HPO_4, 0.40% $CaSO_4$	Increase viscosity	Not viscous enough to maintain shape fidelity Less spreading than 1	344 Pa	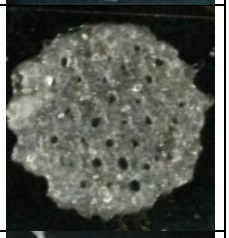
3) 2% alginate, 0.12% Na_2HPO_4, 0.40% $CaSO_4$, **2.5% HA**	Increase viscosity, biocompatibility, and potential osteoconductivity	Inhomogeneous, discontinuous flow Too viscous Stringy	3572 Pa	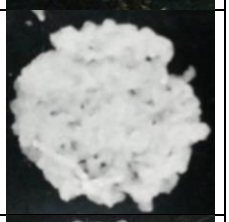
4) 2% alginate, 0.12% Na_2HPO_4, **0.20% $CaSO_4$,** 2.5% HA	Decrease viscosity	Not viscous enough to maintain shape fidelity	351 Pa	
5) 2.5% alginate, 0.15% Na_2HPO_4, 0.20% $CaSO_4$, 2.5% HA	Increase viscosity	Printed well High shape fidelity	1154 Pa	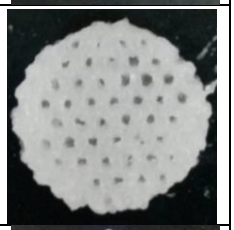
6) 2.5% alginate, 0.15% Na_2HPO_4, 0.20% $CaSO_4$, 2.5% HA, **0.72% NaCl**	Simulating Na^+ present in hydrogel when made with α-MEM	Printed well High shape fidelity	647 Pa	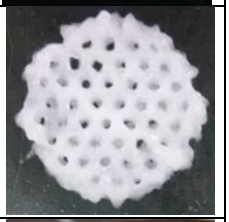
7) Control 2.5% alginate, 0.15% Na_2HPO_4, 0.20% $CaSO_4$	Control for cell culture studies	Not viscous enough to maintain shape fidelity Lines spread	42 Pa	

3.3.2 Rheology

Rheological assessments were conducted to obtain a quantifiable classification of hydrogel printability. The storage moduli of the hydrogel formulations were determined at the end of a 20 minute time sweep at an oscillatory stress of 1.0 Pa. This time period serves to simulate the 20 minute gelation period that the hydrogels experience before they are 3D printed. G' values are stated in Table 3.2 and depicted in Figure 3.1. The optimal range was determined to be between 600-1200 Pa, exhibited by formulations 5 and 6, as lower and higher values proved to result in prints of poor quality. Corresponding loss modulus and complex viscosity values after the 20 minute gelation period are stated in Table 3.3.

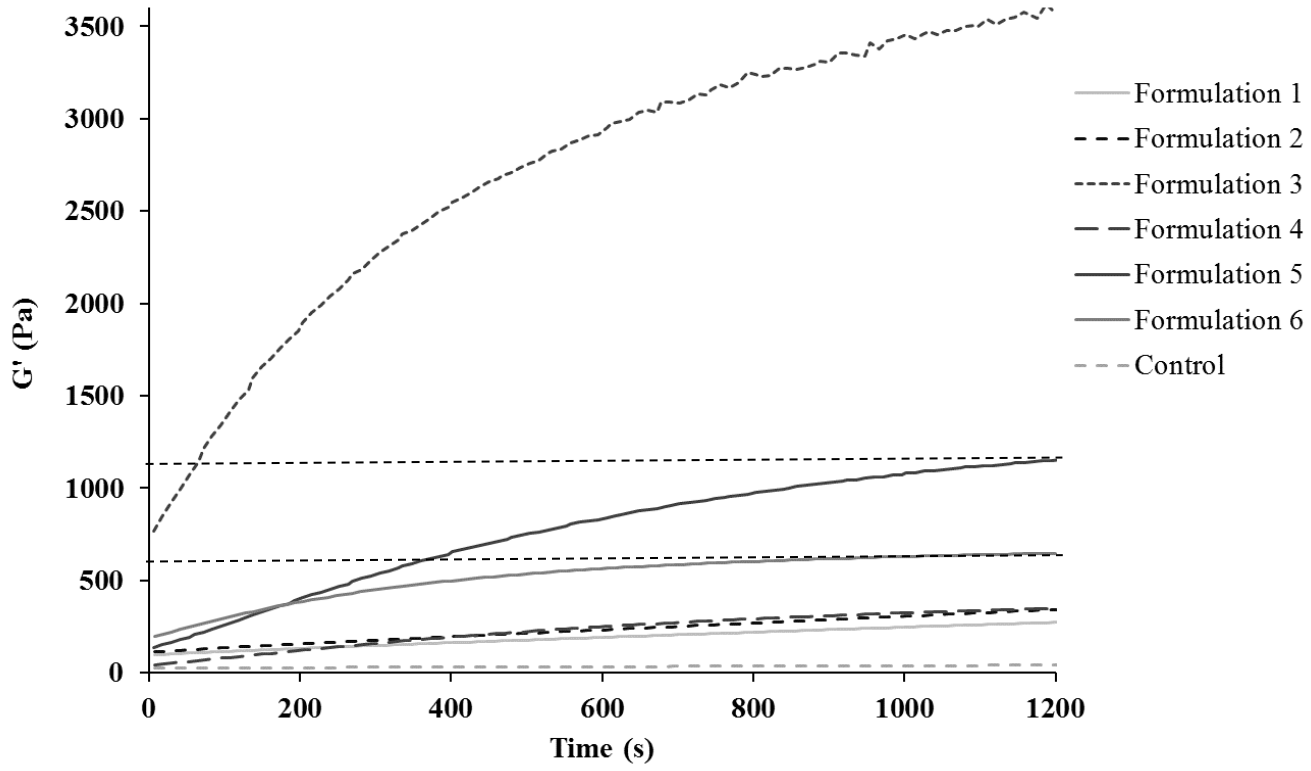

Figure 3.1: Storage moduli profile of hydrogel formulations during 20 minute time sweep

Table 3.3: Summary of rheological values after 20 minute gelation period

Formulation	Storage Modulus (Pa)	Loss Modulus (Pa)	|η*| (Pa-s)
1	275	17	44
2	344	32	55
3	3572	150	569
4	351	29	56
5	1154	73	184
6	647	72	104
Control	42	37	9

As formulations 5 and 6 were determined to have optimal rheological properties for 3D printing, their recovery properties were investigated. Formulation 7 was included as a control. A pre-shear conditioning step at 50.44/s was conducted for 30 seconds following the initial time sweep to simulate extrusion during 3D printing and to break up the hydrogel crosslinks. The recovery profile was then obtained via a time sweep for 20 minutes at a low oscillatory stress of 1.0 Pa, depicted in Figure 3.2.

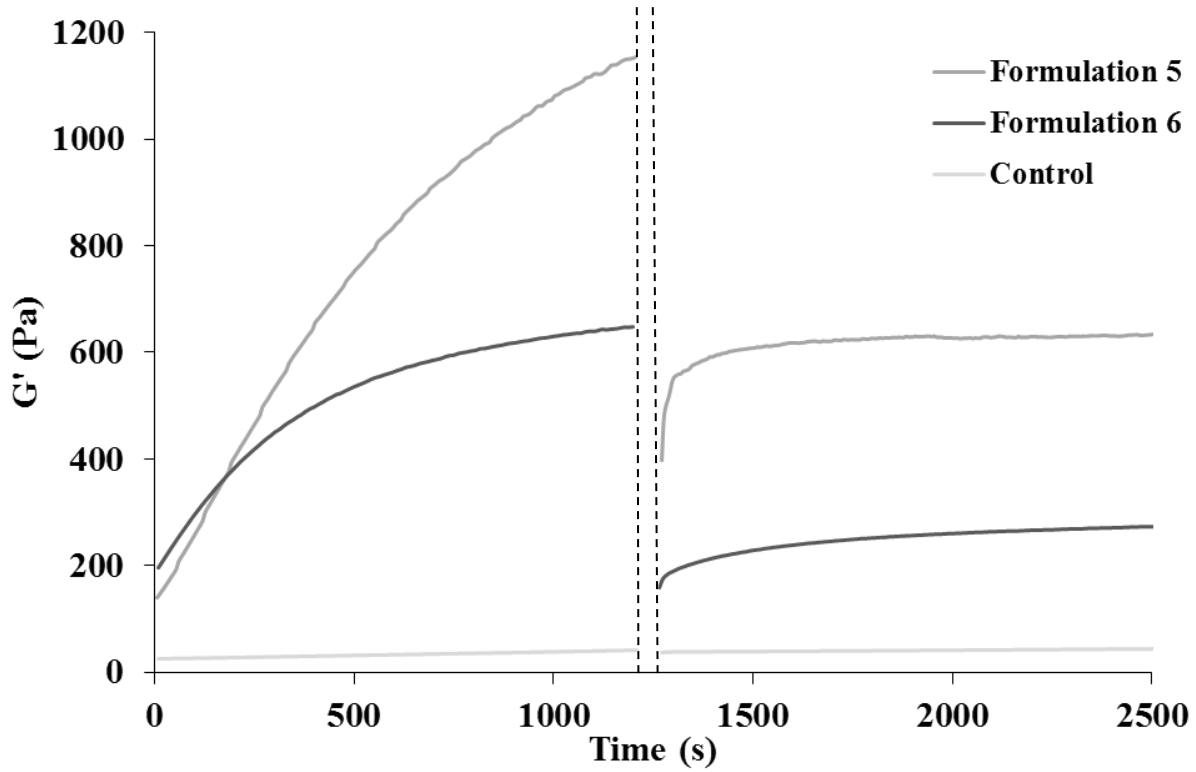

Figure 3.2: Recovery profile of select formulations after applied pre-shear, time period defied by dotted lines

3.3.3 Optimal formulation characterization

The X-ray diffraction patterns of optimal hydrogel formulations 5 and 6 and the control formulation 7 are shown in Figure 3.3. Optimal formulations exhibited characteristic peaks of hydroxyapatite including those at 25.6°, 31.6°, 32.3°, 33.8° and 39.1°, depicted in pattern c). Formulation 6 exhibits an additional peak at 45.2° due to the presence of NaCl. As expected, the control lacked any major crystalline peaks due to its mainly organic composition.

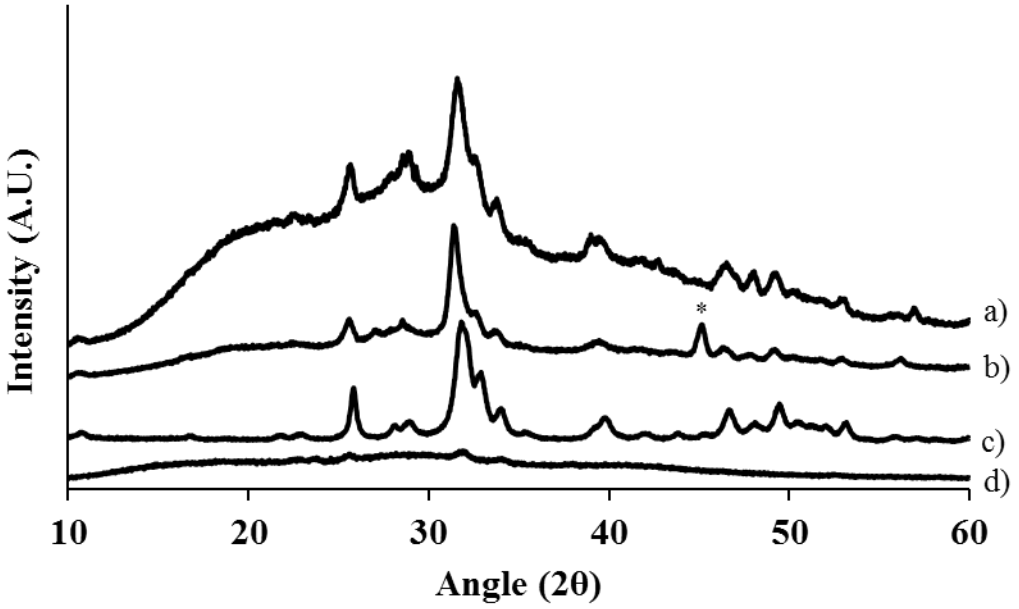

Figure 3.3: XRD patterns of a) formulation 5, b) formulation 6, c) hydroxyapatite and d) control (*) indicates major additional NaCl peak

Thermogravimetric profiles of optimal hydrogel formulations 5, 6 and the control are shown in Figure 3.4. An increase in inorganic content compared to that of the control was observed in formulations 5 and 6. The weight percent of the residue of formulation 5 was determined to be 54.4% while that of formulation 6 was determined to be 56.6%. Formulation 6 had a slightly higher percent residue due to the presence of NaCl. The control had a much lower percent residue at 30.7% due to the lack of hydroxyapatite incorporated into the hydrogel.

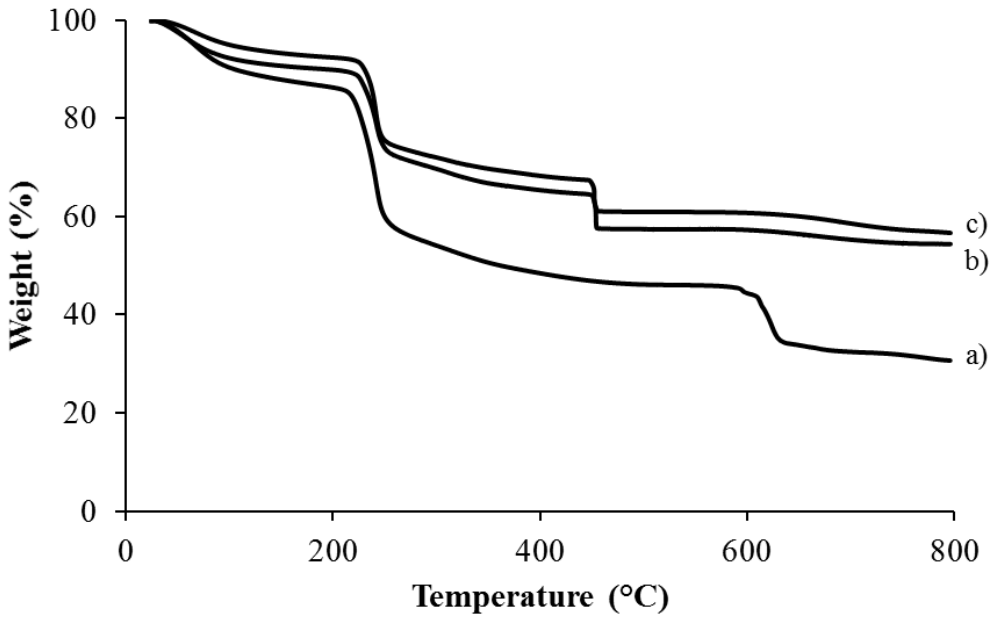

Figure 3.4: TGA curves of a) control, b) formulation 5 and c) formulation 6

3.3.4 Degradation studies in α-MEM

3.3.4.1 Diameter change

Degradation properties of formulations 5 and 6 in α-MEM were investigated to determine the potential of the hydrogels to maintain integrity over 14 days. The control was included to compare degradation properties of optimal hydrogels with those of a formulation lacking hydroxyapatite, which is hypothesized to have an effect on cell viability in *in vitro* cultures. Figure 3.5 shows that after immersion in the calcium bath for 1 hour, scaffolds composed of formulations 5 and 6 shrunk in diameter by 23.5% and 24.9% respectively, due to further crosslinking of the alginate chains. Swelling values were calculated compared to the scaffold diameter measured after immersion in the calcium bath. After incubation in α-MEM for 14 days, formulation 5 scaffolds exhibited increased swelling up to 32.7%. Similarly, formulation 6 scaffolds exhibited increased swelling up to 33.0% after 14 days. The only statistical significant

difference between formulation 5 and 6 was observed after 1 day of incubation. The control scaffolds exhibited different degradation properties throughout the study due to the difference in initial morphology of the printed scaffolds. After incubation in the calcium bath, control hydrogels only shrunk on average by 2.8%, which is statistically significantly different from the shrinkage exhibited by formulation 5 and 6 scaffolds. Additionally, the control continued to shrink on day 1 by 4.3% whereas formulations 5 and 6 exhibited significant swelling. After incubation for 14 days, the control scaffolds only swelled up to 3.3%. These values are also statistically significantly different from those of formulations 5 and 6 at each time point.

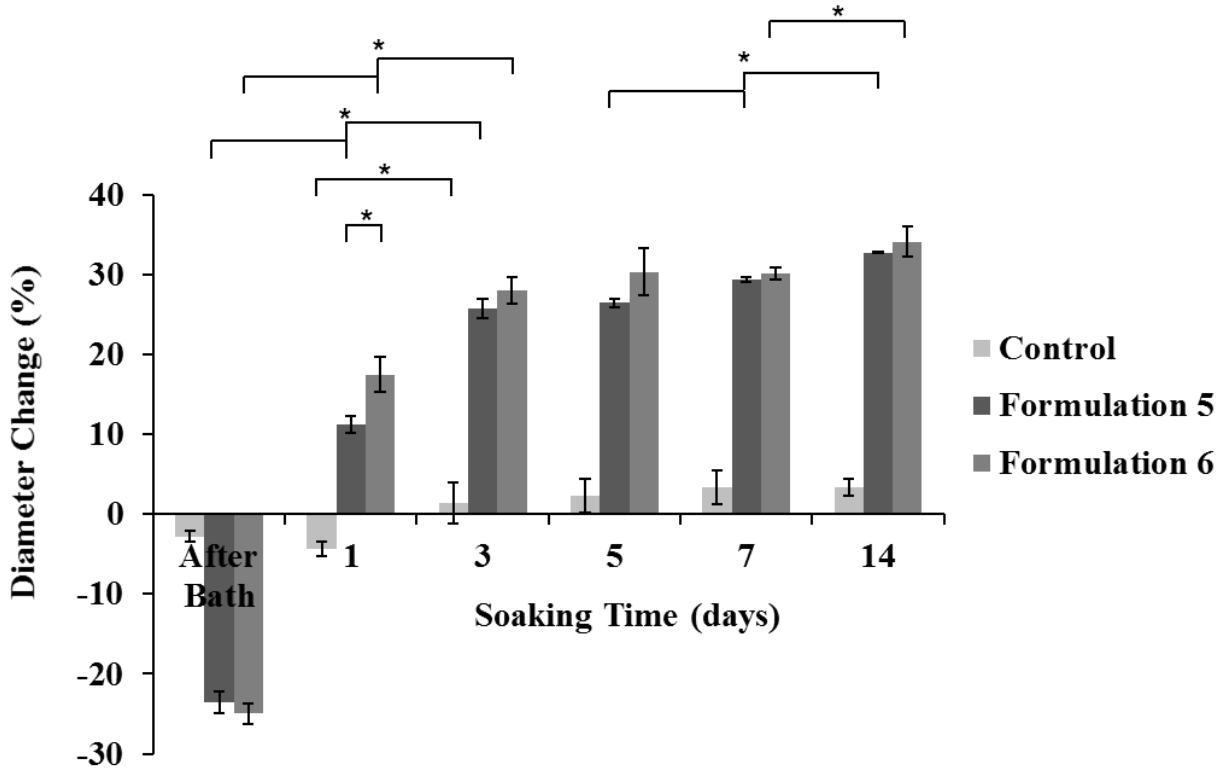

Figure 3.5: Diameter change of select scaffold formulations at various time points throughout degradation study ($p < 0.05$, ANOVA, n = 3)

3.3.4.2 Dynamic mechanical analysis

The compressive moduli of 3D printed formulations 5, 6, and the control were also determined after incubation in the calcium bath and on days 1, 3, 5, 7 and 14 in α-MEM. Figure 3.6 shows a continuous decrease in the compressive moduli of both formulation 5 and 6 scaffolds over 14 days. The average compressive modulus for formulation 5 scaffolds was determined to be 10.3 kPa after immersion in the calcium bath and continually decreased over 14 days to a value of 2.4 kPa. Similarly, formulation 6 scaffolds exhibited an average compressive modulus of 8.6 kPa after immersion in the calcium bath and continually decreased to 2.8 kPa after 14 days. The control scaffolds exhibited limited change in compressive modulus throughout the 14 days starting at 4.7 kPa after the calcium bath and decreasing to 2.7 kPa after incubation for 14 days.

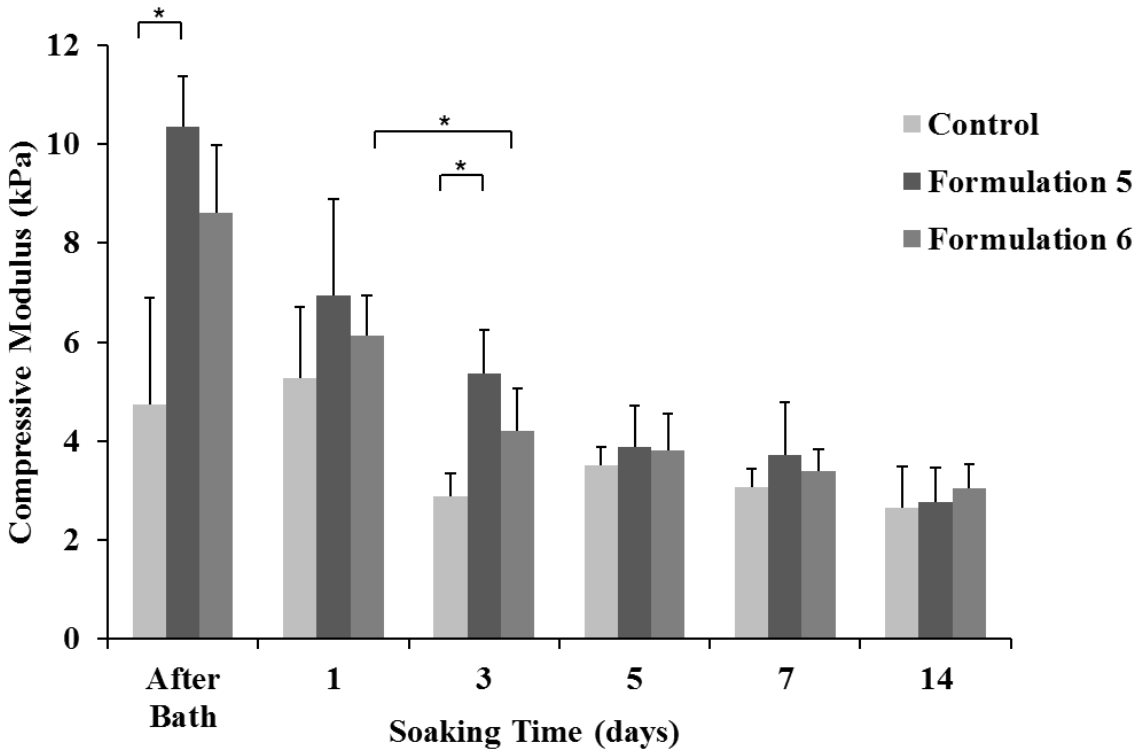

Figure 3.6: Compressive moduli of select scaffold formulations throughout degradation study ($p < 0.05$, ANOVA, n = 3)

3.3.5 Bioprinting and viability of encapsulated MC3T3 cells

MC3T3-E1 cells were successfully encapsulated into the control and optimal alginate-PVA-HA hydrogel formulations and 3D printed into scaffolds with a diameter of 1.5 cm. Compared to the control, the alginate-HA scaffolds have significantly higher shape fidelity, shown in Figure 3.7.

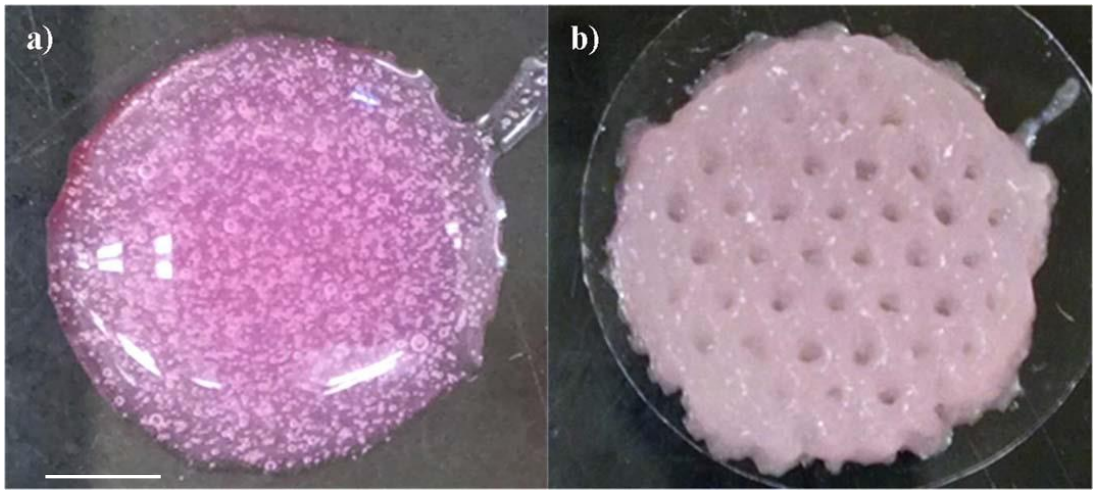

Figure 3.7: Images of 3D bioprinted a) control and b) optimal alginate-polyvinyl alcohol-hydroxyapatite hydrogel formulations embedded with MC3T3-E1 cells (Scale bar 3.75 mm)

Cell viability analysis after 3D printing alginate-PVA-HA hydrogel scaffolds and incubation in the calcium bath revealed average viability values of 95.6% and 77.5%, respectively, seen in Figure 3.8. Cells encapsulated in the control formulation exhibited average viability values of 60.1% and 22.5% after 3D printing and incubation in the calcium bath, respectively. Cell viability was statistically significantly higher in the alginate-PVA-HA printed scaffolds compared to the control scaffolds after both printing and incubation in the calcium

bath. The difference in viability after incubation in the calcium bath was not significant for alginate-PVA-HA scaffolds, but was statistically significantly lower for the control scaffolds.

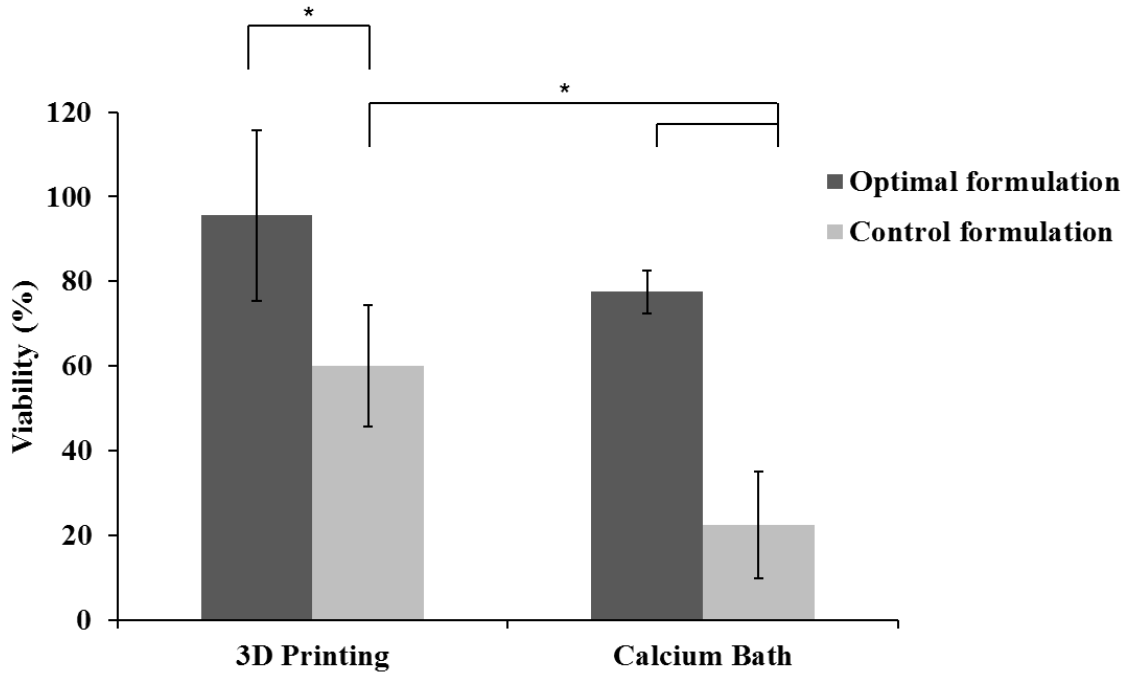

Figure 3.8: Cell viability after 3D printing and incubation in the calcium bath ($p < 0.05$, ANOVA, $n \geq 4$)

3.4 Discussion

3.4.1 Hydrogel printability

Material selection is the most important step when applying 3D printing technology to develop constructs intended to promote tissue regeneration. The material must be printable, or have sufficient viscoelasticity to allow extrusion through a small needle followed by recovery, while also being biocompatible and not eliciting an adverse immune response. Furthermore, it is of great interest that the material has the capability to encapsulate and support live cells throughout the printing process. For bone tissue engineering, the development of a hydrogel

material capable of 3D bioprinting scaffolds of uniform cell distribution has potential to promote enhanced healing compared to conventional scaffolds for bone regeneration. Alginate is a perfect candidate for 3D bioprinting due to its controllable gelation process and natural hydrogel structure, similar to that of the native extracellular matrix.

The gelation mechanism of alginate has been thoroughly investigated and is such that divalent cations, such as calcium, form intermolecular bonds with two deprotonated carboxylate groups of one alginate G block and two hydroxyl groups of another.[120] Alginate undergoes a sol-gel transition as a result of crosslinking of lateral "egg box" multimers.[114] The rate of this gelation process can be controlled by adjusting the concentration of both alginate and calcium, as well as through addition of retardation agents such as sodium dihydrogen phosphate.[55] The mechanism by which Na_2HPO_4 slows down the gelation of alginate is through a chemical reaction with $CaSO_4$, resulting in the formation of calcium phosphate. This precipitation leaves less calcium available in solution for the immediate gelation of alginate. Thus, once all of the phosphate ions have reacted with calcium ions, the calcium is then made available to crosslink the alginate G blocks uniformly throughout the suspension.[126] The ability to control the gelation rate of alginate ultimately results in control of the extent of crosslinking and thus rheological properties defining the printability of the hydrogel throughout the 3D printing process. The inherent shear-thinning property of alginate results in a decrease in the hydrogel viscosity with an increase in shear rate.[47] Thus, as the hydrogel is extruded through the needle and the shear rate increases, the viscosity decreases to allow the hydrogel to flow more easily as continuous strands.

Efforts to investigate printability of alginate formulations of various compositions are summarized in Table 3.2, and correlating rheological values are listed in Table 3.3. The

cylindrical scaffold design was chosen as a model system to determine the optimal formulations that achieved prints of high shape fidelity. The optimal formulations will also be suitable to print larger, more complex designs, which will be investigated in future studies. As an injectable alginate hydrogel formulation with a gelation time defined as optimal in a surgical setting has been developed in our laboratory, it was hypothesized that a hydrogel optimal for 3D printing could be developed as well.[155] Thus, formulation 1 was adapted from our previous studies due to its optimal injectability. This composition served as a baseline formulation on which we modified, based on our knowledge of alginate's gelation mechanism, to develop an ideal formulation for 3D printing. Yet, the concentration of alginate and thus viscosity of the original formulation was too low to maintain shape fidelity. In formulation 2, the concentration of alginate was increased compared to formulation 1, but the hydrogel was still of low viscosity and the resulting printed scaffold of poor quality. A polyvinyl alcohol-hydroxyapatite suspension was added in formulation 3 to increase the viscosity of the formulation as well as to increase the biocompatibility and osteoconductivity of the resulting scaffold. Yet, the viscosity and storage modulus of this formulation were too high to allow sufficient yielding of the hydrogel, resulting in discontinuous extrusion and scaffolds of poor quality. The calcium concentration was decreased in formulation 4 in order to decrease the number of crosslinks and thus storage modulus of the hydrogel. However, the resulting viscosity was too low to produce printed scaffolds of high shape fidelity. An alternate approach was taken to increase the viscosity by increasing the alginate concentration in formulation 5. The phosphate concentration was increased concurrently to prevent premature gelation as a result of the increased number of crosslinking sites. The slight increase in alginate concentration did result in an optimal viscosity capable of producing 3D printed scaffolds of high shape fidelity. Thus, formulation 5 was

defined as an optimal formulation. As the main objective of this study is to encapsulate live cells within the hydrogel, formulation 6 simulates the composition of the hydrogel when made with cell culture media, which is a crucial modification for bioprinting. The increased content of sodium ions present in the cell culture media has potential to interact with the alginate gelation process and was an important modification to investigate. As seen in Table 3.2, formulation 6 produced printed scaffolds of high shape fidelity and was deemed an optimal formulation as well. Formulation 7 lacked the incorporation of the PVA-hydroxyapatite suspension and was included to investigate the printability of a formulation that would serve as a control for future cell culture studies. This formulation displayed very low viscosity and produced printed scaffolds of very low quality with no porosity. This suggests that the presence of the PVA-hydroxyapatite suspension plays a crucial role in altering the viscosity of the overall suspension and thus resulting printability.

3.4.2 Rheology

Figure 3.1 shows the storage moduli profile of the investigated hydrogel formulations during a 20 minute time sweep to simulate the gelation process. As seen in Table 3.3, all formulations displayed G' values greater than G" values, signifying that all are classified as gels. Formulations 5 and 6, which were the only formulations that resulted in 3D printed scaffolds of high quality, expressed a storage modulus value between 600-1200 Pa after the gelation period. The storage modulus value can be correlated to the physical printability observed as the formulations were elastic enough to allow continuous extrusion through the 430 μm needle and recovery upon deposition, while viscous enough to maintain shape fidelity once printed. Formulations with G' values higher and lower than this range resulted in prints of poor quality as

they were either too soft to maintain high shape fidelity or too stiff to allow continuous extrusion. This expresses the sensitivity of the gelation and viscosity of the system and the role each constituent has on the resulting properties, thus highlighting the achievement of obtaining a novel formulation ultimately allowing 3D bioprinting with high cell viability.

It is of the most importance that the hydrogel possesses sufficient viscoelasticy; the property that allows the hydrogel network to deform upon extrusion but recover once deposited so that the 3D printed layers remain distinct and produce an overall structure of high shape fidelity.[156] Figure 3.2 shows the recovery properties of the optimal and control formulations. Following the application of a pre-shear of 50.44/s, all formulations healed and displayed recovery of their storage modulus. The extent to which the hydrogel recovers is not of a great concern as the scaffold is added to a calcium bath to induce further crosslinking after printing. Thus, the shear thinning and viscoelastic properties of the alginate hydrogel formulations prevent complete destruction of the hydrogel network. This suggests that the optimal formulations have potential to provide a suitable environment capable of protecting cells through the extrusion process.

3.4.3 Optimal formulation characterization

As expected, Figure 3.3 shows that optimal formulations exhibited characteristic X-ray diffraction peaks of hydroxyapatite while the control lacked crystallinity due to its highly organic composition. Formulation 6 exhibited an additional peak at 45.2° due to diffraction of the (220) plane of sodium chloride. Slight peak shifting and broadening are observed due to possible in situ formation of nano-sized, poorly crystalline hydroxyapatite and/or additional calcium phosphate phases as a result of precipitation of calcium and phosphate ions during the gelation

process.[125,132] As hydroxyapatite is the main mineral component of natural bone, its presence increases the osteoconductivity of the hydrogel, and thus improves the scaffolds' potential for bone defect repair. Additionally, including hydroxyapatite in a PVA suspension allows it to be homogenously suspended throughout the hydrogel while simultaneously increasing the viscosity of the hydrogel and mechanical properties and biocompatibility of the resulting scaffold.

The thermogravimetric profiles exhibited in Figure 3.4 show the quantification of inorganic residue present in the optimal formulations 5 and 6 compared to that of the control. Decomposition of the alginate hydrogels begins around 26 °C with the loss of water. Losses attributed to the rupture of the alginate chains and monomers occur around 190 °C and 620 °C. The addition of the polyvinyl alcohol-hydroxyapatite suspension in formulations 5 and 6 modifies the loss profile compared to that of the control. A significant increase in percent residue is observed due to the presence of HA, as well as an additional loss around 450°C which can be attributed to PVA. The loss profile of formulation 6 reveals a slight increase in percent residue due to the presence of NaCl. As PVA is a hydrophilic polymer that has been reported to be highly biocompatible in cell culture studies and is approved by the FDA as polymer coatings, it contributes not only to the viscosity of the suspension but to the biocompatibility as well.[55]

3.4.4 Degradation studies in α-MEM

3.4.4.1 Diameter change

An investigation of the hydrogel degradation properties was conducted in order to determine whether the 3D printed scaffolds composed of optimal formulations maintain structural integrity and have potential to support cell life up to 14 days in α-MEM cell culture media. The control was included to compare degradation properties of optimal hydrogels with

those of a formulation lacking hydroxyapatite, which is hypothesized to have a positive effect on *in vitro* cell viability.[157] Figure 3.5 shows that after immersion in the calcium bath for 1 hour, scaffolds composed from formulations 5 and 6 shrunk significantly in diameter. This can be attributed to further crosslinking of alginate G blocks with the free calcium ions in the bath and thereby compression of the alginate chains into the egg box structure.[50] Formulation 6 represents the hydrogel composition when modified for cell incorporation; specifically containing the total amount of sodium ions present in the hydrogel when formulation 5 is made with α-MEM. This modification was investigated to gain an understanding of degradation and swelling properties of hydrogels made for cell encapsulation studies, as the incorporation of cell culture media is integral for cell survival. This is specifically important as the main mechanism in which alginate hydrogels degrade is through ion exchange between the calcium ions crosslinked with the G blocks in the egg-box structure and the sodium ions in the surrounding media. Once the sodium ion replaces the calcium ion in the binding site between the two G blocks, the crosslink is destroyed as alginate does not bind with monovalent cations. This results in relaxation and opening of the polymer G chains, permitting media to penetrate the hydrogel matrix and cause swelling.[57,158] It was important to investigate if the increased presence of sodium ions within the hydrogel enhanced the degradation properties. Figure 3.5 shows that scaffolds of both optimal hydrogel formulations exhibited initial significant swelling after placed in α-MEM. The difference between the two was only significant on day 1, due to the increased ratio of non-gelling ion to gelling ions in formulation 6. Thus, this suggests that a similar swelling profile will occur over 14 days when formulation 5 is made with α-MEM for cell culture studies. It is important that the scaffolds remained stable as a drastic increase in swelling in the presence of cells could make it more difficult for cells to interact with each other to form a network, and

deterioration of the alginate crosslinks could affect cell stabilization within the matrix. Swelling stabilized after day 3 in the media, suggesting that ion exchange between the hydrogels and surrounding media was also stabilized. As the main degradation mechanism is due to ion exchange and is not enzymatic, this suggests that alginate hydrogels will maintain integrity *in vitro*.[56] The control exhibited different degradation properties due to the difference in initial morphology and lack of porosity of the printed scaffolds. The change in diameter over the 14 day period was minimal and statistically significantly lower than formulations 5 and 6. The lack of porosity displayed throughout the degradation study suggests that cells encapsulated in the control formulation *in vitro* may suffer from limited diffusion of nutrients and waste. Thus, the novel specific composition of this alginate-polyvinyl alcohol-hydroxyapatite formulation is able to produce 3D printed scaffolds with sufficient stability and potential to support cell life and activities for 14 days in culture.

3.4.4.2 Dynamic mechanical analysis

Although the compressive moduli of the 3D printed scaffolds are relatively weak compared to 3D printed scaffolds for bone repair reported in literature, the modulus values for both optimal formulations after further crosslinking in the calcium bath represent scaffolds of sufficient mechanical properties for surgical handling.[151] Incubation in α-MEM resulted in a continuous decrease in the compressive moduli of both formulation 5 and 6 scaffolds over 14 days, which is depicted in Figure 3.6. This occurrence can be correlated to the swelling of the hydrogels due to ion exchange with the sodium ions present in the surrounding media. The destruction of the crosslinks between the alginate G blocks and calcium ions weakens the hydrogel structure. It has been hypothesized that the hydrogel reaches an equilibrium with the

surrounding media around day 3, which is also corroborated by the slowing decrease in compressive modulus at this time. As the compressive modulus decreases similarly for formulation 5 and 6 printed scaffolds over 14 days, it is hypothesized that a hydrogel composed of α-MEM for cell encapsulation will experience a similar decreasing compressive modulus profile. These findings also prove the maintenance of integrity of the novel alginate-polyvinyl alcohol-hydroxyapatite scaffolds for 14 days in cell culture, providing a stable matrix for the cells to proliferate, mature and initiate bone regeneration. The control exhibited a less drastic change in compressive modulus, correlating with the lack of porosity and minimal swelling during this incubation period.

3.4.5 Bioprinting and viability of encapsulated MC3T3 cells

MC3T3-E1 cells were successfully incorporated into the optimal alginate-PVA-HA hydrogel formulation and 3D printed into scaffolds of high shape fidelity, seen in Figure 3.7, as neither the cell culture media nor cell suspension affects the printability of the system. Cell encapsulation within the hydrogel matrix provides the scaffold with increased potential for tissue healing as post-fabrication seeding processes may pose difficulties for uniform cell infiltration and thus tissue regeneration.[8] As the MC3T3 cell line is an osteoblast precursor, survival and proliferation of the encapsulated cells throughout the scaffold provides potential to lead to new bone deposition uniformly throughout the defect.

Viability was assessed directly after printing and after incubation in the calcium bath separately to determine if these two processes cause damage to the encapsulated cells. After 3D printing, it was determined that approximately 95.6% of the encapsulated cells in the optimal alginate-PVA-HA formulation were viable, proving that the process was not harmful to the cells

and that the hydrogel formulation was successful in providing protection. After incubation in the calcium bath, the viability decreased to 77.5%, which may be attributed to the further crosslinking of the alginate matrix in the presence of calcium. Such contraction of the hydrogel matrix and shrinkage of the scaffolds, exhibited in Figure 5, has the potential to impose additional stress on the cells and may result in cell death. However, as the viability is still relatively high, the surviving cells still have the potential to recover and proliferate by further incubation *in vitro*, which will be investigated in future studies.[159] In comparison, only about 60.1% of cells were viable after 3D printing the control formulation. This can be due to the reduced viscosity of the suspension and thus increased stress experienced by the cells during the extrusion process, as printing parameters maintained constant throughout all formulations. Thus, the incorporation of PVA-hydroxyapatite suspension not only increases the viscosity of the formulation, but indirectly increases cell viability after printing as well. Furthermore, the viability of cells encapsulated in the control formulation after incubation in the calcium bath reduces to 22.5%. This low value can be attributed to the lack of porosity of the printed scaffolds. Thus, when the cells are immersed in the calcium bath for an hour, they are isolated from the nutrients provided by the surrounding cell culture media. Additionally, after incubation in the sodium citrate solution, the printed scaffolds had to be physically broken apart to release the cells for viability measurements. This may be due to the limited infiltration of sodium citrate into the alginate matrix and minimal crosslink disruption as a result of the lack of scaffold porosity. The application of physical force to the scaffold may have resulted in harm to the encapsulated cells and caused additional cell death.

3.5. Conclusions

In the work in this chapter, a novel alginate-polyvinyl alcohol-hydroxyapatite hydrogel formulation with optimal rheological properties for 3D bioprinting has been developed and employed to result in 3D printed scaffolds of high cell viability. Numerous alginate hydrogels of varying compositions were extensively investigated to identify which concentrations possessed viscoelastic properties allowing continuous hydrogel extrusion and sufficient recovery to produce scaffolds of high shape fidelity. It was determined that the presence of a PVA-hydroxyapatite suspension played a significant role in the viscosity and printability of the formulations, as well as cell viability after 3D printing. 3D printed scaffolds composed of optimal formulations displayed sufficient integrity and mechanical properties over a 14 day incubation period in cell culture media, suggesting potential to provide a suitable environment for cells for *in vitro* culture. This is supported by the ability of the optimal alginate-hydroxyapatite formulation to protect cells during 3D printing and incubation in a calcium bath. Thus, this system will be implemented further in future *in vitro* studies to investigate the ability of the encapsulated MC3T3 cells to differentiate and regenerate new bone. Additionally, scaffolds of more complex, irregular designs will be printed to assess the capability of this optimal formulation in printing large-scale, personalized defects. Thus, bioprinting of this novel alginate-polyvinyl alcohol-hydroxyapatite hydrogel formulation to produce scaffolds for bone repair has the potential to provide individualized treatment of defects and promote enhanced, uniform healing.

Chapter 4

In vitro evaluation of 3D bioprinted tri-polymer network scaffolds for bone tissue regeneration

4.1. Introduction

Three-dimensional (3D) printing of live cells into tissue engineered scaffolds of complex architectures provides an alternative method to treat and heal irregular tissue defects. The application of additive manufacturing for tissue engineering enables biomaterial scaffolds to be constructed layer by layer into 3D replicas of repaired damaged tissues or organs for patients in need.[135,136] Although various materials have been utilized to 3D print live cells into scaffolds at initial high cell viability, *in vitro* evaluations of the scaffolds' ability to support cellular growth and activities are necessary before implementing these scaffolds for healing *in vivo*.[160]

Polymeric hydrogel materials are often used to 3D bioprint cells into tissue engineered scaffolds due to their inherent high water content and fibrillar structure, resembling that of the native extracellular matrix (ECM).[30,32] Both natural and synthetic polymers, including chitosan, alginate, polyethylene glycol, polycaprolactone and many more are used to 3D print tissue substitutes for skin, bone, liver, and other tissues and organs.[89,93,141,161] It is crucial that the material of choice possesses optimal printability as well as provides a suitable environment mimicking that of the natural tissue to support cell life and promote innate physiological behaviors.[97,162] The natural bone environment includes inorganic hydroxyapatite (HA) minerals and organic collagen fibers, which is also the major structural component in the ECM.[92] Conventional methods for 3D printing scaffolds for bone tissue engineering often use ceramic materials composed of HA and limit the inclusion of live cells throughout the fabrication

process.[16,163] 3D bioprinting live cells with a hydrogel is a favorable approach to supply a homogeneous cell population throughout the scaffolds to promote enhanced homogeneous healing.

The environment in which cells live plays a vital role in the physiological morphology and behavior they express in *in vitro* culture.[79,164] For example, they must be provided with proper attachment sites to form integrin binding complexes to the matrix. The integrin receptors on the cell cytoskeleton have an affinity for complexes such as ligands and RGD modalities in which they will attach to.[80,86] They will then begin to exhibit stretched morphology favorable for cell migration as opposed to rounded morphology expressed by cells experiencing improper attachment to the matrix.[165,166] Additionally, the mechanical properties of the scaffolds must be appropriate to support cell proliferation and provide stability to counter cellular contractile forces imposed during migration throughout the matrix.[167,168] Lawyer *et al.* reported that the stiffness of the scaffolds greatly impacts the migration and proliferation abilities of the cells in the scaffold.[169] Thus, it has been concluded that a synergistic effect exists between the biological and mechanical properties of the scaffold which plays a significant role in determining the physiological behavior of the encapsulated cells. These properties must be investigated and understood before the scaffold can be implemented *in vivo*.

Thus, in the work in this chapter we initially evaluated the ability of our previously developed novel alginate-polyvinyl alcohol (PVA)-HA hydrogel formulation and to support cellular life and functions in *in vitro* culture.[170] We have 3D printed pre-osteoblastic MC3T3 cells into scaffolds for bone tissue regeneration and assessed the proliferation of these cells encapsulated within the scaffolds. A systematic approach was taken to improve the proliferation

within the scaffolds, eventually leading to the development of a novel tri-polymer formulation with the addition of collagen hydrogel.

4.2. Materials and methods

4.2.1 Preparation of hydrogel-cell suspension

Mouse calvaria 3T3-E1 cells were encapsulated in the alginate-PVA-HA hydrogel for 3D printing. Cells were cultured in alpha modified eagles medium (α-MEM, Fisher Scientific) supplemented with 10% fetal bovine serum (FBS, Corning Cellgro) and 1% penicillin-streptomycin (Fisher Scientific) under an atmosphere of 5 % CO_2 at 37 °C. At 90 % confluence, cells were harvested and re-concentrated in the supplemented α-MEM for encapsulation.

An alginate-polyvinyl alcohol-hydroxyapatite formulation developed previously in our laboratory was used for 3D bioprinting of honeycomb and alternating rectilinear scaffold designs.[170] Briefly, alginic acid sodium salt (medium viscosity; MP Biomedicals LLC) was added to sterile supplemented α-MEM at 2.5% (w/v) of the final suspension and mixed with a sodium phosphate dibasic anhydrous (Na_2HPO_4, ≥ 99%, Fisher Scientific) solution in supplemented α-MEM at 0.15 % (w/v) of the final suspension. Hydroxyapatite (HA) was prepared via a metathesis reaction.[154] HA powder was then added at 2.5 % (w/v) of the final suspension to a sterile-filtered 1 % (w/v) polyvinyl alcohol (PVA, Fisher Scientific) solution and mixed on a stirring plate for 15 minutes. The HA-PVA suspension was added to the alginate-phosphate suspension, mixed until homogeneous, and incubated in a waterbath at 37 °C while the MC3T3 cells were prepared for encapsulation. 100 μL of the MC3T3 cell suspension at a final concentration of 1.0 x 10^6 cells/mL was added to the formulation and mixed gently until homogeneously suspended. A calcium sulfate anhydrous ($CaSO_4$, 99%, Alfa Aesar) solution in

supplemented α-MEM at 0.20% (w/v) of the final suspension was then added and mixed for 40 seconds to initiate gelation. The hydrogel was transferred to the EMO-25 extruder and allowed to gelate for 30 minutes before 3D printing. A control formulation of the same concentrations but without incorporation of the PVA-HA suspension was included to investigate the effect of the presence of hydroxyapatite in 3D printed scaffolds on cell proliferation. For the control formulation, the volumes of the alginate suspension and Na_2HPO_4 solution were increased so that the cells were added to a hydrogel of equi-volume with the alginate-HA formulation. Hydrogel preparation was conducted as previously described.

4.2.2 3D bioprinting

The HyRel System 30 3D printer with a modified EMO-25 extruder was used to conduct 3D bioprinting of MC3T3 cells encapsulated in an alginate-PVA-HA hydrogel. After gelating for 30 minutes in the extruder, 3D printing was initiated and the hydrogel-cell suspension was extruded through a 23 gauge, 430 μm needle into pre-determined scaffold designs. The computer software programs Repetrel and Slic3r were used to construct a G-code file to print a 1.5 cm cylindrical scaffold with a honeycomb infill pattern at a 40% infill density. The control formulation was also printed according to this design. To determine if a different infill design would have an effect on cell proliferation, an alternating rectilinear G-code file was created in which every two layers were rotated 45°. All other parameters remained constant. After printing was complete, scaffolds were transferred to a 1.0 % (w/v) $CaCl_2$ (Calcium chloride anhydrous, Fisher Scientific) bath in α-MEM for 1 hour in the incubator at 5 % CO_2 and 37 °C for further crosslinking of the alginate chains. Crosslinked scaffolds were then added to a 24 well plate with 1 mL of fresh α-MEM and returned to the incubator. Media was refreshed every other day during

the entire period of *in vitro* studies. A schematic of the 3D bioprinting process can be seen in Figure 4.1.

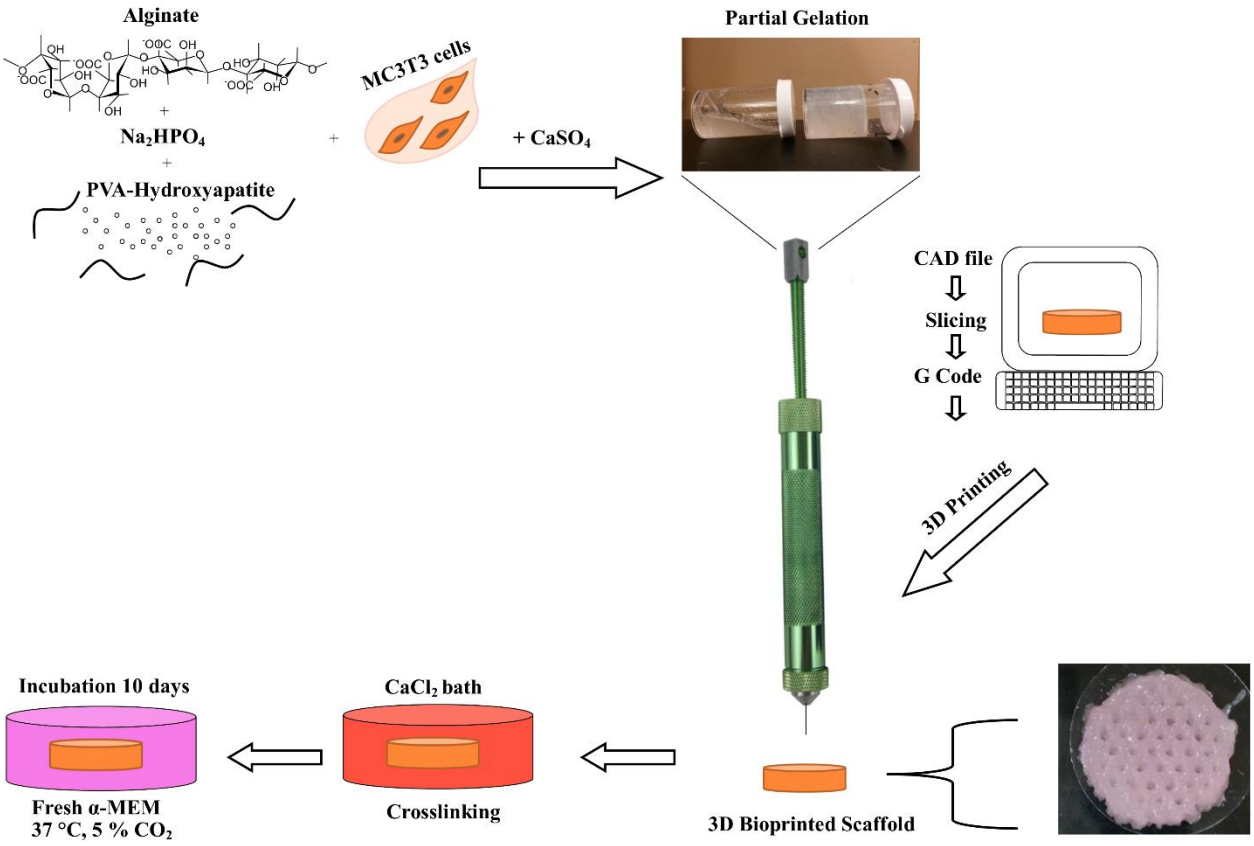

Figure 4.1: Schematic of 3D bioprinting process

4.2.3 In vitro proliferation

The proliferation of MC3T3 cells encapsulated in 3D printed alginate hydrogels over 10 days was assessed using an alamarBlue assay (Fisher Scientific). Healthy cells metabolize the dye and reduce resazurin to the fluorescent molecule, resorufin. The extent of reduction can be quantified via spectroscopy and directly correlates with the number of healthy, metabolically

active cells present in the scaffolds. An increase in reduction thereby signifies an increase in cell number and thus proliferation. At select time points, 3D printed scaffolds were chosen for analysis and incubated in 0.1 M sodium citrate (Fisher Scientific) solution in a 1.5 mL centrifuge tube for 1 hour to dissociate the alginate-calcium bonds. The suspensions were then centrifuged at 1400 rpm for 5 minutes to form a cell pellet. The media was removed and 1 mL of fresh media and 100 μL of alamarBlue dye were added to the centrifuge tube, which was then incubated at an atmosphere of 5 % CO_2 at 37 °C for 4 hours. 200 μL aliquots were then added to a 96 well plate and the absorbance was read using a spectrometer (Biotek, USA) at 570 nm and a reference wavelength of 600 nm. The reduction of the alamarBlue was then calculated according to the equation provided by the manufacturer.

4.2.4 Effects of calcium bath

In efforts to increase the proliferation of the MC3T3 cells in the 3D printed scaffolds of original and alternating infill designs, the concentration of the calcium bath was decreased to 0.5 % (w/v) $CaCl_2$.

4.2.4.1 Diffusion properties of 3D printed scaffolds

To investigate the diffusion properties of the 3D printed hydrogel scaffolds, fluorescein isothiocyanate (FITC)-dextran (40kDa, Fisher Scientific) was added to the hydrogel formulations before the addition of $CaSO_4$ at a final concentration of 0.084 mg/mL. Dextran was incorporated to serve as a model molecule to obtain insight on the diffusion properties of nutrients and waste through the scaffolds, as it is a small polysaccharide. Scaffolds of the original and alternating infill designs and the control formulation were 3D printed and crosslinked with either 0.5 %

(w/v) or 1.0 % (w/v) $CaCl_2$ (n=4 each) for 1 hour. The scaffolds were then added to a 24 well plate and incubated with 1 mL of α-MEM in a waterbath at 37 °C. To obtain a release profile, aliquots were taken and read with a fluorescent plate reader (excitation:490 nm, emission:520 nm) with media replenished at 2 hours and refreshed every 24 hours. Permeability coefficients were calculated using FITC-dextran flux from the linear region of the release profile. Diffusion coefficients were calculated using scaffold thickness of 0.15 cm and partition coefficient k=1.0.

4.2.4.2 Calcium cytotoxicity analysis

MC3T3 cells were grown and cultured as previously described for investigation of the effect of the calcium bath on cellular proliferation. Cells were seeded at a concentration of 2.0 x 10^5 cells/mL in 24 well plates and allowed to attach for 4 hours. They were then introduced to a 0 %, 0.5 % (w/v) or 1.0 % (w/v) $CaCl_2$ solution in α-MEM (n=3 each) for 30 minutes, simulating scaffold incubation in the calcium bath. Cells were then rinsed with 1 x PBS solution, and 1 mL of fresh α-MEM was added to each well before incubation at 37 °C and 5 % CO_2 atmosphere. Proliferation analyses were conducted as previously described.

4.2.5 Addition of collagen content

Type I collagen was extracted from rat tails and dissolved in 0.02 M acetic acid, resulting in a collagen solution with a concentration of 5.6 mg/mL.[111,127,171] To form a collagen gel, the pH of 5 mL of this solution was raised to 7 using sodium hydroxide and incubated overnight in a waterbath at 37 °C. The precipitates were collected via filtration and air dried for 20 minutes. The hydrogel formulation used for 3D bioprinting was prepared as previously described with 5.0 % (w/v) of the wet collagen gel added to the alginate-phosphate suspension and mixed

homogeneously before the addition of the PVA-HA suspension. Gelation, 3D printing, and proliferation analyses were then conducted as previously described.

As an alternative method to increase proliferation and limit damage inflicted on the cells due to the presence of calcium, the duration of the calcium bath was decreased to 30 minutes for both 0.5 % (w/v) and 1.0 % (w/v) $CaCl_2$ concentrations. Additionally, scaffolds were rinsed in 1x phosphate buffer saline (PBS) for 30 seconds to remove excess calcium from the scaffolds before incubation in fresh cell culture media. Proliferation analyses were then conducted as previously described.

In final efforts to increase proliferation, the collagen content was increased to 6.5 % (w/v). Scaffolds were 3D printed, added to the calcium bath, rinsed with 1 x PBS, and proliferation analyses were conducted as previously described.

4.2.6 Mechanical properties

To investigate the mechanical properties of scaffolds composed of the alginate-PVA-HA-increased collagen (6.5 % (w/v)) formulation, scaffolds were 3D printed as previously described and incubated in either 0.5 % (w/v) or 1.0 % (w/v) $CaCl_2$ for 30 minutes. Scaffolds were rinsed with 1x PBS after which the diameters were measured with a micrometer. Scaffolds were then transferred to a 24 well plate, incubated with 1 mL of α-MEM supplemented with 1 % (w/v) penicillin. They were then incubated in a waterbath at 37 °C for 10 days, with the media exchanged every other day.

Dynamic mechanical analysis (DMA) was completed using a DMA 2980 Dynamic Mechanical Analyzer (T.A. Instrument Inc., New Castle, DE) in compression mode. Scaffold diameters were measured before loading onto the 40 mm sandwich fixtures. A uniform stress

rate of 0.5 N per minute was ramped from 0 to 18 N. The stress-strain curve was obtained and the compressive modulus was calculated from the slope of the linear elastic region within the initial 15% strain.

4.2.7 Statistical analysis

Results were statistically analyzed using one-way analysis of variance (ANOVA) and expressed as mean ± standard deviation. Statistical significance was defined as $p < 0.05$.

4.3 Results

4.3.1 3D printing of scaffolds with different infill geometries

Scaffolds of original and alternating infill geometries were 3D printed and are shown in Figure 4.2a and 4.2b, respectively. The control formulation, shown in Figure 4.2c, was unable to produce scaffolds of high shape fidelity and thus lacked the macroporosity achieved by the alginate-PVA-HA formulation. All scaffolds are 1.5 cm in diameter.

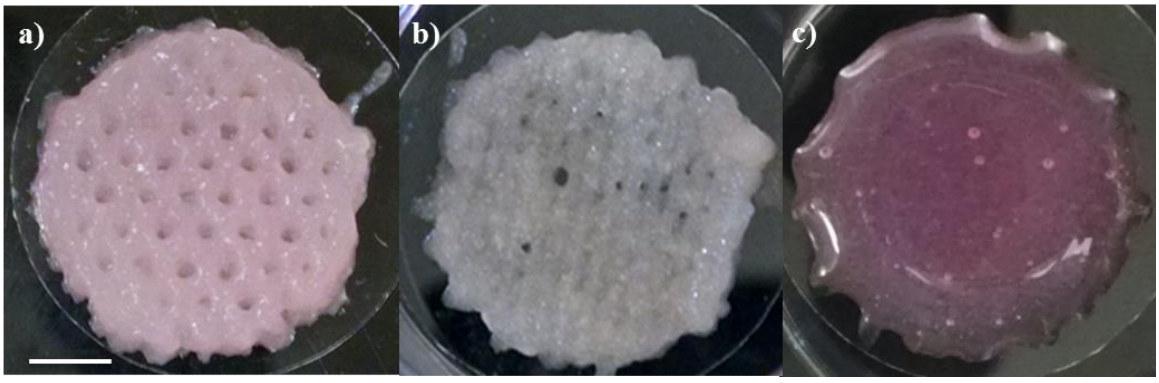

Figure 4.2: 3D printed a) original design b) alternating design and c) control scaffolds (Scale bar 3.75 mm)

4.3.2 Evaluation of proliferation

4.3.2.1 Infill geometry

Cellular reduction of alamarBlue and thus cell number over 10 days showed little to no proliferation of MC3T3 cells in any of the 3D bioprinted scaffolds, as shown in Figure 4.3. No statistical differences in cellular reduction were observed between scaffolds of original and alternating infill designs. A slight increase in reduction was observed for scaffolds of original and alternating designs from day 1 to day 4, whereas a decrease in reduction was seen in control scaffolds during the same time period.

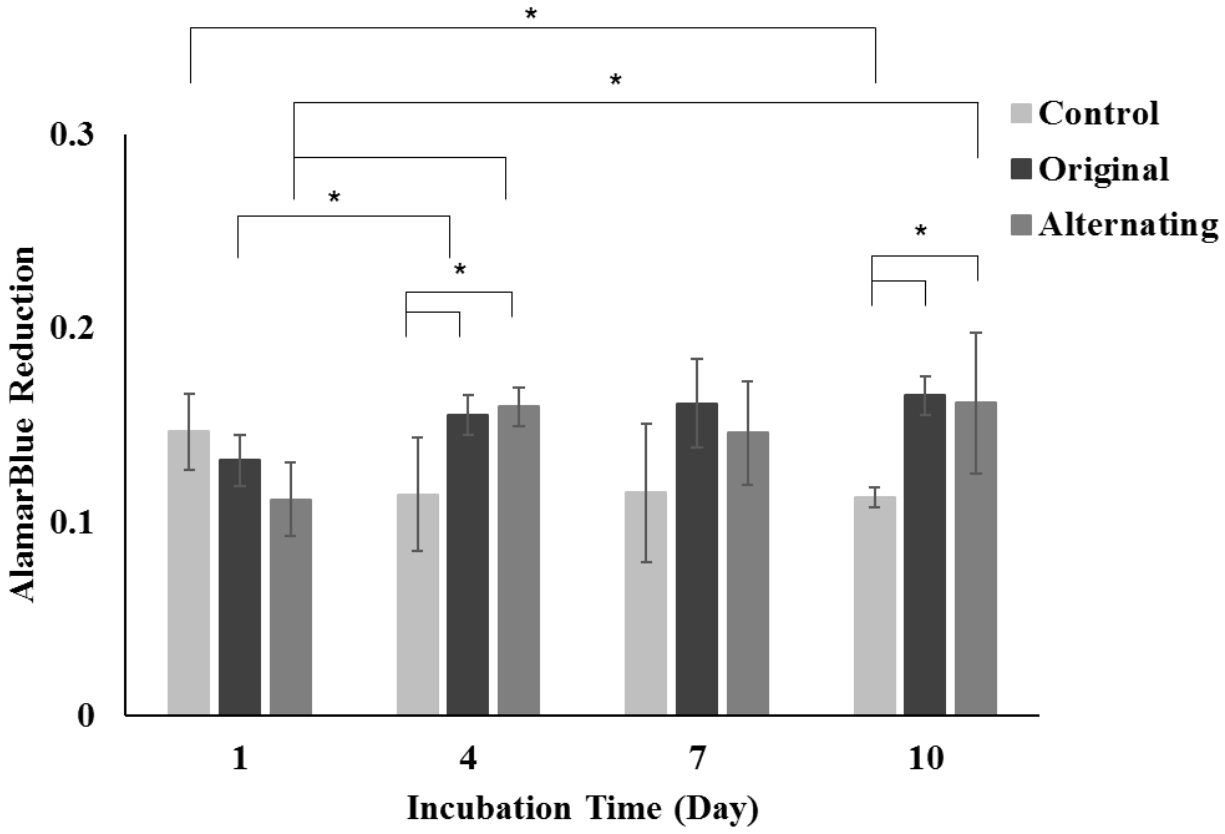

Figure 4.3: Proliferation of cells in 3D bioprinted scaffolds after 1 % (w/v) $CaCl_2$ bath ($p < 0.05$, ANOVA, $n \geq 3$)

4.3.2.2 Effects of calcium bath

The decrease in calcium concentration of the calcium bath from 1.0 % to 0.5 % (w/v) $CaCl_2$ for bioprinted scaffolds of original and alternating infill designs resulted in a slight increase in cellular reduction of alamarBlue on day 1, but no further increase in cell number was observed over 7 days, as seen in Figure 4.4. A slight decrease in reduction and thus cell number was observed on day 7 for both scaffold types.

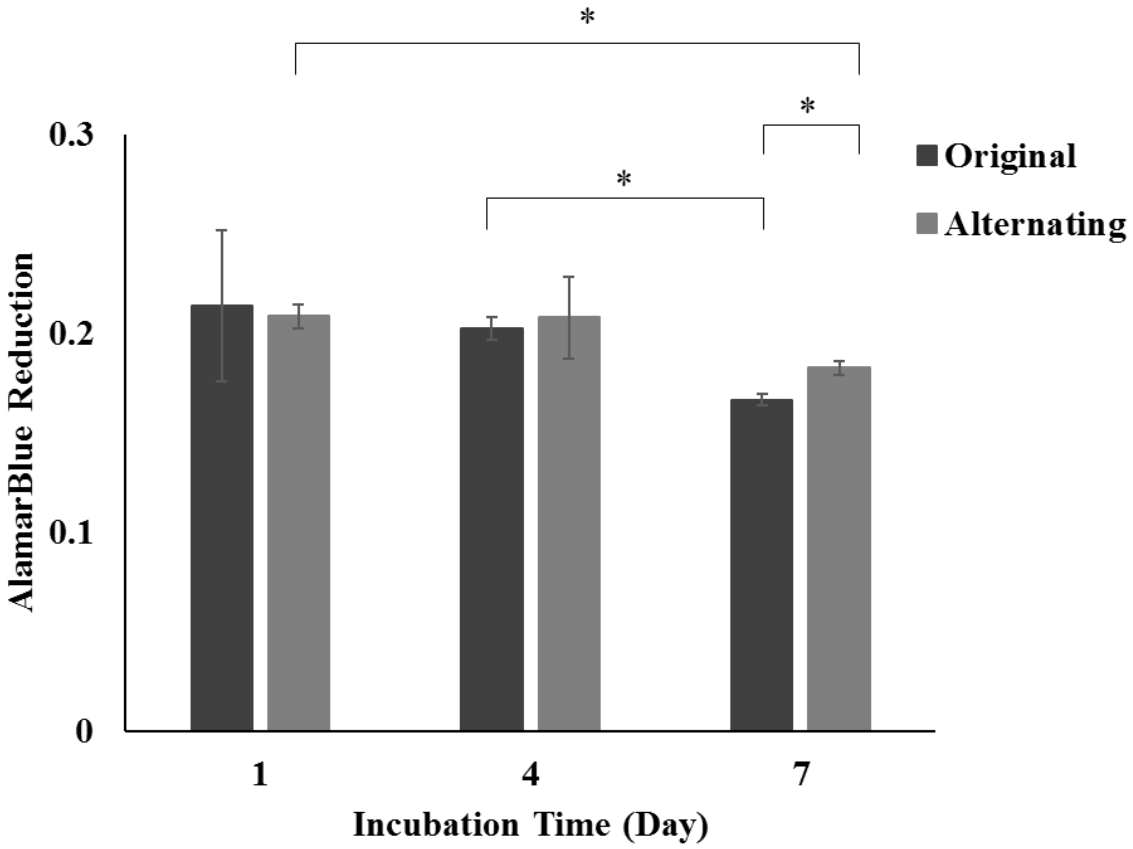

Figure 4.4: Proliferation of 3D bioprinted scaffolds after 0.5 % (w/v) $CaCl_2$ bath ($p < 0.05$, ANOVA, n = 2)

4.3.2.2.2 Calcium cytotoxicity analysis

Figure 4.5 shows the reduction of alamarBlue by MC3T3 cells with or without incubation in a calcium bath. After exposure to calcium for 30 minutes, cells incubated in 0.5 % and 1.0 % $CaCl_2$ exhibited 6.1 % and 7.3 % less reduction, respectively, compared to the control in which cells were not exposed to calcium. The difference in reduction from the control was only statistically significant for cells in scaffolds incubated in 1.0 % $CaCl_2$ baths.

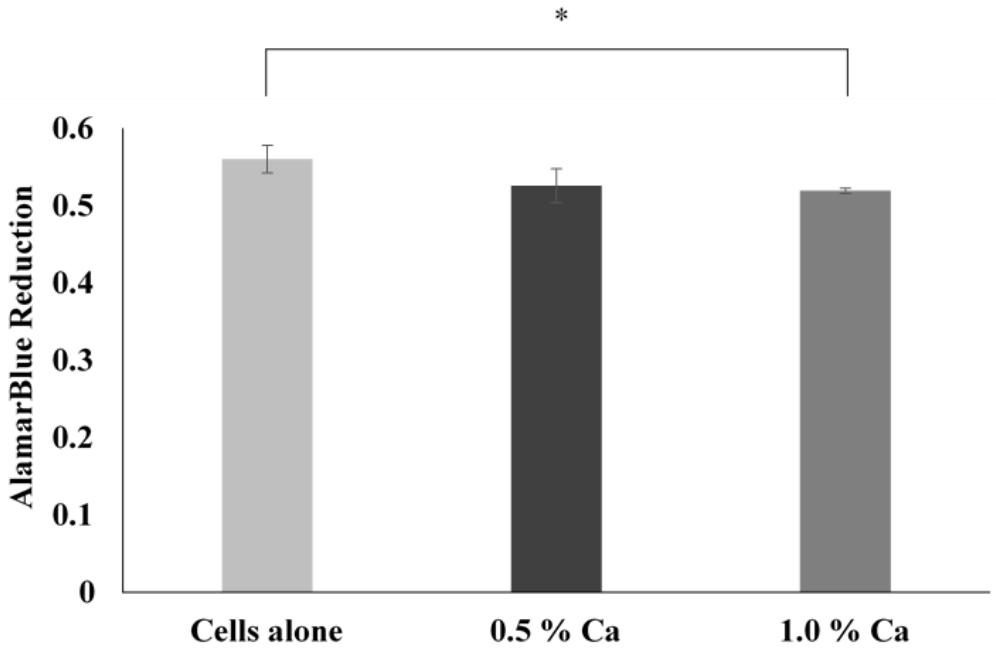

Figure 4.5: Cytotoxic study of MC3T3 cells incubated in calcium baths of various concentrations ($p < 0.05$, ANOVA, n = 3)

4.3.2.2.3 Scaffold diffusion properties

The cumulative release profile of FITC-dextran from the 3D printed scaffolds after incubation in the calcium bath is shown in Figure 4.6a. Dextran was incorporated to serve as a

model molecule and obtain insight on the diffusion properties of nutrients and waste through the scaffolds. Figure 4.6a shows the release profile over 3 days, while Figure 4.6b shows a zoomed in profile of the first 1.5 hours of incubation in fresh cell culture media. Release from the scaffolds during incubation in the calcium bath was difficult to accurately quantify and was thus not included as the precipitated calcium present in the aliquots interfered with the fluorescent readings and all values were amplified. During incubation in fresh cell culture media for three days, approximately 11, 8, and 5 µg of FITC-dextran were released from the control, original and alternating design scaffolds incubated in 1.0 % (w/v) $CaCl_2$, respectively. Approximately 14, 10 and 6 µg of FITC-dextran were released from control, original and alternating design scaffolds incubated in 0.5 % (w/v) $CaCl_2$, respectively.

a)

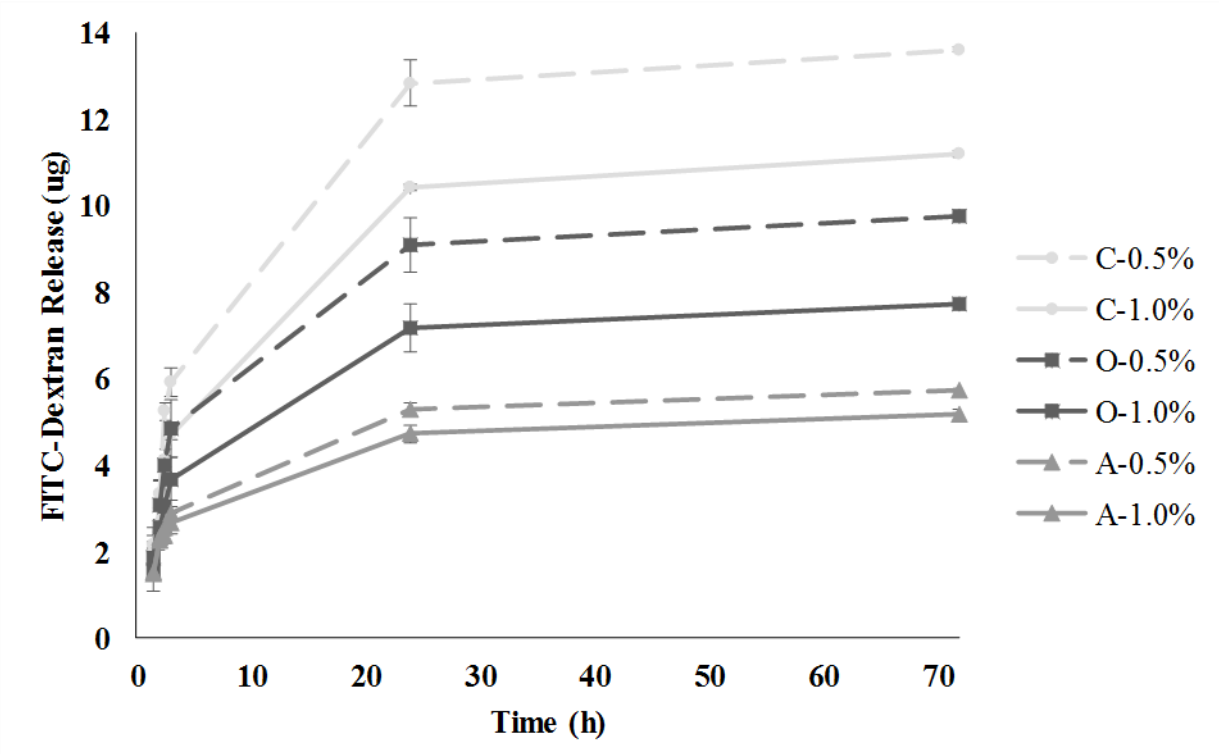

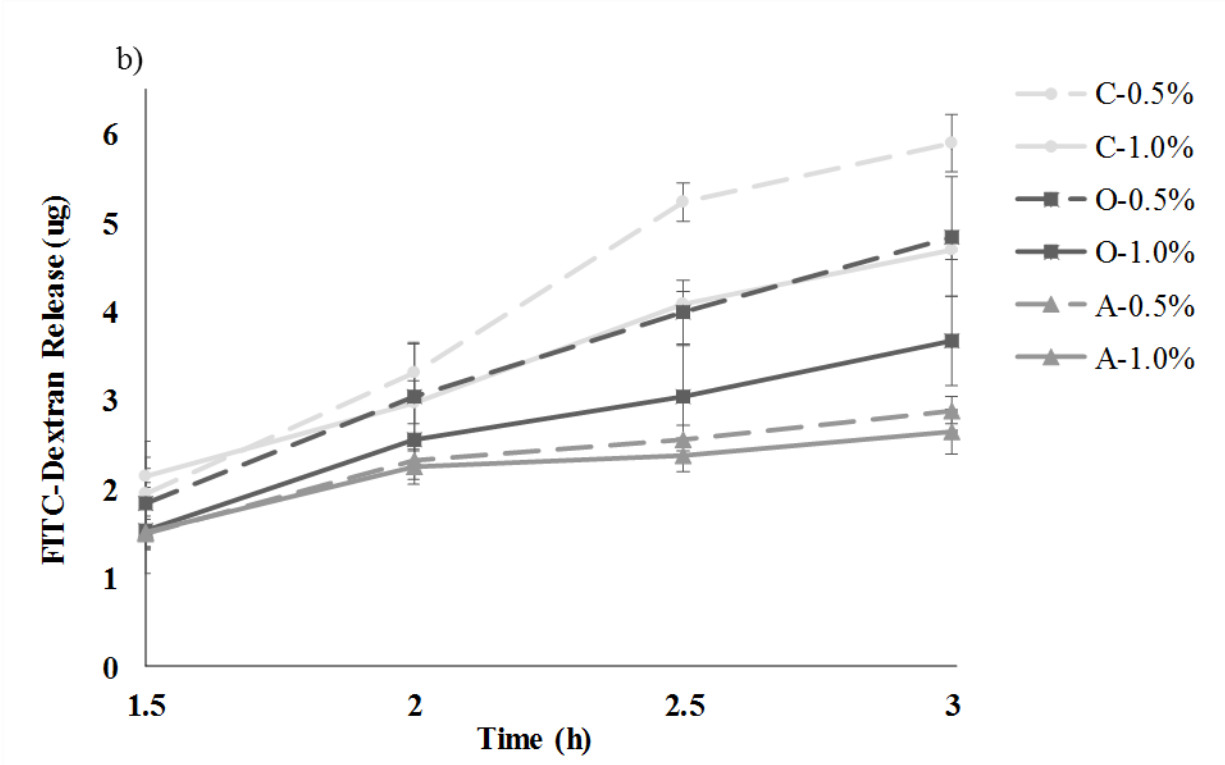

Figure 4.6: a) Cumulative release profile of FITC-dextran from scaffolds with control (C), original (O) and alternating (A) infill designs incubated in 0.5 % or 1.0 % $CaCl_2$ b) Magnified release profiles of 1.5-3 hours

Figure 4.7 shows the permeability coefficient of FITC-dextran released from each scaffold type incubated in both 0.5 % and 1.0 % (w/v) $CaCl_2$ baths, calculated from the release profile from 1.5 to 3 hours. For each infill design, scaffolds incubated in 0.5 % (w/v) $CaCl_2$ baths expressed greater permeability than those incubated in 1.0 % (w/v) $CaCl_2$ baths. Scaffolds of the original infill design displayed the greatest permeability values. Diffusion coefficients were calculated and are listed in Table 4.1.

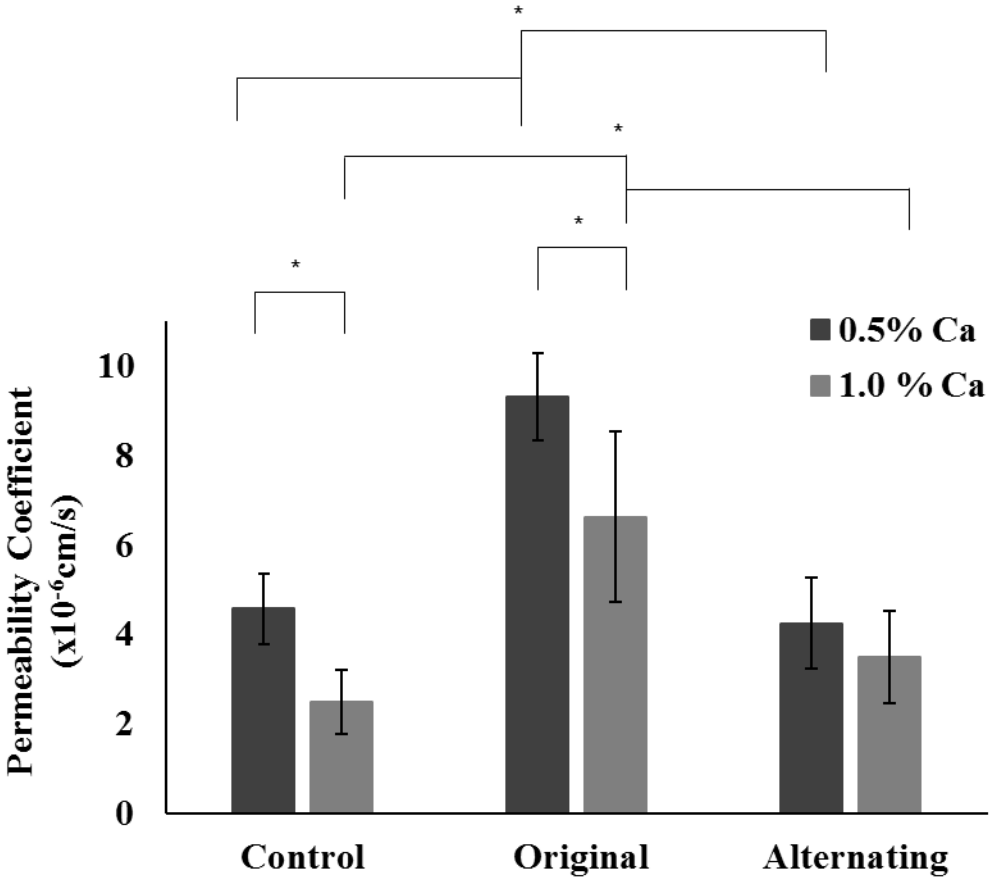

Figure 4.7: Permeability coefficients of FITC-dextran released from 3D printed scaffolds ($p <$ 0.05, ANOVA, n = 3)

Table 4.1: Diffusion coefficients of FITC-dextran from 3D printed scaffolds

Infill geometry	Diffusion Coefficient (cm^2/s)	
	0.5 % (w/v) $CaCl_2$	1.0 % (w/v) $CaCl_2$
Control	7.31E-07	3.97E-07
Original	1.49E-06	1.06E-06
Alternating	6.80E-07	5.59E-07

4.3.2.3 Effect of collagen content

Reduction of alamarBlue by cells 3D bioprinted into scaffolds with 5.0 % (w/v) collagen under various conditions can be seen in Figure 4.8a. Cells 3D printed into collagen containing scaffolds incubated under all conditions exhibited greater reduction on day 1 compared to cells printed in scaffolds without collagen. A significant change in cell number was not observed over 10 days for prints incubated in the 0.5 % (w/v) $CaCl_2$ bath for 1 hour. When the duration of the calcium bath was decreased to 30 minutes and a 1x PBS rinsing step was added, a significant increase in reduction was observed on day 1, however, no significant increase in reduction was observed over 10 days. Scaffolds incubated in 1.0 % (w/v) $CaCl_2$ baths for 30 minutes exhibited lower reduction on day 1 followed by a slight increase in reduction until day 7 and a decrease on day 10. The addition of a 1x PBS rinsing step resulted in a slight increase in reduction over 10 days.

Figure 4.8b shows cellular reduction of alamarBlue in scaffolds printed with increased collagen content. When the collagen content was increased to 6.5 % (w/v), printed scaffolds incubated in 0.5 % (w/v) $CaCl_2$ for 30 minutes showed comparable reduction to prints with 5.0 % (w/v) collagen for the duration of the study, with a slight decrease in reduction observed on

day 7 but an increase on day 10. Cells printed in scaffolds with 6.5 % (w/v) collagen and incubated in a 1.0 % (w/v) $CaCl_2$ bath showed significantly higher reduction at each time point. Additionally, an increase in reduction was observed until day 7 in culture, followed by a slight decrease in reduction on day 10.

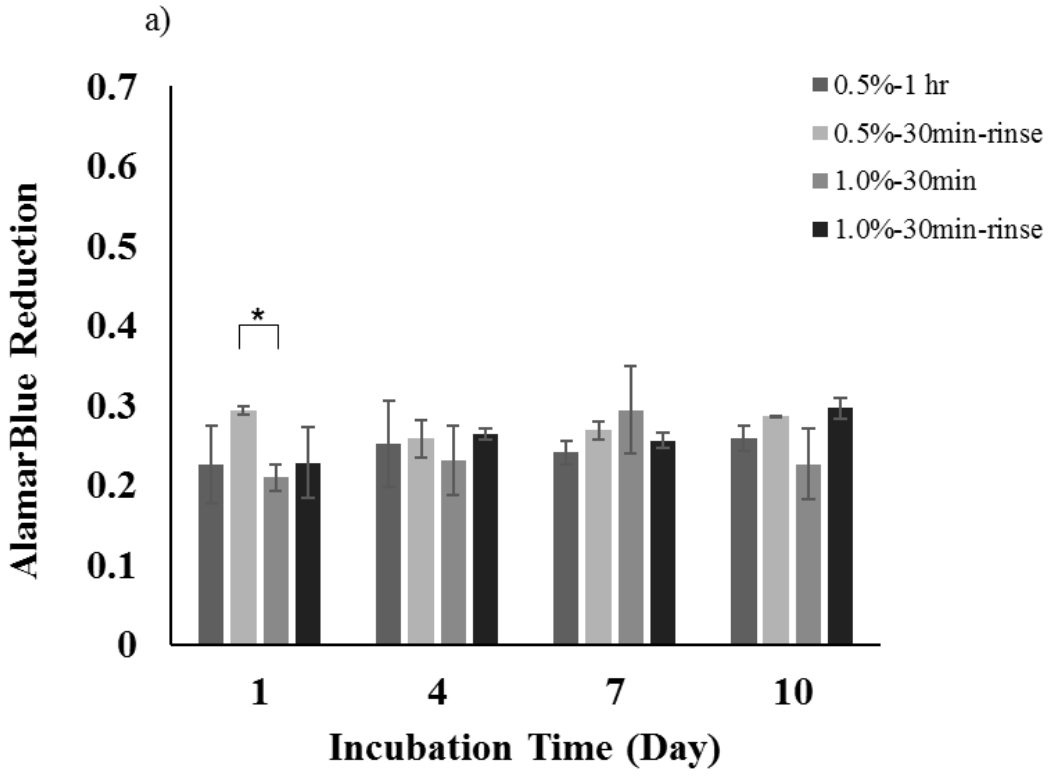

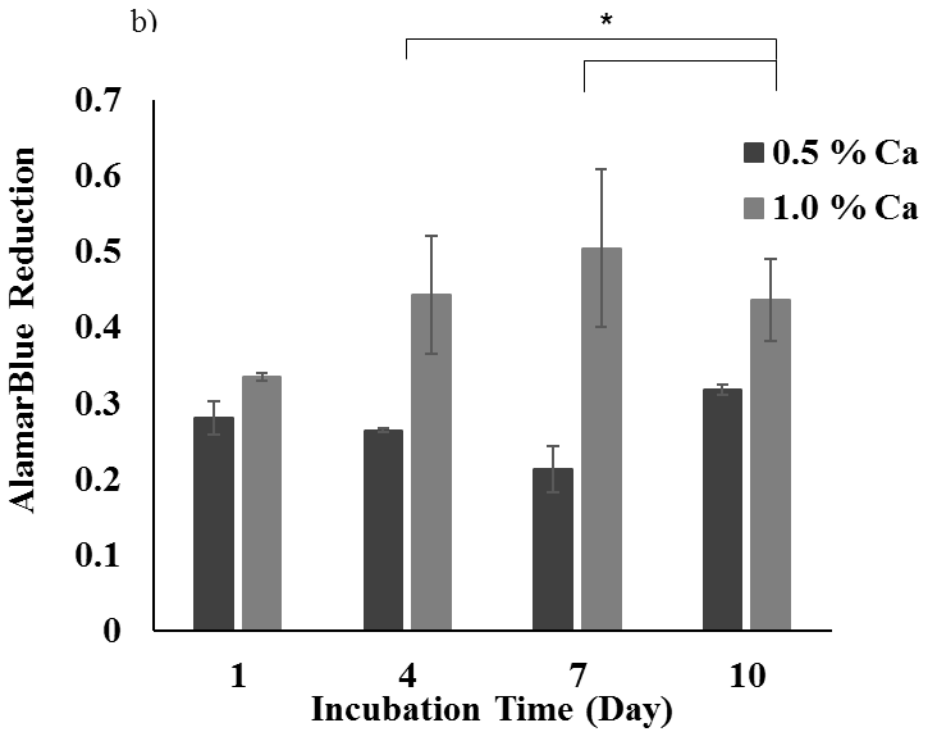

Figure 4.8: AlamarBlue reduction by cells 3D printed into scaffolds with a) 5.0 % (w/v) and b) 6.5 % (w/v) collagen incubated in 0.5 % (w/v) and 1.0 % (w/v) $CaCl_2$ baths ($p < 0.05$, ANOVA, n = 2)

4.3.3 Mechanical properties

The compressive moduli of 3D printed scaffolds with increased collagen content (6.5% (w/v)) incubated in a 0.5 % or 1.0 % (w/v) $CaCl_2$ bath for 10 days in *in vitro* culture conditions are shown in Figure 4.9. Initially after 1 day in culture, scaffolds incubated in 1.0 % (w/v) and 0.5 % (w/v) $CaCl_2$ had average compressive modulus values of 9.5 kPa and 8.0 kPa, respectively. Scaffolds incubated in both calcium bath concentrations displayed a statistically significant decrease in compressive moduli on day 4 but did not continue to significantly decrease for the duration of the study. After day 1, scaffolds incubated in 1.0 % $CaCl_2$ continued to display

higher compressive moduli values than those incubated in 0.5% $CaCl_2$ for the duration of the study, although only statistically significant on day 7.

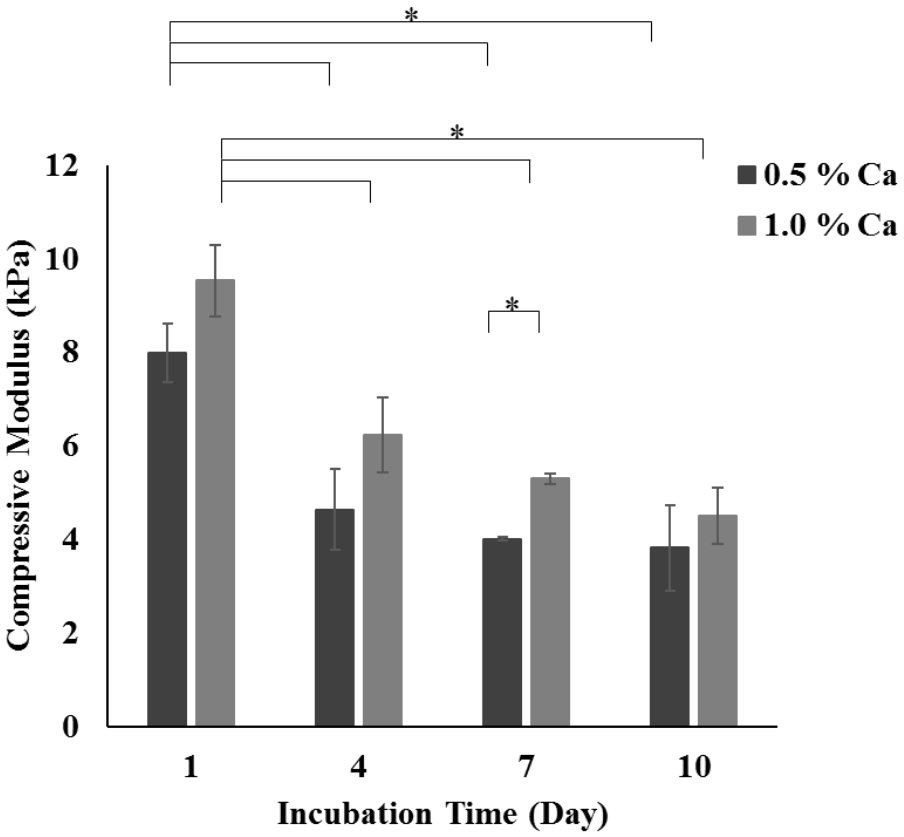

Figure 4.9: Compressive moduli of increased collagen scaffolds throughout degradation study ($p < 0.05$, ANOVA, n = 2)

4.4 Discussion

4.4.1 Proliferation

As we previously identified an optimal hydrogel formulation capable of 3D bioprinting scaffolds of high shape fidelity and initial cell viability, it was important to further investigate the capability of the hydrogel scaffolds to support long-term cellular life and activities. Before cells

can differentiate and begin to form new tissue, it is crucial that they form a cellular network within the hydrogel matrix and begin to migrate and proliferate.[172] In order to follow the natural progression of processes resulting in tissue formation, there must first exist cell adhesion ligands within the hydrogel matrix mimicking those present in the native extracellular matrix that promote cell attachment and bind to transmembrane integrin receptors on the cell surface.[166] If these adhesions sites aren't present within the matrix, cells may remain viable but unable to attach and spread throughout the matrix, resulting in a rounded morphology that prevents migration and proliferation. Alginate, a polysaccharide derived from algae, is a widely used biocompatible hydrogel material that has been reported to promote limited cell adhesion on its own.[173] Thus, alginate is commonly chemically modified with RGD peptide sequences or combined with additional elements to provide cells with adhesion ligands to enhance cell attachment.[74,85] In this work, we originally incorporated polyvinyl alcohol and hydroxyapatite in the form of a suspension into our alginate formulation to increase the biocompatibility and promote cell attachment throughout the scaffolds. Polyvinyl alcohol has been reported to be highly biocompatible polymer promoting cellular activities.[55] Hydroxyapatite, as it is the main mineral component in natural bone, was incorporated in the hydrogel to provide an environment favorable for promoting MC3T3 cell differentiation into osteoblasts and enhancing calcium phosphate deposition. It has also been reported that cells have the ability to attach to HA particles.[174,175]

4.4.1.1 Effects of infill geometry

Scaffolds of varying infill geometries were 3D printed using a novel alginate-PVA-HA formulation to investigate the effect of the geometry on cellular activities and proliferation. An

original design with a honeycomb infill and 60% macro-porosity was first investigated, followed by an alternating rectilinear infill design, also of 60% macro-porosity. A control formulation, lacking the PVA-HA suspension, was included to determine the effect of the suspension on both printability and cell proliferation. Figure 4.3 shows that MC3T3 cells encapsulated in the alginate-PVA-HA formulation and 3D printed into scaffolds of original design showed a constant reduction profile and thus limited proliferation in *in vitro* culture for 10 days. As a significant decrease in cell number was not observed, it can be concluded that the cells are not dying but are alive and merely abstaining from appropriate metabolic and physiological activities, such as proliferation. This indicates that the formulation did not provide a favorable enough environment suitable for substantial cell attachment and proliferation. As previously discussed, cells must bind to the matrix via integrins in their cytoskeletons and ligands within the matrix in order to form a network and proliferate sufficiently. Thus, although originally hypothesized to be capable of promoting adhesion, the presence of the polyvinyl alcohol-hydroxyapatite suspension alone was not enough to promote cell spreading and migration necessary for proliferation. Similarly, cells encapsulated in scaffolds with the alternating infill design showed limited proliferation throughout the scaffold within the 10 day time period. Although drastic changes in infill geometry and porosity have been shown to affect proliferation in PLA-collagen scaffolds for osteochondral regeneration, it was not observed in this study.[139] This suggests that for our scaffolds, the material selection and lack of cell adhesion modalities had a greater effect on proliferation than the infill design. When the control formulation was used to print scaffolds of the original infill design, the resulting scaffolds lacked the intended macro-porosity of the design. This is because the PVA-HA suspension provides the formulation with an optimal viscosity for 3D printing scaffolds of high shape fidelity. Thus, control scaffolds

supported slightly lower cell numbers than the scaffolds printed with the optimal formulation throughout the *in vitro* study, but cells were still viable. Although the cells exhibited a slight decrease in reduction from day 1 to day 4, suggesting cell death, the scaffolds did not decrease in cell number for the remainder of the study. This suggests that the degree of microporosity within the control scaffolds was sufficient to support cell life, but was unable to promote cell proliferation, similar to scaffolds of the original and alternating infill designs.

4.4.1.2 Effects of calcium bath

As cell exposure to high concentrations of calcium has been reported to negatively affect cellular activities, the concentration of the calcium bath in this study was reduced to 0.5 % (w/v) $CaCl_2$ in hope to increase cell proliferation throughout the scaffolds.[159] Although a low concentration of calcium is present in the cytoplasm to promote vital cell functions such as attachment, motility and signal transduction, cell exposure to high concentrations of calcium for extended periods of time has been reported to damage the cell membrane and even program cell apoptosis.[159,176] Thus, it was important that we investigate the effect of the calcium bath on cell proliferation. Although an initial increase in cell number was observed on day 1 when the concentration of the calcium bath was reduced, Figure 4.4 shows that an increase in proliferation was still not observed for 7 days for cells 3D printed in scaffolds of either original or alternating infill designs.

4.4.1.2.1 Calcium cytotoxicity analysis

To further investigate if the calcium bath had a negative effect on MC3T3 cell activity, cells were seeded in a well plate and exposed to 0.5 % or 1.0 % (w/v) $CaCl_2$ for 30 minutes. This

simulated the incubation of the printed scaffolds in calcium baths for further crosslinking of the alginate chains. As cells incubated in both calcium bath concentrations exhibited reduction levels close to that of cells without incubation in calcium, shown in Figure 4.5, it can be concluded that the metabolic activity of the cells was not significantly affected by exposure to calcium concentrations of 0.5 % (w/v) and 1.0 % (w/v), agreeing with results reported in literature.[98] Lee *et al.* [76] showed that MC3T3 cells encapsulated in 1.0 % and 2.0 % alginate beads exposed to 1.0 % (w/v) $CaCl_2$ for 1 hour displayed initial viability over 98 % and expressed substantial proliferation in *in vitro* culture. Thus, in this case, the calcium bath at concentrations less than or equal to 1.0 % (w/v) did not negatively affect the cells or inhibit their proliferation in 3D printed scaffolds.

4.4.1.2.2 Scaffold diffusion properties

The release of FITC-dextran from 3D printed scaffolds was quantified in order to determine whether the 3D printed scaffolds provided the encapsulated cells with sufficient nutrient influx and waste removal to support cell life and appropriate physiological functions. The extent of crosslinking of the alginate chains with calcium ions has an effect on the diffusion properties of the resulting hydrogel. Calcium and other divalent cations bind with the carboxyl and hydroxyl groups of the alginate G blocks in the polymer backbone to form egg box structures.[50] Lateral stacking of these egg boxes results in crosslinking and contraction of the alginate matrix. Thus, during incubation in the calcium bath, calcium ions diffuse into the scaffolds to further crosslink, resulting in shrinkage of the 3D printed scaffolds.

Figure 4.6a shows the release profile for each scaffold type over 3 days. For each scaffold type, scaffolds incubated in 0.5 % (w/v) $CaCl_2$ baths showed a greater release than those

incubated in 1.0 % (w/v) $CaCl_2$ baths. This can be attributed to the fact that the lower calcium concentration results in a lower degree of crosslinking and thus lower mechanical properties of the scaffolds.[38,155,177] Thus, the weaker scaffolds are prone to a greater degree of media intake and swelling, leading to increased diffusion of the FITC-dextran out of the matrix and into the surrounding media.[178] Figure 4.6a also shows a greater final release of FITC-dextran for the control scaffolds. Because the control scaffolds lack the intended macro-porosity exhibited by the other scaffold designs, the calcium influx, crosslinking and scaffold shrinkage are minimal during incubation in the calcium bath. As diffusion is limited during this period, there was minimal release of FITC-dextran from the matrix out into the calcium bath. Thus, a greater amount of FITC-dextran was released for the remainder of the study. Similarly, it can be inferred from the release profile that the scaffolds of the alternating infill design released the most FITC-dextran during the calcium bath. This can be due to the fact that the alternating design resulted in scaffolds of increased interconnected infill with the same degree of porosity. Thus, the scaffolds exhibited a greater degree of crosslinking during this time period, resulting in a greater amount of FITC-dextran being squeezed out of the matrix into the surrounding media. Scaffolds of the alternating infill design reach lower cumulative release values for the remainder of the study as there was less FITC-dextran to start with after the calcium bath. Scaffolds of the original infill design exhibited an intermediate release value as the macro-porosity allowed release of FITC-dextran during the calcium bath but not to the extent reached by scaffolds of the alternating infill design. Thus, a greater amount of FITC-dextran was released from scaffolds of the original infill design compared to the alternating infill design for the remainder of the study.

The permeability and diffusion coefficients of FITC-dextran released from the 3D printed scaffolds of various infill geometries were determined using the linear region of the initial 1.5

hours in incubation in after the calcium bath, seen in Figure 4.6b. Figure 4.7 shows the permeability coefficients and Table 4.1 reports the diffusion coefficients of FITC-dextran. All values are greater than those reported in literature, indicating the scaffolds are sufficient for proper nutrient diffusion and waste removal to support cell life.[179,180] As previously discussed, the scaffolds of the alternating infill design released the most FITC-dextran in the calcium bath, resulting in a lower permeability coefficient for the following incubation period. For each scaffold type, the permeability is greater for scaffolds crosslinked in the 0.5 % (w/v) $CaCl_2$ bath compared to those in the 1.0 % (w/v) $CaCl_2$ bath as expected. As previously described, this is due to the lower degree of crosslinking as a result of the formation of fewer calcium alginate bonds.

As all scaffold types exhibit sufficient diffusivity to support cellular life and activities in *in vitro* culture, it can be concluded that the extent of crosslinking and thereby diffusion properties of the 3D printed scaffolds are not deterring the encapsulated cells from proliferating throughout the matrix.

4.4.1.3 Effect of collagen content

Collagen was incorporated into the hydrogel formulation to provide the encapsulated cells with adhesion ligands necessary to promote cellular attachment, as collagen is a ligand present in the native extracellular matrix that binds with integrins on the cytoskeleton.[181,182] The incorporation of collagen did not significantly affect the viscosity and thus printability of the hydrogel formulation. In order for a scaffold of high shape fidelity to be printed, it is of the most importance that the hydrogel be continuously extruded and not too viscous to clog the needle.[170] Also, it must not negatively impact the capability of the formulation to protect the encapsulated cells throughout the printing process and shield them from the shear stresses applied during

extrusion.[97] As the collagen was incorporated in a gel state, it did not impose additional stress or difficulties during printing.

Initially, the addition of 5.0 % (w/v) collagen to 3D bioprinted scaffolds of the alternating infill design that were incubated in 0.5 % (w/v) $CaCl_2$ bath for 1 hour showed a slight increase in proliferation until day 4 but remained relatively constant for the remainder of the study, seen in Figure 4.8a. A decrease in the calcium bath duration and addition of a rinsing step resulted in an increase in cell number on day 1, providing a more favorable initial environment for cell survival. However, the cell number remained constant throughout the study as before. As the mechanical properties of the scaffold also play a critical role in affecting cell proliferation, the concentration of the calcium bath was increased to 1.0 % (w/v) $CaCl_2$ to provide the scaffold with enhanced crosslinking as well as stiffness. This achieved a proliferation profile more closely resembling that as expected, with a slight increase in cell number until day 7 followed by a slight decrease on day 10. The addition of the rinsing step to remove excess calcium ions resulted in a slight increase in cell number until day 10. Although the collagen showed promise in improving cell proliferation throughout the scaffolds, the limited increase in cell number suggested that the hydrogel matrix composition could be modified further to achieve a more optimal environment for enhancing cell proliferation and natural physiological behaviors. Thus, the collagen content was further increased to provide the cells with increased ligand binding site density in hope to enhance attachment and proliferation.

An increase in collagen content to 6.5 % (w/v) in scaffolds incubated in 0.5 % (w/v) $CaCl_2$ bath for 30 minutes did not have a significant effect on proliferation, shown in Figure 4.8b. Although the cells were provided with an increase in ligand density and thus initial attachment sites, the lower amount of calcium ions available in the bath resulted in the formation

of fewer crosslinks. This proved the importance of the synergistic presence of ligands and scaffold mechanical rigidity as soft scaffolds were unable to support proliferation.[184] When the calcium bath concentration was increased to 1.0 % (w/v) $CaCl_2$, an increase in reduction and thus cell proliferation was observed until day 7 in culture. The increased collagen content and alginate-calcium crosslinks offered a scaffold with sufficient adhesion ligands and appropriate mechanical rigidity necessary for cells to attach and proliferate. The slight decrease in cell number, although not significant, observed on day 10 can be attributed to a decrease in metabolic activity. MC3T3 cells have been reported to reach a quiescent state by day 9 in *in vitro* culture.[183] At this point, they exit the G1 cellular growth phase, and enter the G0 phase in which the cells stop dividing and lose their metabolic activity. As alamarBlue is a measure of metabolic activity and a cell's ability to reduce resazurin, a decrease in reduction at day 10 doesn't signify cell death but cell maturation. At this stage, an external stimuli is necessary to induce the cells to proceed with differentiation. Thus, it can be inferred that the MC3T3 cells in the 3D printed scaffolds are ready for differentiation. However, external biological cues and osteogenic media including ascorbic acid and β-glycerophosphate are necessary to promote differentiation into osteoblasts. Thus, the 3D printed scaffolds with increased collagen content and appropriate mechanical rigidity have a great potential to support cellular proliferation and achievement of a state ready for differentiation.

4.4.2 Mechanical properties

Mechanical rigidity and integrity of the 3D printed scaffolds also has a significant effect on the ability of cells to effectively attach to and proliferate throughout the matrix.[184,185] Figure 4.9 shows that after 1 day in culture, scaffolds incubated in 1.0 % $CaCl_2$ exhibited higher

compressive moduli values than those incubated in 0.5 % $CaCl_2$. This can be attributed to the increased calcium content available to crosslink the alginate chains, as previously discussed. With increased time in culture, scaffolds incubated in both calcium concentrations exhibited a decrease in compressive modulus, due to ion exchange between calcium ions involved in the crosslinking with alginate carboxyl groups with sodium ions in the surrounding media.[38] Thus, as crosslinks are broken, scaffolds uptake media, swell, and lose their mechanical stability. It was determined that the increase in initial crosslinks throughout the scaffolds incubated in 1.0 % $CaCl_2$ baths provided the mechanical stability necessary that when coupled with the increased collagen and thus ligand content resulted in the most favorable environment for cell proliferation. Scaffolds incubated in 1.0 % $CaCl_2$ provided a more rigid matrix on day 7 which is a crucial time point for cell proliferation and migration. The matrix needs to provide the cells with a rigid substrate to withstand the contractile forces imposed by cells during migration.[186,187] Thus, a synergistic effect exists in which the mechanical properties coupled with the biological environment must both be sufficient for the cells to achieve significant proliferation.

As MC3T3 cells are pre-osteoblasts in origin, they prefer and achieve optimal proliferation on stiff substrates with compressive moduli closer to that of natural bone.[188] Thus, a further increase in the compressive modulus of the scaffolds may result in a more optimal environment to promote proliferation and differentiation of MC3T3 cells. This could be achieved by increasing the hydroxyapatite content in the formulation as long as the viscosity and printability of the hydrogel isn't affected.

4.4.3 Conclusions

In the work described in this chapter, we have systematically investigated methods to increase the proliferation of MC3T3 cells 3D printed into scaffolds composed of a novel hydrogel formulation. It was determined that only the synergistic effect of sufficient ECM ligand density coupled with proper mechanical rigidity provided a suitable environment for proliferation. The enhanced collagen content was necessary to provide the cells with sufficient attachment sites to the matrix while the increased calcium content in the calcium bath was necessary to provide sufficient crosslinking and adequate mechanical resistance to withstand cell contractile forces necessary for proper migration. Separately, these factors did not promote cell proliferation. It was determined that all scaffolds exhibited diffusion properties to necessary support sufficient nutrient influx and waste removal. The proliferation profile achieved by MC3T3 cells 3D printed in scaffolds with increased collagen content suggests that by day 10 in culture the cells are waiting to receive external cues to begin differentiation. Thus, future *in vitro* differentiation and *in vivo* studies must be conducted to determine if the MC3T3 cells have maintained their natural physiological functions and bone making capabilities after 3D printing and crosslinking of the scaffolds. This *in vitro* evaluation of our novel 3D printed tri-polymer alginate-PVA-HA-collagen scaffolds shed light on the scaffolds' ability to support cell viability and potential to promote differentiation in future studies.

Chapter 5

Conclusions and Future work

5.1 Conclusions

In this work, novel alginate hydrogel systems were developed to aid in the progression of more personalized methods for treating defective bone tissue. The gelation properties of alginate hydrogel formulations were thoroughly investigated and control of gelation kinetics was established through introduction of a retardation agent as well as by varying the concentrations of the constituents. A novel alginate-collagen-hydroxyapatite hydrogel formulation was developed with a gelation time suitable in a surgical setting. Novel *in situ* formation of this system results in an environment more closely mimicking that of natural bone, and has potential as an injectable bone tissue substitute through less invasive means. Not only can this system be implemented to fill irregular bone defects and breaks but it can be implemented to fill areas of osteoporotic bone as well. This would promote healing of the area and prevent further progression of the weakened bone and future injuries by inducing formation of new, strong bone. The unique gelation properties also allow incorporation of drugs and/or cells to treat osteoporosis and enhance further new bone formation.

The innate material properties and versatility of alginate then allowed translation of the novel hydrogel system to application in the ever-growing, popular field of 3D printing technology. A systematic investigation was conducted and a novel alginate-polyvinyl alcohol-hydroxyapatite hydrogel formulation suitable for 3D printing scaffolds of high shape fidelity was developed. Rheology of the formulations was completed to understand the differences in storage moduli associated with printability and determine what range enabled the hydrogel to be easily

extruded and recover upon deposition, forming scaffolds of high shape fidelity. The degradation properties of the scaffolds were then investigated and it was determined that scaffolds maintained integrity over 14 days in culture, indicating they are capable of physically supporting cell life over this time period. Most importantly, live MC3T3 cells were incorporated into the optimal alginate-PVA-HA hydrogel formulation and 3D printed at high viability rates. Collectively, the results of this study suggest that this formulation has potential to 3D bioprint structures capable of supporting cell life in culture, with the novel composition providing an environment favorable of promoting tissue regeneration.

Finally, *in vitro* studies were conducted to assess the scaffolds' ability to promote proliferation of MC3T3 cells and potential for their differentiation into osteoblasts. Initial results showed limited proliferation of cells encapsulated in the original alginate-PVA-HA scaffolds. Further efforts to increase proliferation showed that the concentration and duration of the calcium bath have a less effect on proliferation than the composition of the formulation itself. Thus, a novel alginate-PVA-HA-collagen tri-polymer formulation was developed, providing an environment most favorable for proliferation. It was determined that this was due to the synergistic effect presented by the presence of increased adhesion ligand density within the collagen with the increased mechanical properties as a result of increased crosslinking. This systematic investigation shed light on properties of the hydrogel formulation and resulting scaffolds necessary for MC3T3 proliferation and developed an environment with potential to promote differentiation and thereby new bone formation.

Thus, the development of these alginate hydrogel systems can provide opportunities for enhanced, uniform, personalized healing of defective bone tissue due to their gelation properties

suitable for various applications and superior compositions incorporating collagen and hydroxyapatite, the two main components of natural bone.

5.2 Future work

5.2.1 Drug delivery

To expand the applications of the alginate hydrogel systems, their use in drug delivery may be investigated. Model drugs or proteins, such as bovine serum albumin (BSA), may be incorporated into the alginate suspension before the addition of the calcium sulfate for encapsulation at levels of high efficiency within the alginate matrix. The formulation then may be either 3D printed and further crosslinked or be injected into an irregular mold to set before incubation in a waterbath at 37 °C for 7-14 days. The model drugs or proteins may be conjugated with fluorescent molecules such as Alexa Fluor 488 or FITC so that their release from the matrix into the surrounding media can be quantified via absorbance, read with a spectrometer. The burst release and/or sustained release profiles can then be determined and the hydrogel system's capacity as a drug carrier can be determined. Potential applications include incorporation of alendronate, a biophosphonate that hinders bone resorption of osteoclasts, into the alginate matrix for sustained release to help treat osteoporosis.

5.2.2 3D printing scaffolds of irregular architectures

As it is of interest to apply 3D printing of these novel alginate hydrogel scaffolds in a clinical setting, the ability of the hydrogel formulation to 3D print large scaffolds with irregular geometries and high shape fidelity should be investigated. Such scaffolds would possess a

jagged, irregular perimeter and size more closely resembling those of a natural bone defect. An example of the proposed scaffold is presented in Figure 5.1.

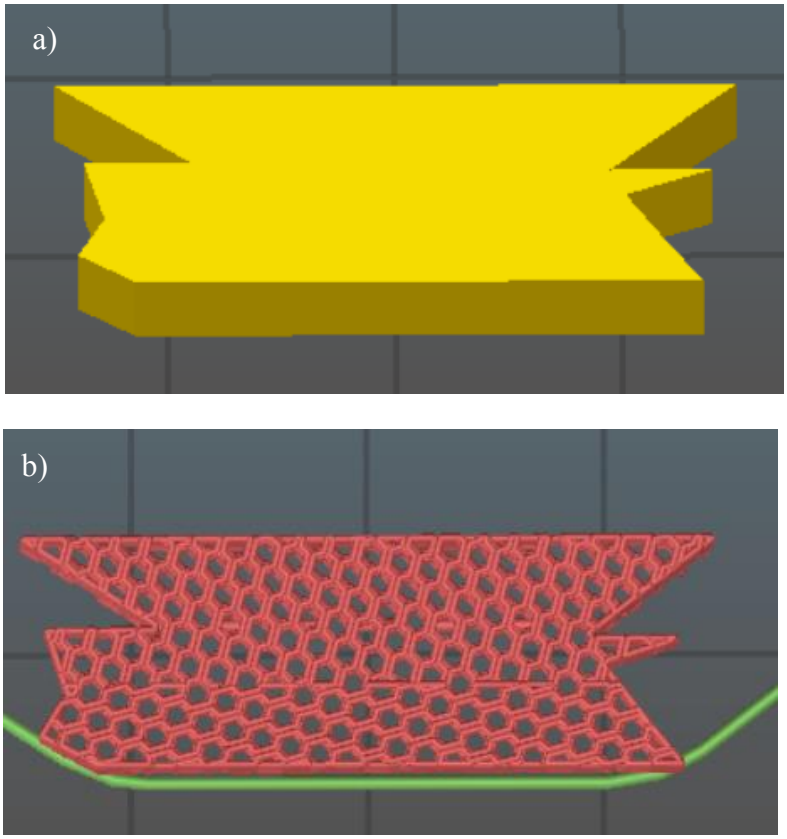

Figure 5.1: Example of a) CAD model and b) sliced .stl file of proposed irregular scaffold design

Once scaffolds of such architecture are 3D printed with high shape fidelity, application for bioprinting large scale, personalized scaffolds from a patient's CT scan or MRI can be employed. Thus, reconstruction and repair of non-load bearing, such as craniofacial, bone tissue can be achieved.

5.2.3 Further in vitro evaluation

Before the tri-polymer 3D bioprinted scaffolds can be implemented for bone healing *in vivo,* further *in vitro* evaluations must be completed to assess the scaffolds ability to promote differentiation of MC3T3 cells into osteoblasts and thus deposition of new bone. 3D printed scaffolds should be cultured in osteogenic media, in the presence of ascorbic acid and β-glycerophosphate, for 14 to 21 days. Levels of alkaline phosphatase (ALP), a by-product of osteoblast activity, can be quantified throughout the study via a colormetric assay kit. P-nitrophenol phosphate (pNNP) is dephosphorylated in the presence of ALP and can be quantified via absorbance measurements. Absorbance values can be directly correlated to the amount of ALP secreted by the cells, which is increased when osteoblasts are depositing new bone.

Levels of RUNX2, a protein reflecting MC3T3 differentiation into osteoblasts, can also be measured via PCR analysis through the duration of *in vitro* studies. RUNX2 is an early marker of bone formation as it is upregulated in immature osteoblasts, and should show an increase at about 14 days in culture.

Levels of osteocalcin and osteopontin, proteins produced by mature osteoblasts, can be measured as late markers of bone formation via ELISA kits. Osteocalcin is a non-collagenous protein in bone. Osteopontin is an organic, extracellular structural protein in bone that strongly binds to calcium based minerals, playing a vital role in bone remodeling by anchoring osteoclasts to the mineral matrix of bone. Increased levels of both proteins reflect an increase in bone density, which should occur through 14-21 days in culture. Additionally, at this stage histology can be conducted to obtain physical sections and assess the quality of new bone tissue formation.

5.2.4 In vivo evaluation

Once 3D bioprinted scaffolds show successful promotion of MC3T3 differentiation into osteoblasts and express significant signs of new bone formation *in vitro*, movement can be made towards *in vivo* testing. Tri-polymer scaffolds encapsulating MC3T3 cells of either conventional or irregular architecture can be 3D printed and implanted into rat calvarial bone tissue defects of matching geometry. New bone formation can then be monitored and evaluated over 2 months via histology, assessing the scaffolds capability to promote bone tissue regeneration *in vivo*. Completion of *in vivo* studies would thus contribute to possible alternative methods to treat personalized bone defects of patients in need of bone healing or reconstruction.

References

1) Nerem RM, Sambanis A. Tissue engineering: from biology to biological substitutes. Tissue Eng. 1995; 1: 3-13.

2) O'Brien FJ. Biomaterials & scaffolds for tissue engineering. Mater. Today. 2011; 14: 88-95.

3) Place ES, Evans ND, Stevens MM. Complexity in biomaterials for tissue engineering. Nat. Mater. 2009; 8: 457-470.

4) Stock UA, Vacanti JR. Tissue engineering: Current state and prospects. 2001; 52: 443-451.

5) Atala A. Tissue engineering and regenerative medicine: Concepts for clinical application. Rejuvenation Res. 2004; 7: 15-31.

6) Nau T, Teuschl A. Regeneration of the anterior cruciate ligament: Current strategies in tissue engineering. World J. Orthop. 2015; 6: 127-136.

7) Yang S, Leong KF, Du Z, Chua CK. The design of scaffolds for use in tissue engineering. Part I. Traditional factors. Tissue Eng. 2001; 7: 679-689.

8) Chan BP, Leong KW. Scaffolding in tissue engineering: general approaches and tissue-specific considerations. Eur. Spine J. 2008; 17: 467-479.

9) Karp JM, Dalton PD, Schoichet MS. Scaffolds for tissue engineering. MRS Bulletin. 2003; 301-306.

10) Freed LE, Vunjak-Novakovic G, Biron RJ, Eagles DB, Lesnoy DC, Barlow SK, Langer R. Biodegradable polymer scaffolds for tissue engineering. Biotechnology. 1994; 12: 689-693.

11) Rey C, Combes C, Drouet C, Glimcher MJ. Bone mineral: update on chemical composition and structure. Osteoporosis Int. 2009; 20: 1013-1021.

12) Al-Munajjed AA, Gleeson JP, O'Brien FJ. Development of a collagen calcium–phosphate scaffold as a novel bone graft substitute. Stud. Health Technol. Inf. 2008; 133: 11–20.

13) Lebourg M, Suay Anton J, Gomez Ribelles JL. Hybrid structure in PCL-HAp scaffold resulting from biomimetic apatite growth. J Mater Sci Mater Med 2010; 21: 33-44.

14) Burg KJL, Porter S, Kellam JF. Biomaterial developments for bone tissue engineering. Biomaterials. 200; 21: 2347-2359.

15) Polo-Corrales L, Latorre-Esteves M, Ramirez-Vick JE. Scaffold design for bone regeneration. J. Nanosci. Nanotechnol. 2014; 14: 15-56.

16) Amini AR, Laurencin CT, Nukavarapu SP. Bone tissue engineering: Recent advances and challenges. Crit. Rev. Biomed. Eng. 2012; 40: 363-408.

17) LeGeros RZ, Chohayeb A, Shulman A. Apatitic calcium phosphates: possible restorative materials. J. Dent. Res. 1982; 61: 343.

18) Bose S, Roy M, Bandyopadhyay A. Recent advances in bone tissue engineering scaffolds. Trends Biotechnol. 2012; 30: 546-554.

19) Al-Munajjed AA, Plunkett NA, Gleeson JP, Weber T, Jungreuthmayer C, Levingstone T, Hammer J, O'Brien FJ. Development of a biomimetic collagen–hydroxyapatite scaffold for bone tissue engineering using a SBF immersion technique. J. Biomed. Mater. Res., Part B App. Biomater. 2009; 90: 584-591.

20) Hollister SJ. Porous scaffold design for tissue engineering. Nat. Mater. 2005; 4: 518-524.

21) Sheikh Z, Najeeb S, Khurshid Z, Verma V, Rashid H, Glogauer M. Biodegradable materials for bone repair and tissue engineering applications. Mater. 2015; 8: 5744-5794.

22) Stevens MM. Biomaterials for bone tissue engineering. Mater. Today. 2008; 11: 18-25.

23) Yu X, Tang X, Gohil SV, Laurencin CT. Biomaterials for bone regenerative engineering. Adv. Healthc. Mater. 2015; 4: 1268-1285.

24) Chen Z, Liu H, Liu X, Cui FZ. Injectable calcium sulfate/mineralized collagen-based bone repair materials with regulable self-setting properties. J. Biomed. Mater. Res. Part A. 2011; 99A: 554-563.

25) El-Sherbiny IM, Yacoub MH. Hydrogel scaffolds for tissue engineering: Progress and challenges. Glob. Cardiol. Sci. Pract. 2013; 2013: 316-342.

26) Ahmed EM. Hydrogel: Preparation, characterization, and applications: A review. J. Adv. Res. 2015; 6: 105-121.

27) Calo E, Khutoryanskiy VV. Biomedical applications of hydrogels: A review of patents and commercial products. Eur. Poly. J. 2015; 65: 252-267.

28) Bhattarai N, Gunn J, Zhang M. Chitosan-based hydrogels for controlled, localized drug delivery. Adv. Drug Deliv. Rev. 2010; 62: 83-99.

29) Nicodemus GD, Bryant SJ. Cell encapsulation in biodegradable hydrogels for tissue engineering applications. Tissue Eng. Part B Rev. 2008; 14: 149-165.

30) Kirchmajer DM, Gorkin III R, in het Panhuis M. An overview of the suitability of hydrogel-forming polymers for extrusion-based 3D printing. J. Mater. Chem. B. 2015; 3: 4105-4117.

31) Zhu J, Marchant RE. Design properties of hydrogel tissue engineering scaffolds. Expert Rev. Med. Devices. 2011; 8: 607-626.

32) Caliari SR, Burdick JA. A practical guide to hydrogels for cell culture. Nature Methods. 2016; 13: 405-414.

33) Jeong B, Kim SW, Bae YH. Thermosensitive sol-gel reversible hydrogels. Adv. Drug Deliv. Rev. 2002; 54: 37-53.

34) Fu SZ, Ni PY, Wang BY, Chu BY, Zheng L, Luo F, Luo JC, Qian ZY. Injectable and thermo-sensitive PEG-PCL-PEG copolymer/collagen/n-HA hydrogel composite for guided bone tissue regeneration. Biomaterials. 2012; 33:4801-4809.

35) Nguyen KT, West JL. Photopolymerizable hydrogels for tissue engineering applications. Biomaterials. 2002; 23: 4307-4314.

36) Arakawa C, Ng R, Tan S, Kim S, Wu B, Lee M. Photopolymerizable chitosan-collagen hydrogels for bone tissue engineering. J. Tissue Eng. Regen. Med. 2017; 11: 164-174.

37) Amini AA, Nair LS. Injectable hydrogels for bone and cartilage repair. Biomed. Mater. 2012; 7: 024105.

38) Kuo C, Ma P. Ionically crosslinked alginate hydrogels as scaffolds for tissue engineering: Part 1. Structure, gelation rate and mechanical properties. Biomaterials. 2001; 22: 511-521.

39) Qin XH, Gruber P, Markovic M, Plochberger B, Klotzsch E, Stampfl J, Ovsianikov A, Liska R. Enzymatic synthesis of hyaluronic acid vinyl esters for two-photon microfabrication of biocompatible and biodegradable hydrogel constructs. Polym. Chem. 2004; 5: 6523-6533.

40) Gong CY, Shi S, Dong PW, Kan B, Gou ML, Wang XH, Li XY, Luo F, Zhao X, Wei YQ, Qian ZY. Synthesis and characterization of PEG-PCL-PEG thermosensitive hydrogel. Int. J. Pharm. 2009; 365: 89-99.

41) Hoare TR, Kohane DS. Hydrogels in drug delivery: Progresses and challenges. Polymer. 2008; 49:1993-2007.

42) Gibas I, Janik H. Review: Synthetic polymer hydrogels for biomedical applications. Chem. Chem. Technol. 2010; 4: 297- 304.

43) Lee KY, Mooney DJ. Hydrogels for tissue engineering. Chem. Rev. 2001; 101: 1869-1879.

44) Zhao W, Jin X, Cong Y, Liu Y, Fu J. Degradable natural polymer hydrogels for articular cartilage tissue engineering. J. Chem. Technol. Biotechnol. 2013; 88: 327-339.

45) Kondiah PJ, Choonara YE, Kondiah PP, Marimuthu T, Kumar P, du Toit LC, Pillay V. A review of injectable polymeric hydrogel systems for application in bone tissue engineering, Molecules. 2016; 21: 1580.

46) Tan H, Marra KG. Injectable, biodegradable hydrogels for tissue engineering applications. Materials. 2010; 3: 1746-1767.

47) Augst AD, Kong HJ, Mooney DJ. Alginate hydrogels as biomaterials. Macromol. Biosci. 2006; 6: 623-633.

48) Coma V. Polysaccharide-based biomaterials with antimicrobial and antioxidant properties. Polimeros. 2013; 23: 287-297.

49) McHugh D. Chapter 2 - Production, Properties and Uses of Alginates. *Production and Utilization of Products from Commercial Seaweeds*. Rome: Food and Agriculture Organization of the United Nations, 1987. Print.

50) Grant G, Morris E, Rees D, Smith P, Thom D. Biological interactions between polysaccharides and divalent cations: The egg-box model. FEBS Lett. 1973; 15: 195-198.

51) Marriott AS, Bergstrom E, Hunt AJ, Thomas-Oates J, Clark JH. A natural template approach to mesoporous carbon spheres for use as green chromatographic stationary phases. RSC Adv. 2014; 4: 222-228.

52) Lee KY, Mooney DJ. Alginate: properties and biomedical applications. Prog. Polym. Sci. 2012; 37: 106-126.

53) Fang Y, Al-Assaf S, Phillips GO, Nishinari K, Funami T, Williams OPA, Li L. Multiple steps and critical behaviors of the binding of calcium to alginate. J. Phys. Chem. B. 2007; 111: 2456-2462.

54) Sun J, Tan H. Alginate-based biomaterials for regenerative medicine applications. Materials 2013; 6:1285-1309.

55) Cho SH, Lim SM, Han DK, Yuk SH, Im GI, Lee JH. Time-dependent alginate/polyvinyl alcohol hydrogels as injectable cell carriers. Journal of Biomaterials Science, Polymer Edition 2009: 20:7-8, 863-876.

56) Kong HJ, Kaigler D, Kim K, Mooney DJ. Controlling rigidity and degradation of alginate hydrogels via molecular weight distribution. Biomacromol. 2004; 5: 1720-1727.

57) LeRoux MA. Guilak F, Setton LA. Compressive and shear properties of alginate gel: Effects of sodium ions and alginate concentration. J. Biomed. Mater. Res. 1999; 47: 46-53.

58) Andersen T, Strand B, Formo K, Alsberg E, Christensen B. Alginates as biomaterials in tissue engineering. Carbohydr. Chem. 2012; 37: 227-258.

59) Smidsrod O, Skjak-Braek G. Alginate as immobilization matrix for cells. Trends Biotechnol. 1990; 8: 71-78.

60) Szekalska M, Pucilowska A, Szymanska E, Ciosek P, Winnicka K. Alginate: Current use and future perspectives in pharmaceutical and biomedical applications. Int. J. Polym. Sci. 2016; 2016: 1-17.

61) Pereira R, Carvalho A, Vaz DC, Gil MH, Mendes A, Bartolo P. Development of novel alginate based hydrogel films for wound healing applications. Int. J. Biol. Macromolec. 2013; 52: 221-230.

62) Yu W, Jiang YY, Sun TW, Qi C, Zhao H, Chen F, Shi Z, Zhu YJ, Chen D, He Y. Design of a novel wound dressing consisting of alginate hydrogel and simvastatin-incorporated mesoporous hydroxyapatite microspheres for cutaneous wound healing. RSC Adv. 2016; 6: 104375-104387.

63) Tonnesen HH, Karlsen J. Alginate in drug delivery systems. Drug Dev. Ind. Pharm. 2002; 28: 621-630.

64) Bhattarai RS, Dhandapani NV, Shrestha A. Drug delivery using alginate and chitosan beads: An overview. Chron. Young Sci. 2011; 2: 192-196.

65) Anal AK, Stevens WF. Chitosan-alginate multilayer beads for controlled release of ampicillin. Int. J. Pharm. 2005; 290: 45-54.

66) Zhao J, Guo B, Ma PX. Injectable alginate microsphere/PLGA-PEG-PLGA composite hydrogels for sustained drug release. RSC Adv. 2014; 4: 17736-17742.

67) Hwang SJ, Rhee GJ, Lee KM, Oh KH, Kim CK. Release characteristics of ibuprofen from excipient-loaded alginate gel beads. Int. J. Pharm. 1995; 116: 125-128.

68) Kassem MA, Abdel MI, Assak TE, Al Badrawy AA. Preparation and evaluation of certain hydrophilic drug-loaded microspheres. Int. Res. J. Pharm. 2012; 2: 82-90.

69) Wu J, Kong T, Yeung KWK, Shum HC, Cheung KMC, Wang L, To MKT. Fabrication and characterization of monodisperse PLGA-alginate core-shell microspheres with monodisperse size and homogeneous shells for controlled drug release. Acta Biomater. 2013; 9: 7410-7419.

70) Zhang J, Wang Q, Wang A. In situ generation of sodium alginate/hydroxyapatite nanocomposite beads as drug-controlled release matrices. Acta Biomater. 2010; 6: 445-454.

71) Sun Q, Silva EA, Fritton JC, Mooney DJ, Schaffler MB, Grossman PM, Rajagopalan S. Sustained release of multiple growth factors from injectable polymeric system as a novel therapeutic approach towards angiogenesis. Pharm. Res. 2010; 27: 264-271.

72) Gombotz WR, Wee SF. Protein release from alginate matrices. Adv. Drug Deliv. Rev. 2012; 64: 194-205.

73) Gu F, Amsden B, Neufeld R. Sustained delivery of vascular endothelial growth factor with alginate beads. J. Control. Release. 2004; 96: 463-472.

74) Andersen T, Auk-Emblem P, Dornish M. 3D cell culture in alginate hydrogels. Microarrays 2015; 4: 133-161.

75) Lan SF, Safiejko-Mroczka B, Starly B. Long-term cultivation of HepG2 liver cells encapsulated in alginate hydrogels: A study of cell viability, morphology and drug metabolism. Toxicol. In Vitro. 2010; 24: 1314-1323.

76) Lee BH, Li B, Guelcher SA. Gel microstructure regulates proliferation and differentiation of MC3T3-E1 cells encapsulated in alginate beads. Acta Biomater. 2012; 8: 1693-1702.

77) Yao R, Zhang R, Lin F, Luan J. Biomimetic injectable HUVEC-adipocytes/collagen/alginate microsphere co-cultures for adipose tissue engineering. Biotechnol. Bioeng. 2013;110:1430-1443.

78) Hunt NC, Shelton RM, Grover LM. An alginate hydrogel matrix for the localized delivery of a fibroblast/keratinocyte co-culture. Biotechnol. J. 2009; 4: 730-737.

79) Rosso F, Giordano A, Barbarisi M, Barbarisi A. From cell-ECM interactions to tissue engineering. J. Cell. Physio. 2004; 199: 174-180.

80) Wu C. Focal adhesion: A focal point in current cell biology and molecular medicine. Cell Adh. Migr. 2007; 1:13-18.

81) Narayanan LK, Huebner P, Fisher MB, Spang JT, Starly B, Shirwaiker RA. 3D-bioprinting of polylactic acid (PLA) nanofiber-alginate hydrogel bioink containing human adipose-derived stem cells. ACS Biomater. Sci. Eng. 2016; 2: 1732-1742.

82) Rowley JA, Madlambayan G, Mooney DJ. Alginate hydrogels as synthetic extracellular matrix materials. Biomaterials 1999; 20: 45-53.

83) Wu Z, Su W, Xu Y, Kong B, Sun W. Bioprinting three-dimensional cell-laden tissue constructs with controllable degradation. Sci. Rep. 2016; 6: 24474.

84) Sayyar B, Dodd M, Marquez-Curtis L, Janowska-Wieczorek A, Hortelano G. Fibronectin-alginate microcapsules improve cell viability and protein secretion of encapsulated Factor IX-engineered human mesenchymal stromal cells. Artif. Cells Nanomed. Biotechnol. 2015; 43: 318-327.

85) Kang SW, Cha BH, Park H, Park KS, Lee KY, Lee SH. The effect of conjugating RGD into 3D alginate hydrogels on adipogenic differentiation of human adipose-derived stromal cells. Macromolec. Biosci. 2011; 11: 673-679.

86) Alsberg E, Anderson KW, Albeiruti A, Franceschi RT, Mooney DJ. Cell-interactive alginate hydrogels for bone tissue engineering. J. Dent. Res. 2001; 80: 2025-2029.

87) Zhang SM, Cui FZ, Liao SS, Zhu Y, Han L. Synthesis and biocompatibility of porous nano-hydroxyapatite/collagen/alginate composite. J. Mater. Sci.: Mater. Med. 2003; 14: 641-645.

88) Wong KV, Hernandez A. A review of additive manufacturing. ISRN Mech. Eng. 2012; 2012: 1-10.

89) Sears NA, Seshadri DR, Dhavalikar PS, Cosgriff-Hernandez E. A review of three-dimensional printing in tissue engineering. Tissue Eng. Part B Rev. 2016; 22: 298-310.

90) Rengier F, Mehndiratta A, von Tengg-Kobligk H, Zechmann CM, Unterhinninghofen R, Kauczor HU, Giesel FL. 3D printing based on imaging data: review of medical applications. Int. J. CARS. 2010; 5: 335-341.

91) Grunberger T, Domrose R. Direct metal laser sintering: Identification of process phenomena by optical in-process monitoring. Laser Tech. J. 2015; 12: 45-48.

92) Bose S, Vahabzadeh S, Bandyopadhyay A. Bone tissue engineering using 3D printing. Mater. Today 2013; 16: 496-504.

93) Chia HN, Wu BM. Recent advances in 3D printing of biomaterials. J. Biol. Eng. 2015; 9: 1-14.

94) Park SH, Park DS, Shin JW, Kang YG, Kim HK, Yoon TR, Shin JW. Scaffolds for bone tissue engineering fabricated from two different materials by the rapid prototyping technique: PCL versus PLGA. J. Mater. Sci.: Mater. Med. 2012; 23: 2671-2678.

95) Li J, He L, Zhou C, Zhou Y, Bai Y, Lee FY, Mao JJ. 3D printing for regenerative medicine: From bench to bedside. MRS Bull. 2015; 40: 145-153.

96) Shim JH, Kim JY, Park M, Park J, Cho DW. Development of a hybrid scaffold with synthetic biomaterials and hydrogel using solid freeform fabrication technology. Biofabrication 2011; 3: 034102.

97) Chung JHY, Naficy S, Yue Z, Kapsa R, Quigley A, Moulton SE, Wallace GG. Bio-ink properties and printability for extrusion printing living cells. Biomater. Sci. 2013; 1: 763-773.

98) Khalil S, Sun W. Bioprinting endothelial cells with alginate for 3D tissue constructs. J. Biomech. Eng. 2009; 131: 111002-1-8.

99) Xu T, Zhao W, Zhu JM, Albanna MZ, Yoo JJ, Atala A. Complex heterogeneous tissue constructs containing multiple cell types prepared by inkjet printing technology. Biomaterials 2013; 34: 130-139.

100) Malda J, Visser J, Melchels FP, Jüngst T, Hennink WE, Dhert WJA, Groll J, Hutmacher DW. 25th Anniversary Article: Engineering Hydrogels for Biofabrication. Adv. Mater. 2013; 25: 5011-5028.

101) Wang ZY, Zhang QZ, Konno M, Saito S. Sol-gel transition of alginate solution by the addition of various divalent cations: A rheological study. Biopolymers 1994; 34: 737-746.

102) Trombetta R, Inzana JA, Schwarz EM, Kates SL, Awad HA. 3D printing of calcium phosphate ceramics for bone tissue engineering and drug delivery. Ann. Biomed. Eng. 2016; 1-22.

103) Pati F, Song TH, Girdhardi R, Jang J, Kim SW, Cho DW. Ornamenting 3D printed scaffolds with cell-laiden extracellular matrix for bone tissue regeneration. Biomaterials 2015; 37: 230-241.

103) Hench LL, Splinter RJ, Allen WC, Greenlee TK. Bonding mechanisms at the interface of ceramic prosthetic materials. Biomed. Mater. Res. 1971; 5: 117-141.

104) Nery EB, Lynch KL, Hirthe WM, Mueller KH. Bioceramic implants in surgically produced infrabony defects. Periodont. 1975; 46: 328-333.

105) LeGeros RZ. Calcium phosphate materials in restorative dentistry: A review. Adv. Dent. Res. 1988; 2: 164-180.

106) Brown WE, Chow LC. Dental Restorative Cement Pastes, U.S. Patent No. 4, 518, 430, May 21, 1985.

107) Manjubala I, Scheler S, Bossert J, Jandt K. Mineralisation of chitosan scaffolds with nano-apatite formation by double diffusion technique. Acta Biomater. 2006; 2:75-84.

108) Kikuchi M, Itohv S, Ichinose S, Shinomiya K, Tanaka J. Self-organization mechanism in a bone-like hydroxyapatite/collagen nanocomposite synthesized in vitro and its biological reaction in vivo. Biomaterials 2001; 22: 1705-1711.

109) Ficai A, Andronescu E, Voicu G, Ghitulica C, Vasile BS, Ficai D, Trandafir V. Self-assembled collagen/hydroxyapatite composite materials. J. Chem. Eng. 2010; 160: 794-800.

110) Qu H, Xia Z, Knecht D, Wei M. Synthesis of dense collagen/apatite composites using a biomimetic method. J. Am. Ceram. Soc. 2008; 91: 3211–3215.

111) Xia Z, Yu X, Wei M. Biomimetic collagen/apatite coating formation on Ti6Al4V substrates. J. Biomed. Mater. Res., Part B App. Biomater. 2012; 100: 871–881.

112) Xia Z, Yu X, Jiang X, Brody H, Rowe D, Wei, M. Fabrication and characterization of biomimetic collagen–apatite scaffolds with tunable structures for bone tissue engineering. Acta Biomater. 2013; 9: 7308-7319.

113) Ma G, Li Q, Wang K, Binling C, Kennedy J, Nie J. Injectable hydrogels based on chitosan derivative/polyethylene glycol dimethacrylate/N,N-dimethylacrylamide as bone tissue engineering matrix. Carbohydr. Polym. 2010; 79: 620-627.

114) Bucke, C. Methods Enzymol. 1987: 135, 175.

115) Watson BM, Kasper FK, Engel PS, Mikos AG. Synthesis and characterization of injectable, biodegradable, phosphate-containing, chemically cross-linkable, thermoresponsive macromers for bone tissue engineering. Biomacromolecules 2014; 15: 1788-1796.

116) Coutinho DF, Sant SV, Shin H, Oliveira JT, Gomes ME, Neves NM, Khademhosseini A, Reis RL. Modified gellan gum hydrogels with tunable physical and mechanical properties. Biomaterials 2010; 31: 7494-7502.

117) McHugh D. Chapter 2 - Production, Properties and Uses of Alginates. *Production and Utilization of Products from Commercial Seaweeds*. Rome: Food and Agriculture Organization of the United Nations, 1987. Print.

118) Martinsen A, Skjak-Braek G, Smidsrod O. Alginate as immobilization material: I. correlation between chemical and physical properties of alginate gel beads. Biotechnol. Bioeng. 1989; 33: 79-89.

119) Sotome S, Uemura T, Kikuchi M, Chen J, Itoh S, Tanaka J, Tateishi T, Shinomiya K. Synthesis and in vivo evaluation of a novel hydroxyapatite/collagen–alginate as a bone filler and a drug delivery carrier of bone morphogenetic protein. Mater. Sci. and Eng. C Mater. Biol. Appl. 2004; 24: 341–347.

120) Brayner R, Coradun T, Fievet-Vincent F, Livage J, FIevet F. Algal polysaccharide capsule-templated growth of magnetic nanoparticles. New J. Chem. 2005; 29: 681–685.

121) Braccini I, Grasso RP, Perez S. Conformational and configurational features of acidic polysaccharides and their interactions with calcium ions: a molecular modeling investigation. Carbohydr. Res. 1999; 317:119-130.

122) Parhi P, Ramanan A, Ray AR. Preparation and characterization of alginate and hydroxyapatite-based biocomposite. J. Appl. Polym. Sci. 2006; 102: 5162–5165.

123) Li W, Zhao P, Lin C, Wen X, Katsanevakis E, Gero D, Felix O, Liu Y. Natural polyelectrolyte self-assembled multilayers based on collagen and alginate: Stability and cytocompatibility. Biomacromolecules 2013;14: 2647-2656.

124) Jin HH, Lee CH, Lee WK, Lee JK, Park HC, Yoon SY. In-situ formation of the hydroxyapatite/chitosan–alginate composite scaffolds. Mater. Lett. 2008; 62: 1630–1633.

125) Tampieri A, Sandri M, Landi E, Celotti G, Roveri N, Mattioli-Belmonte M, Virgili L, Gabbanelli F, Biagini G. HA/alginate hybrid composites prepared through bio-inspired nucleation. Acta Biomater. 2005; 1: 343–351.

126) Tan R, Niu X, Gan S, Feng Q. Preparation and characterization of an injectable composite. J. Mater. Sci.: Mater. Med. 2009; 20: 1245–1253.

127) Rajan N, Habermehl J, Coté MF, Doillon CJ, Mantovani D. Preparation of ready-to-use, storable and reconstituted type I collagen from rat tail tendon for tissue engineering applications. Nat. Protoc. 2007; 1: 2753–2758.

128) Lu L, Qi YS, Zhou CR, Jiao YP. Rapidly *in situ* forming biodegradable hydrogels by combining alginate and hydroxyapatite nanocrystal. Sci. China Tech. Sci. 2010; 53: 272−277.

129) Rho JY, Kuhn-Spearing L, Zioupos P. Mechanical properties and the hierarchical structure of bone. Med. Eng. Phys. 1998; 20:92-102.

130) Noor Z. Nanohydroxyapatite application to osteoporosis management. J. Osteoporosis 2013; 2013: 1-6.

131) Chang SC, Rowley JA, Tobias G, Genes NG, Roy AK, Mooney DJ, Vacanti CA, Bonassar LJ. Injection Molding of Chondrocyte/alginate Constructs in the Shape of Facial Implants. J. Biomed. Mater. Res. 2001; 55:503-511.

132) Teng S, Shi J, Peng B, Chen L. The effect of alginate addition on the structure and morphology of hydroxyapatite/gelatin nanocomposites. Compos. Sci. Technol. 2006; 66: 1532-1538.

133) Kramer ER, Morey AM, Staruch M, Suib SL, Jain M, Budnick JI, Wei M. Synthesis and characterization of iron-substituted hydroxyapatite via a simple ion-exchange procedure. J. Mater. Sci. 2013; 48: 665-673.

134) Wang L, Li Y, Li C. In situ processing and properties of nanostructured hydroxyapatite/alginate composite. J. Nanopart. Res. 2009; 11: 691-699.

135) Regis M, Marin E, Fedrizzi L, Pressacco M. Additive manufacturing of trabecular titanium orthopedic implants. MRS Bull. 2015: 40: 137- 144.

136) Do AV, Khorsand B, Geary SM, Salem AK. 3D printing of scaffolds for tissue regeneration applications. Adv Healthc Mater. 2015; 4: 1742-1762.

137) Mandrycky C, Wang Z, Kim K, Kim DH. 3D bioprinting for engineering complex tissues. Biotechnol. Adv. 2016; 34: 422-434.

138) Radenkovic D, Solouk A, Seifalian A. Personalized development of human organs using 3D printing technology. Med. Hypotheses 2016; 87: 30-33.

139) Holmes B, Zhu W, Li J, Lee JD, Zhang LG. Development of novel three-dimensional printed scaffolds for osteochondral regeneration. Tissue Eng. Part A 2015; 21: 403-415.

140) Koch L, Deiwick A, Schlie S, Michael S, Gruene M, Coger V, Zychlinski D, Schambach A, Reimers K, Vogt PM, Chichkov B. Skin Tissue Generation by Laser Cell Printing. Biotechnol. Bioeng. 2012; 109: 1855-1863.

141) Murphy SV, Atala A. 3D bioprinting of tissues and organs. Nature Biotechnol. 2014; 32: 773-785.

142) Markstedt K, Mantas A, Tournier I, Martínez Ávila H, Hägg D, Gatenholm P. 3D bioprinting human chondrocytes with nanocellulose–alginate bioink for cartilage tissue engineering applications. Biomacromolecules 2015; 16: 1489-1496.

143) Hsieh FY, Lin HH, Hsu SH. 3D bioprinting of neural stem cell-laden thermoresponsive biodegradable polyurethane hydrogel and potential in central nervous system repair. Biomaterials 2015; 71: 48-57.

144) Inzana JA, Olvera D, Fuller SM, Kelly JP, Graeve OA, Schwarz EM, Kates SL, Awad HA. 3D printing of composite calcium phosphate and collagen scaffolds for bone regeneration. Biomaterials 2014; 35: 4026-4034.

145) Jakus AE, Rutz AL, Shah RN. Advancing the field of 3D biomaterial printing. Biomed. Mater. 2016; 11: 1-11.

146) Senatov FS, Niaza KV, Zadorozhnyy MY, Maksimkin AV, Kaloshkin SD, Estrin YZ. Mechanical properties and shape memory effect of 3D printed PLA-based porous scaffolds. J. Mech. Behav. Biomed. Mater. 2016; 57: 139-148.

147) Van Vlierberghe S, Dubruel P, Schacht E. Biopolymer-based hydrogels as scaffolds for tissue engineering applications: A review. Biomacromolecules 2011; 12: 1387-1408.

148) Wang S, Lee JM, Yeong WY. Smart hydrogels for 3D bioprinting. Int. J. Bioprinting 2015; 1: 3-14.

149) Rutz AL, Hyland KE, Jakus AE, Burghardt WR, Shah RN. Multimaterial bioink method for 3D printing tunable, cell-compatible hydrogels. Adv. Mater. 2015; 27: 1607–1614.

150) Kong HJ, Smith MK, Mooney DJ. Designing alginate hydrogels to maintain viability of immobilized cells. Biomaterials 2003; 24: 4023-4029.

151) Luo Y, Lode A, Sonntag F, Nies B, Gelinsky M. Well-ordered biphasic calcium phosphate-alginate scaffolds fabricated by multi-channel 3D plotting under mild conditions. J. Mater. Chem. B 2013; 1: 4088- 4098.

152) Jia J, Richards DJ, Pollard S, Tan Y, Rodriguez J, Visconti RP, Trusk T, Yost MJ, Yao H, Markwald RR, Mei Y. Engineering alginate as bioink for bioprinting. Acta Biomater. 2014; 10: 4323-4331.

153) Neufurth M, Wang X, Schroder HC, Feng Q, Diehl-Seifert B, Ziebart T, Steffen R, Wang S, Muller WEG. Engineering a morphogenetically active hydrogel for bioprinting of bioartificial tissue derived from human osteoblast-like SaOS-2 cells. Biomaterials 2014; 35: 8810-8819.

154) Peng F, Veilleux E, Schmidt M, Wei M. Synthesis of hydroxyapatite nanoparticles with tailorable morphology and carbonate substitutions using precipitation method. J. Nanosci. Nanotechnol. 2012; 11: 1-9.

155) Bendtsen ST, Wei M. Synthesis and characterization of a novel injectable alginate-collagen-hydroxyapatite hydrogel for bone tissue regeneration. J. Mater. Chem. B 2015; 3: 3081-3090.

156) Kesti M, Muller M, Becher J, Schnabelrauch M, D'Este M, Eglin D, Zenobi-Wong M. A versatile bioink for three-dimensional printing of cellular scaffolds based on thermally and photo-triggered tandam gelation. Acta Biomater. 2015; 11: 162-172.

157) Rajkumar M, Meenakshisundaram N, Rajendran V. Development of nanocomposites based on hydroxyapatite/sodium alginate: Synthesis and characterization. Mater. Charact. 2001; 62: 469-479.

158) Segeren AJM, Boskamp JV, van den Tempel M. Rheological and swelling properties of alginate gels. Faraday Discuss. Chem. Soc. 1974; 57: 255-262.

159) Cao N, Chen XB, Schreyer DJ. Influence of calcium ions on cell survival and proliferation in the context of an alginate hydrogel. ISRN Chem. Eng. 2012; 2012: 1-9.

160) Godbey WT, Atatla A. In vitro systems for tissue engineering. Ann. N.Y. Acad. Sci. 2002; 961: 10–26.

161) Kundu J, Shim JH, Jang J, Kim SW, Cho DW. An additive manufacturing-based PCL-alginate-chondrocyte bioprinting scaffold for cartilage tissue regeneration. J Tissue Eng. Regen. Med. 2015; 9: 1286-1297.

162) Zhao Y, Li Y, Mao S, Sun W, Yao, R. The influence of printing parameters on cell survival rate and printability in microextrusion-based 3D cell printing technology. Biofabrication 2015; 7: 045002.

163) Thavornyutikam B, Chantarapanich N, Sitthiseripratip K, Thouas GA, Chen Q. Bone tissue engineering scaffolding: computer-aided scaffolding techniques. Prog Biomater. 2014; 3: 61-102.

164) Wozniak MA, Modzelewska K, Kwong L, Keely PJ. Focal adhesion regulation of cell behavior. Biochimica et Biophysica Acta. 2004; 1692: 103-119

165) Parsons JT, Horwitz AR, Schwarts MA. Cell adhesion: integrating cytoskeletal dynamics and cellular tension. Nat. Rev. Mol. Cell Biol. 2010; 11: 633-643.

166) Khalili AA, Ahmad MR. A review of cell adhesion studies for biomedical and biological applications. Int. J. Mol. Sci. 2015; 16: 18149-18184.

167) Khatiwala CB, Peyton SR, Putnam AJ. Intrinsic mechanical properties of the extracellular matrix affect the behavior of pre-osteoblastic MC3T3-E1 cells. Am. J. Physiol. Cell Physiol. 2006; 290: C1640-C1650.

168) Matyah M, Despang F, Ikonomidou C, Gelinsky M. Swelling and mechanical properties of alginate hydrogels with respect to promotion of neural growth. Tissue Eng. Part C Methods. 2014; 20: 401-411.

169) Lawyer T, McIntosh K, Clavijo C, Potekhina L, Mann BK. Formulation changes affect material properties and cell behavior in HA-based hydrogels. Int. J. Cell Biol. 2012; 2012: 1-9.

170) Bendtsen ST, Quinnell SP, Wei M. Development of a novel alginate-polyvinyl alcohol-hydroxyapatite hydrogel for 3D bioprinting bone tissue engineered scaffolds. J. Biomed. Mater. Res. A. 2017; 105: 1457-1468.

171) Yu X, Xia Z, Wang L, Peng F, Jiang X, Huang J, Rowe DW, Wei M. Controlling the structural organization of regenerated bone by tailoring tissue engineering scaffold architecture. J. Mater. Chem. 2012; 22: 9721-9730.

172) Matsumura K, Hayami T, Hyon SH, Tsutsumi S. Control of proliferation and differentiation of osteoblasts on apatite-coated poly(vinyl alcohol) hydrogel as an artificial articular cartilage material. J. Biomed. Mater. A. 2010; 92A: 1225-1232.

173) Derby B. Bioprinting: inkjet printing proteins and hybrid cell-containing materials and structures. J. Mater. Chem. 2008; 18: 5717-5721.

174) Li L, Crosby K, Sawicki M, Shaw LL, Wang Y. Effects of surface roughness of hydroxyapatite on cell attachment and proliferation. J. Biotechnol. Biomater. 2012; 2: 2-5.

175) Peng F, Yu X, Wei M. In vitro cell performance on hydroxyapatite particles/poly(L-lactic acid) nanofibrous scaffolds with an excellent particle along nanofiber orientation. Acta Biomater. 2011; 7: 2585-2592.

176) Maeno S, Niki Y, Matsumoto H, Morioka H, Yatabe T, Funayama A. Toyama Y, Taguchi T, Tanaka J. The effect of calcium ion concentration on osteoblast viability, proliferation and differentiation in monolayer and 3D culture. Biomaterials. 2005; 26: 4847-4855.

177) Wan LQ, Jiang J, Arnold DE, Guo XE, Lu HH, Mow VC. Calcium concentration effects on the mechanical and biochemical properties of chondrocyte-alginate constructs. Cell. Mol. Bioeng. 2008; 1: 93-102.

178) Torelli-Souza RR, Cavalcante Bastos LA, Nunes HGL, Camara CA, Amorim RVA. Sustained release of an antitumoral drug from alginate-chitosan hydrogel beads and its potential use as colonic drug delivery. J. Appl. Polym. Sci. 2012; 126: E408-E417.

179) Bhattacharya M, Malinen MM, Lauren P, Lou YR, Kuisma SW, Kanninen L, Lille M, Corlu A, GuGuen-Guillouzo C, Ikkala O, Laukkanen A, Urtti A, Yliperttula M. Nanofibrillar cellulose hydrogel promotes three-dimensional liver cell culture. J. Control. Release. 2012; 164: 291-298.

180) Mannermaa E, Reinisalo M, Ranta VP, Vellonen KS, Kokki H, Saarikko A, Kaarniranta K, Urtti A. Filter-cultured ARPE-19 cells as outer blood-retinal barrier model. Eur. J. Pharm. Sci. 2010; 40: 289-296.

181) Farndale RW, Lisman T, Bihan D, Hamaia S, Smerling CS, Pugh N, Konitsiotis A, Leitinger B, de Groot PG, Jarvis GE, Raynal N. Cell-collagen interactions: the use of peptide Toolkits to investigate collagen-receptor interactions. Biochem. Soc. Trans. 2008; 36: 241-250.

182) Pawelec KM, Best SM, Cameron RE. Collagen: a network for regenerative medicine. J. Mater. Chem. B. Mater. Biol. Med. 2016; 4: 6484-6496.

183) Quarles LD, Yohay DA, Lever LW, Caton R, Wenstrup RJ. Distinct proliferative and differentiated stages of murine MC3T3-E1 cells in culture: an in vitro model of osteoblast development. J. Bone Miner. Res. 1992; 7: 683-692.

184) Ahearne M. Introduction to cell-hydrogel mechanosensing. Interface Focus. 2014; 4: 20130038.

185) Janson IA, Putnam AJ. Extracellular matrix elasticity and topography: material-based cues that affect cell function via conserved mechanisms. J. Biomed. Mater. Res. A. 2015; 103: 1246-1258.

186) Lo CM, Wang HB, Dembo M, Wang Yl. Cell movement is guided by the rigidity of the substrate. Biophysical J. 2000; 79: 144-152.

187) Discher D, Janmey P, Wang YL. Tissue cells feel and respond to the stiffness of their substrate. Science. 2005; 310: 1139-1143.

188) Khatiwala CB, Peyton SR, Metzke M, Putnam AJ. The regulation of osteogenesis by ECM rigidity in MC3T3-E1 cells requires MAPK activation. J. Cell. Physiol. 2007; 211: 661-672.